Durham E-Theses

On Statistical QoS Provisioning for Smart Grid

YOU, MINGLEI

On Statistical QoS Provisioning for Smart Grid

Minglei You

A Thesis presented for the degree of
Doctor of Philosophy

Department of Engineering
University of Durham
United Kingdom

June 2018

To my beloved wife

and

my Parents.

On Statistical QoS Provisioning for Smart Grid

Minglei You

Abstract

Current power system is in the transition from traditional power grid to Smart Grid. A key advantage of Smart Grid is its integration of advanced communication technologies, which can provide real-time system-wide two-way information links. Since the communication system and power system are deeply coupled within the Smart Grid system, it makes Quality of Service (QoS) performance analysis much more complex than that in either system alone. In order to address this challenge, the effective rate theory is studied and extended in this thesis, where a new H transform based framework is proposed. Various scenarios are investigated using the new proposed effective rate framework, including both independent and correlated fading channels. With the effective rate as a connection between the communication system and the power system, an analysis of the power grid observability under communication constraints is performed. Case studies show that the effective rate provides a cross layer analytical framework within the communication system, while its statistical characterisation of the communication delay has the potential to be applied as a general coupling point between the communication system and the power system, especially when real-time applications are considered.

Besides the theoretical QoS performance analysis within Smart Grid, a new Software Defined Smart Grid testbed is proposed in this thesis. This testbed provides a versatile evaluation and development environment for Smart Grid QoS performance studies. It exploits the Real Time Digital Simulator (RTDS) to emulate different power grid configurations and the Software Defined Radio (SDR) environment to implement the communication system. A data acquisition and actuator module is developed, which provides an emulation of various Intelligent Electronic Devices (IEDs). The implemented prototype demonstrates that the proposed testbed has the potential to evaluate real time Smart Grid applications such as real time voltage stability control.

Declaration

The work in this thesis is based on research carried out at Department of Engineering, Durham University, England. No part of this thesis has been submitted elsewhere for any other degree or qualification and it is all my own work unless referenced to the contrary in the text.

Parts of this work have been published in the form of refereed papers:

- **Chapter 2**

  – **Minglei You**, Qitao Liu and Hongjian Sun, *"New Communication Strategy for Spectrum Sharing Enabled Smart Grid Cyber-Physical System"*, IET Cyber-Physical Systems: Theory and Applications, 2017, 2(3), pp. 136-142.

- **Chapter 3**

  – **Minglei You**, Hongjian Sun, Jing Jiang and Jiayi Zhang, *"Effective Rate Analysis in Weibull Fading Channels"*, IEEE Wireless Communications Letters, 2016, 5(4), pp. 340-343.

  – **Minglei You**, Xiaolin Mou and Hongjian Sun, *"Effective capacity analysis of smart grid communication networks"*, IEEE 20th International Workshop on Computer Aided Modelling and Design of Communication Links and Networks (CAMAD), Surrey, UK, 2015, pp. 196-200.

- **Chapter 4**

  – **Minglei You**, Hongjian Sun, Jing Jiang and Jiayi Zhang, *"Unified Framework for the Effective Rate Analysis of Wireless Communication Systems*

over MISO Fading Channels", IEEE Transactions on Communications, 2017, 65(4), pp. 1775-1785.

– **Minglei You** and Hongjian Sun, *"Realising energy-aware communication over fading channels under QoS constraints (Invited paper)"*, IEEE International Conference on Ubiquitous Wireless Broadband (ICUWB), Nanjing, China, 2016, pp. 1-4.

- **Chapter 5**

  – **Minglei You**, Jing Jiang, Andrea M. Tonello, Tilemachos Doukoglou, and Hongjian Sun, *"On Statistical Power Grid Observability Performance under Communication Constraints (Invited paper)"*, IET Smart Grid, 2018, 1(2), pp. 40-47.

  – **Minglei You**, Qitao Liu, Jing Jiang and Hongjian Sun (2017), *"Power Grid Observability Redundancy Analysis under Communication Constraints"*, 2017 IEEE/CIC International Conference on Communications in China (ICCC), Qingdao, China, 2017, pp. 1-5.

- **Chapter 6**

  – **Minglei You**, Qitao Liu, and Hongjian Sun (2018), *"A Cognitive Radio Enabled Smart Grid Testbed Based on Software Defined Radio and Real Time Digital Simulator"*, 2018 IEEE International Conference on Communications (ICC), Kansas City, USA, 2018, pp. 1-6.

August 11, 2018

Acknowledgements

I would like to first thank my PhD supervisors, Dr Hongjian Sun and Prof Simon Hogg for giving me the opportunity and guidance in carrying out my research. Dr Hongjian Sun has been very supportive in every aspect of my academic research and provided me many opportunities including project experiences and conferences. His enthusiasm and efforts in research have deeply motivated and encouraged me.

I am very grateful for the Durham Doctoral Scholarship provided by Durham University, which has fully funded my whole PhD degree including both tuition fees and living costs.

I would like to thank Prof Alan Purvis and Mr Peter Baxendale for their time and efforts in reviewing my annual reports. Special thanks to Dr Jing Jiang, who has provided me great help in discussions and academic supports. I would also like to thank Dr Tilemachos Doukoglou and Dr Velissarios Gezerlis from OTE, who have warmly hosted me during my secondment there and provided many helpful suggestions and comments on my work.

I am very lucky to have worked with so many talented and supportive colleagues and friends, especially thanks to Xiaolin Mou, Qitao Liu, Dan Li, Jiangjiao Xu, Weiqi Hua, John Heron, Mengwei Sun, Lei Fan, Meng Xu, Tao Yang, Zizheng Sun, Jingya Yang, Qian Wang and Konstantinos Krestenitis who have provided me joyful memories and helpful discussions.

Finally, I would like to thank my wife and parents. Their care and support have encouraged me in both my study and life.

Contents

List of Figures

List of Tables

Chapter 1

Introduction

1.1   Research Objectives and Solutions

In this thesis, the cross layer analysis framework for QoS provisioning in Smart Grid is firstly investigated, which is followed by an application of this analysis tool in the Smart Grid application performance improvement. Specifically, the focus is placed on the following four research objectives in this thesis.

- **A cross layer QoS analysis method for Smart Grid**

- **A unified framework for effective capacity analysis**

- **Smart Grid application performance improvement considering both power system and communication system aspects**

- **A Software Defined Smart Grid Testbed**

1.1.1   A Cross Layer QoS Analysis Method for Smart Grid

With the integration of advanced communication technologies, many potential real time and high data rate applications have been enabled in Smart Grid. This diver-

sity of applications provides a wider service choice for both customers and providers. But along with this benefit, it also brings a various requirement of QoS performance guarantee. In Smart Grid communication networks, the cyber network is deeply coupled with the physical components. Most application functions are built upon hardware, for example, the measurements from the sensors and meters, or the control command to be executed on the actuators. For active control and monitoring purpose, it demands strict time performances for such applications. On the other hand, Smart Grid has a wide coverage ranges, including power market, system operators, service provider, bulk generation, transmission, distribution and customer domains [3]. Numerous smart devices spines the support for the service infrastructure. In the meantime, this also brings the challenges of a huge volume of data and scarcity of frequency resources. All these challenges require a synthetic consideration of the QoS provisioning in the Smart Grid.

In most studies, only one or several QoS metrics are focused. From the aspect of communication networks, all the layers are designed to be as independent with each other as possible. This brings benefits as other modularized design does, but it also isolated the relations between the QoS metrics. Hence the research will focus on a specific layer when addressing a challenging problem. But in practice, some performances, such as delay, result from the combined effects from every layer. This makes the cross layer analysis method very attractive in QoS provisioning in Smart Grid. As more layers are considered in the cross layer model, the QoS metrics from different layers can provide a wider range of optimization for the performance improvement. However, the cross layer analysis is usually much complex compared to that of a single layer, since more influencing factors and parameters are involved.

In this thesis, the QoS provisioning in Smart Grid is addressed via cross layer analysis. The cross layer model named effective capacity is investigated and further developed. Using the effective capacity as an analysis tool, the Smart Grid application QoS performances are evaluated in case studies in Chapter 3.

1.1.2 A Unified Framework for Effective Capacity Analysis

The effective capacity theory is firstly proposed by Wu and Negi [4], which is the dual concept of the effective bandwidth used in wired communication analysis [5]. The theory is essentially a cross layer analysis model, which considers the network layer queueing features and physical layer channel fading effects. The model provides a statistical quantified relation between several QoS metrics, including delay bound, delay bound violation probability, data rate and channel fading effect. These parameters and factors are of great interest to a wide range of research areas, such as wireless communication networks and Smart Grid. However, only one or part of these parameters are considered in the existing studies, which is due to the complexity of the cross layer analysis within the communication system. The advent of effective capacity theory provides a way to simultaneously consider these parameters, which provide a versatile analysis basis for further QoS provisioning considerations. Hence it has attracted many research interests to further develop this theory in more practical scenarios, such as generalized fading channels [6,7] and various wireless networks [8,9]. Most existing studies are built upon the integral framework proposed by Matthaiou in [10]. This framework is based on multiple antenna systems, which includes the single antenna system as special cases. But this framework is defined based on integral form, which requires further derivations for individual cases. Besides, this derivation procedure needs sophisticated mathematical techniques, which will be illustrated in Chapter 3.

In this thesis, a unified framework for the effective capacity analysis is proposed, which is based on MGF and H transform representation. The H transform can help to reduce the complexity of both computation and representation, which is compared to the traditional integral form. Besides, with the aid of H function properties and features, the H transform representation of the effective capacity has the potential to simplify the application procedure in individual scenarios as well as further derivations based on it. This will be detailed in Chapter 4.

1.1.3 Smart Grid Application Performance Improvement Considering both Power System and Communication System Aspects

Power system and communication system are deeply coupled within Smart Grid system. They both depend on the other, where communication system provides the information link between grid components and power system is the energy source for the communication system. A failure of either system can result in the catastrophic cascade of failure in the whole system [11]. Hence the performance of Smart Grid application should be evaluated and considered from both systems' angle. In existing studies, only a few articles have considered the influences from both power system and communication system. Available mature models for the inter discipline research is mainly on the Demand Side Management application, which has spawned several algorithms where the electricity prices, profits and communication resources are optimized at the same time [12]. There are also studies focusing on other Smart Grid applications that are closely related to the similar services in traditional communication networks, such as video services [13]. These great studies enlightened the cross area research between power system and communication system and stressed the importance of involving Smart Grid application features into algorithm optimization. But these two models are confined to their own models or specific applications, where there is still a lack of much general model or analysis basis for other Smart Grid applications.

In this thesis, the Smart Grid application performance improvement problem is to be addressed by simultaneously considering both power system and communication influences. Due to the uncertainty of wireless communication channel fading effect, a statistical guarantee method is considered instead of deterministic method. This also provides a modelling method for the analysis of communication system influence on the power system performances, which will be detailed in Chapter 5.

1.1.4 A Software Defined Smart Grid Testbed

Since Shannon proposed the analytical framework for information theory in [14], QoS performance related studies have become hot topics in communication area. Various QoS metrics have been well studied in existing literature, such as data rate, latency, reliability, security and redundancy. One important feature of Smart Grid is to integrate advanced communication technologies into the power grid, thus the power system poses many QoS requirements for the potential communication networks. Smart Grid is a system integrating both power system and communication system. Therefore the QoS performance experienced by individual Smart Grid applications is affected by both systems. This means that neither power system or communication system alone may not be sufficient to characterize the QoS performances within Smart Grid. Thus besides theoretical studies, it has attracted a lot of researchers to build a Smart Grid experiment environment for test and evaluation of new methods. Some testbeds are based on pure simulator environment, which provides good flexibility but constrained practicality, while others are based on hardware devices, which provides real world data but with high cost. There are also hybrid testbeds providing a trade-off between software and hardware testbeds, where software and hardware components are integrated and cooperated. In existing testbeds, the communication networks are mostly realized via Ethernet switches or simulators such as NS-3, where the wireless communication network is still under addressed.

In this thesis, a framework of Software Defined Smart Grid testbed is proposed, which exploits RTDS, MBED and USRP to create a highly flexible and scalable real time Smart Grid evaluation environment. The RTDS is exploited to simulate various power system scenarios, while the USRP is used to build a real wireless communication system. The MBED is programmed to interface between power system and communication systems. A prototype is implemented in the Smart Grid lab at Durham University, where various case studies under different Smart Grid scenarios can be evaluated. This will be detailed in Chapter 6.

1.2 Thesis Outline

The thesis is organised as follows.

In Chapter 2, a review of Smart Grid communication networks is performed, where Smart Grid application QoS requirements and provisioning methods are focused on. Smart Grid testbeds are also reviewed, where the state-of-the-art modelling and simulation methods are discussed and investigated.

Chapter 3 introduces the effective capacity theory and its integration based analysis framework. Besides, case studies are given on the application of effective capacity theory in i.n.i.d. Weibull fading scenario as well as the analysis of Smart Grid application QoS performances.

In Chapter 4, a unified framework is proposed for the effective rate analysis of wireless communication systems over MISO fading channels, which is to address the issues in its integral based peer, such as complex in further derivation.

Based on the effective theory, Chapter 5 proposes an inter discipline QoS provisioning method, which aims at improving the power grid observability performance via the optimisation of the communication system resources.

In Chapter 6, a Software Defined Smart Grid testbed framework is proposed, which provides a Smart Grid experimental environment. A prototype is implemented at Smart Grid Lab of Durham University, where several case studies are performed and analysed.

Finally, conclusions are drawn in Chapter 7, where the thesis is summarized and a number of problems are addressed for future investigations.

Chapter 2

Literature Review

The advent of Smart Grid has deeply reformed the operations of the traditional power grid in terms of generation, transmission, distribution and control [15]. By exploiting advanced communication and information technologies, the Smart Grid is expected to achieve full observability and pervasive control of the grid [16]. These features are to be fulfilled by both existing and emerging Smart Grid applications, which request specific communication performances based on their functionalities. In this chapter, the research background on Smart Grid communication network is reviewed. The development of Smart Grid technology is first introduced, which is followed by an investigation of Smart Grid application QoS requirements. Emphasis is placed on the QoS provisioning within Smart Grid, where a cross layer QoS analytical model, namely Effective Capacity theory, is detailed discussed.

2.1   A Brief Introduction to Smart Grid

Smart Grid is the concept proposed to address the increasing need for an effective, reliable, scalable and secure next generation power grid. The grid-wide automation is enabled via the advanced communication technologies, which makes the traditional passive and static power grid become smart and active. By integrating communication networks into the system, two-way information flow is supported within the Smart Grid. The grid network is expected to be achieved via an integration of a magnitude of smart electric devices, such as sensors, controllers and actuators [17].

Power grids have been the fundamental infrastructure for modern nations. To transform from the legend power grid to the Smart Gird, every nation and region has their own requirement and development roadmaps. Some leading examples are the NIST roadmap from the United States [3], Mandate CEN/CENELEC M/441 from the European Union [18], thirteenth five-year plan for Smart Grid from China [19], and fourth strategic energy plan from Japan [20].

In the meantime, since both communication and power research areas are integrated into the Smart Grid, individual organizations also have their own specific focus, which results in different standardization efforts. Representative examples are the International Electro-technical Commission (IEC) Smart Grid standardization roadmap [21], IEEE P2030 guide [22] and Microsoft Smart Energy Reference Architecture [23]. With the efforts of these organizations, there have been several standard information protocols available for the communications within Smart Grid [24], such as IEC 61850 [25] and IEC 61970 [26].

One major difference between Smart Grid and the traditional power grid is the high penetration of renewable energy. In traditional power grid, the energy source for the main generators mainly relies on fossil fuels, including petroleum, coal and natural gas [27]. While in Smart Grid, distributed generators can be spread throughout the power grid, which exploits various renewable energy sources, including wind, solar, tidal, hydro and geothermal [28]. On one hand, the integration of renewable energy sources benefits the Smart Grid in many aspects. The clean energies like wind and solar can help reduce the carbon emission, which has been long criticized in fossil based power generations [29]. Besides, the distributed generators are important supplemental sources for peak load demand [29]. On the other hand, the high penetration of renewable energy also brings new challenges. From power system aspect, the distributed renewable generators have great impacts on both stability and control of the whole grid [30]. While from communication system aspect, the monitor and management of these renewable energy sources poses strict quality of service performance requests, such as data rate, latency and reliability.

In this thesis, the focus is placed on the QoS performance within Smart Grid. Therefore reviews on QoS requirement are performed from both power system and

communication network aspect.

2.2   A Review on QoS Requirement from Power System Aspect

Smart Grid is an integrated system, where a fault within any participating system may result in a cascade of failures. The reliability of power system is particularly important, since many modern systems are built upon power systems and electrical blackouts will often result in a catastrophic cascade of failures in these systems [11]. Therefore there is an increasing need for power grid status monitor and control. In order to make sure the required information properly delivered, it is important to guarantee the QoS performances for the applications from the power system aspect. This will depend on the functions of the applications, and some of them quantified into QoS metrics in communication networks.

2.2.1   Smart Grid Application QoS Requirements

Depending on the specific functions, Smart Grid applications may have various requirements on different QoS metrics, such as data rate, latency, reliability, security and redundancy. A brief review on these QoS metrics is given as follows.

Data Rate

Data rate supported by the communication networks is the most concerned QoS metric, which is the key point on how fast the information can be delivered between Smart Grid components [31]. A simple estimation of the available data rate can be given by the Shannon capacity theory [14], which is defined by the SNR and the allocated bandwidth. These two factors are characterized by the physical communication channels. In wireless communication networks, it is more complicated, since they are involved in the consideration of interference, cost and availability. Individual Smart Grid application will have specific data rate requirement, which depends on the data generation pattern and the package size. For example, in wide

area situation awareness systems, the application provides video streaming services for critical components surveillance. This will require high data to maintain a stable performance. On the contrary, for most control command and sensor measurement in Smart Meter system, the required data rate will be relatively low [32].

Latency

The grid automation is achieved based on the measurements and timely control, which are transmitted via the communication networks. When a package is transmitted through the communication network, it will be delayed along the route [33]. Hence a latency will be experienced by the applications between the information source and sink. Among the contributors of the total latency, the communication delay is an important latency source which should be minimized [34]. The influence of latency on the application performance depends on specific functions. Some applications may tolerant with very large latencies, such as general metering and billing, while others may have very stringent latency requirement, such as protection information and most control commands.

Reliability

Reliability is of the highest priority for power systems. However, in modern systems, various systems are deeply coupled with each other, where a failure can result in a cascade disaster in the depending systems [11]. This is also a typical situation for the Smart Grid, where the power system relies on communication to transmit grid information for monitoring and control, while the communication system relies on power system for the electricity as the power source. Hence the reliability of Smart Grid communication networks is also the critical supporting pillar for the stability of power system [35]. The communication reliability is not only confined to the link outage. For time sensitive applications, a violation of the latency bound can also result in the unstable status of the system [36].

Security

The Electric Power Research Institute (EPRI) report has pointed out that security is one of the most challenging issues for the Smart Grid field deployment [37]. The system should be able to combat against physical attack, as well as protect the privacy of cyber data. The cyber security in Smart Grid is an essential requirement, since the data collected from the smart devices may contain customer information, while grid control command can determine the stability of the whole network.

Redundancy

The network of Smart Grid has the requirement on redundancy, where the system resources are reserved for flexibility and future usage. The Smart Grid can be expanding with time, which needs to accommodate more smart devices, support emerging applications and expand the grid coverage [33]. For the communication networks, it may need to dynamically allocate the resources to support various applications with different features and QoS requirements. For some applications such as power grid observation and status estimation, certain degrees of redundancy will provide a guarantee for the stability of the system operation in case of regional communication failures [38].

2.2.2   Categories of Smart Grid Applications

Integrating advance communication techniques into power grid has enabled many new applications, such as smart meters, demand management and real-time voltage stability enhancement. As can be foreseen, many more kinds of smart grid application will emerge in the near future. Different from the cellular network and other data-oriented networks, the information transmitted via smart grid CPS communication network is essentially physical devices oriented. Due to the various needs, functions and algorithms, the data to be exchanged within the smart grid CPS are usually of different types, which will have different time performance requirements. For example, billing information is usually time insensitive, where a relatively long delay will not impair its performance. However, for typical real time applications,

the measured status at the physical sensors usually changes with time, while the control decision should be delivered to corresponding actuators as soon as possible, because these kinds of information are only valid for a very short period of time. In order to provide better services to different applications, the information of different applications can be categorised into three general classes, namely critical information, important information and informative information, which are summarised in Table 2.1 and detailed as follows.

Critical information (Class 3)

Critical information has the highest priority among all the information classes. Applications require strictly low latency or vital information that has to be transmitted immediately should be categorised into this class. The common features of this kind of information are: (a) rare in occurrence and (b) short in message length. But latency for this kind of information will result in serious consequences. Typical applications include grid control commands, outage detection and restoration and other vital messages for control, protection and management.

Important information (Class 2)

For most real-time applications, such as voltage stability enhancement, demand response and supervisory control and data acquisition (SCADA), they can be categorised as important information. Based on different mechanisms and algorithms, the messages in important information class can be event-driven or periodic generated. The messages can be measurements or control commands. Latency will usually result in a compromised performance.

Informative information (Class 1)

All latency insensitive applications can be categorised as informative information class, such as smart metering, billing information and other information gathering applications. Compared to the critical information and important information classes, messages in informative information class are relatively frequently generated. The messages in this class usually require high throughput, but a significant

delay might not compromise the performance.

Table 2.1: Categories of smart grid applications

information type	Occurrence probability	Delay tolerance	Throughput requirement	Importance
Informative	High	High	High	Low
Important	Medium	Medium	Medium	Medium
Critical	Low	Low	Low	High

2.3   A Review on QoS Provisioning from Communication Network Aspect

2.3.1   Communication Networks

In the research of communication networks, QoS provisioning aims at satisfying the requirements and/or improving the performances of the various supported services. For different services, applications or users, the communication networks should be able to support their specific performance requirements. Usually QoS metrics are used to quantify the performance requirements, such as Signal to Noise Ratio (SNR), throughput, latency, error rate, loss rate and so on [39, 40]. These metrics are determined by the features of considered communication networks, which can be generally categorised into three groups according to the signal propagation medium, namely wired communication networks, power line communication networks and wireless communication networks.

Wired Communication Networks

Wired communication networks are mature and stable in providing information exchanges. They have dedicated wire lines for data transmissions, such as twisted pairs, coaxial cable and optical fibre, which can support the data rate ranging from only a few kilobits per second to several gigabits per second. Besides, the wires provide a fixed and known communication channel, which results in almost constant performances, such as SNR and latency. These features are very favourable in providing critical and essential services when information data exchanges are involved.

Hence wired communication networks are widely applied in backbone networks, as well as fundamental information infrastructures for Smart Grid [27, 33].

From the aspect of Smart Grid, the role of wired communication networks is also very important. It has been identified in the previous discussion that huge data volume, as well as heterogeneous requirements on latency, priority and error rate can be foreseen along with the development of Smart Grid. These QoS requirements can be supported by a wide range of wireline networks, such as SONET/SDH [41], Ethernet [42], DSL [43] and the traditional coaxial cable access network. Since the communication channel is predictable in wired communication networks, the most interested QoS metrics are supported data rate and latency. The former mainly depends on the protocol and wire type, while the later is mostly influence by routing algorithms in network layer [44, 45].

The major disadvantages of the wired communication networks are their flexibility and cost. Despite the many aforementioned merits, the deployment of physical wires is usually complex, which has to be well planned and routed. A change of the grid topology, such as a new renewable generation site or new client buildings, will require new connection wires. Moreover, it may be hard or very expensive to provide wired connections for some physical environment, such as off-shore wind farms or distributed sites in rural areas. As a result, wired communication networks are less flexible, more expensive and lack of scalability than its wireless counterpart.

Power Line Communication Networks

The signal propagation medium of power line communication networks is also physical wires. But it is different from traditional wired communication networks, where the wires are dedicated for communication purpose only. In power line communication, the power line is initially designed for power transmission instead of information transmission [46]. Hence its communication channel characteristics are very harsh and more similar to the wireless communication channels [47]. The data rate supported by power line communication ranges from a few hundred bits per second to millions of bits per second, which depends on the protocols and physical wire conditions.

A great advantage of power line communication is that the power line is part of the fundamental infrastructures within Smart Grid. Hence information exchange within Smart Grid can exploit the existing power lines instead of the deployment of extra communication cables. This feature makes power line communication networks very appealing for the customer domain scenarios such as offices or houses. There have been studies exploiting power line communications to support Smart Grid applications. In [48], the available narrowband and broadband power line communication technologies were analysed for their suitability for enabling Smart Grid, while the regulations and challenges for field deployment were also studied. In [49], the application of power line communication in utility networks was studied, which is over IPv6 protocol and provides the potential to support a large number of Smart Grid applications. In [50], the application of power line communication in Smart Grid medium voltage networks was studied in both simulation and field test. In [51], a comprehensive investigation was performed on power line communication technology and its application for Smart Grid in all voltage levels, from within the home up to high voltage lines.

The major challenge to apply power line communication in smart grid is its channel modelling. Since the power line is not designed for data exchange, the communication through it is very harsh and noisy. The channel is frequency selective and time varying, while the background noise is coloured. Thus the theoretical analysis for power line communication system is hard. These features also result in challenges in QoS provisioning for the Smart Grid applications. Desired data rate and latency can be supported via proper power line communication protocols and standards, such as IEEE P.1901, ITU-T G.9960, ETSI, CENELEC EN 50065, HomePlug AV, Universal Power Line Association (UPA) and HD-PLC [52, 53].

Wireless Communication Networks

Wireless communication technologies exploit air as the signal propagation medium, which frees the devices from wire connections. This wireless feature makes the communication networks very flexible and relatively low cost. Therefore, wireless communication networks are most favourable to span the Smart Grid to its every

corner. Besides, mobile services such as Electrical Vehicles are also enabled.

Wireless communication networks can provide both long range and short range coverages. There are various sophisticated wireless communication technologies available for Smart Grid, such as Wifi networks [54], Zigbee networks [55], cellular networks [56] and cognitive radio networks [57]. These wireless communication technologies provide data rate ranging from 20kbps in Zigbee up to 10Gbps via 5G technologies.

5G and beyond network is currently one of the most hot research areas in wireless communication networks. The ongoing research has also making efforts to provide ultra reliable and ultra low latency communications [58]. Especially, Smart Grid has been identified to be one of the most important scenarios for the potential application of 5G networks [59]. There have been studies on ultra low latency communication methods for both push-based services and request-based services [60], which will be critical to enable various real-time applications. The work in this thesis will also contribute to the theoretical research of this area, since the effective rate theory charaterises the system upper bound performance which also applies to 5G and beyond networks.

But due to the broadcasting nature of wireless communications, the communication channels are prone to attenuation and environmental interference [27]. Hence wireless communication technologies are less reliable than its wired counterpart. Moreover, due to the time varying channel fading and various environmental interference such as shadowing effect, it makes QoS performance very hard to analyse in the wireless communication system.

2.3.2 Delay Sources

It can be indicated from Section 2.2 that, latency performance, also referred as delay performance, is one of the most concerned QoS metrics to the Smart Grid applications. But from the view of the whole communication system, several sources will contribute to the total delay experienced by the application packages. The major sources include queueing delay, channel access delay, transmission delay, propagation delay and processing delay.

Queueing Delay

Queueing delay is the QoS metric studied mainly in the network layer of wireless communication networks. When network service rate cannot meet with traffic source arrival rate, the data not served are buffered as a queue, which results in queueing delay [61]. The queueing behaviours can be analysed via queueing theory, where the communication network is often treated as a queueing model. Its statistical behaviours are characterized by its inter-arrival distribution process, service distribution process, system capacity and the number of parallel servers [61]. Generally speaking, the system capacity and the number of parallel servers depend on the available hardware resources, while the inter-arrival distribution process is described the traffic source statistical characteristics. For the service distribution process, it will be more complex since it not only depends on the routing algorithms used in the network layer, but also influenced by MAC protocol applied in MAC layer, configurations in physical layer and channel capacity fluctuations.

There has been an increasing research interest in queueing delay analysis specifically for Smart Grid, which focuses on modelling the applications, such as power management [62], load balancing [63] and profit optimization [64]. Besides, there are also studies considering specific communication technologies [45], such as machine-to-machine communication networks [65], power line communication networks [51] and IEEE 802.11s [66].

Channel Access Delay

In wireless communication networks, all devices share the same signal propagation medium, i.e. the open air [67]. In order to mitigate the interferences, the devices are regulated via designed channel access mechanisms. These mechanisms can be generally categorized into three types, namely contention based mechanism, contention free mechanism and a mix of them [68]. For contention free mechanism, the channel access has been scheduled, where delay can be generally treated as fixed. But it might not be efficient as contention based mechanisms and will have to face the challenges with a large number of devices, which is very likely to happen in Smart Grid scenarios. On the other hand, contention based channel access mechanism

has better channel usage efficiency, but the channel access delay will be random with cases. Besides, collisions will further complicate the delay analysis, while other factors such as relaying will also result in extra delays.

Due to the development of Smart Grid as well as the increasing demand for QoS guarantees, there have been several modified channel access mechanisms specifically designed for the QoS provisioning purpose, such as IEEE 802.11e, IEEE 802.11af and IEEE 802.11as in IEEE 802.11 series. Moreover, the delay performance of these QoS aware channel access mechanisms is also analysed considering Smart Grid applications, such as IEEE 802.15.4 [69], IEEE 802.11s [70], IEEE 802.11af [71] and IEEE 802.11ah [72].

Transmission Delay

In modern communication networks, information is usually packetized. Transmission delay is defined by the amount of time required to transmit all bits within the packet [73]. Let $d_{\text{transmission}}$ denote the transmission delay, then it can be given by

$$d_{\text{transmission}} = \frac{P_{\text{size}}}{r_{\text{transmission}}}, \tag{2.1}$$

where P_{size} is the number of bits in the packet and $r_{\text{transmission}}$ is the data rate of the link. The transmission delay is also known as store-and-forward delay or packetization delay. When specific MAC and PHY layer protocol is considered, its associated transmission delay is upper bounded, since the maximum packet size is predefined. Usually, the transmission delay is relatively small compared to other delay sources and can be negligible in most cases.

Propagation Delay

The signals propagate as electromagnetic waves in the communication channels [67]. Propagation delay is the amount of time for the signal to travel from the transmitter to the receiver, which is given as follows,

$$d_{\text{propagation}} = \frac{L_{\text{distance}}}{r_{\text{propagation}}}, \tag{2.2}$$

where L_{distance} is the distance between transmitter and receiver, while $r_{\text{propagation}}$ is the signal propagation speed. In wireless communication networks, the speed $r_{\text{propagation}}$ is usually taken as the speed of light ($c = 3 \times 10^8 m/s$). Note that in short range communication scenarios, e.g. IEEE 802.11, the transmission range is normally less than a hundred meters. With this distance, the propagation delay is at the level of $10^{-7}s$, which is negligible comparing to other delays. But in the long distance wireless communication scenarios, satellite communication for instance, the propagation delay can be at the level of hundreds of milliseconds. In such cases, the propagation delay may become the major delay source and cannot be overlooked.

Processing Delay

Processing delay is the time that a packet header been processed by different layers, such as a router checking bit-level errors in packets on reception, or confirming address bits during relay [74]. The processing delays in high speed devices are typically on the order of microseconds or less. But some systems may include complex encryption algorithms, examining or modifying packet contents [73]. In such cases, the processing delay cannot be negligible. The processing delay is related to the processing mechanism and the hardware ability. The processing delay can be reduced with advanced hardware design such as high performance microprocessors, but this is beyond the scope of this thesis.

2.3.3 Empirical Study

As discussed in Section 2.3.2, the total delay experienced by the application has many contributing sources. Single layer analysis can only describe a specific part of the total delay. While the performances between different layers are correlated, more accurate delay study will involve cross layer analysis. A practical way to estimate the total delay experienced by the applications is via empirical measurement. By setting up similar communication systems and application environment, we can estimate the expected achievable delay performances under specific scenarios.

In [75], a field test in Italy was performed to evaluate the communication performances such as throughput and latency of various communication technologies,

including broadband power line, Wifi and fibre optics. In [76], simulations were carried out on WECC 225 bus power system and Poland 2383 bus power system, where fibre optic based Ethernet is considered. Typical Smart Grid applications are assumed, including PMU, state estimation, SCADA, small signal stability, transient stability, voltage stability and post mortem analysis. In [77], the LTE wireless cellular network was used for the Smart Grid automation, and a round trip time was estimated to be below 100 ms. In [78], the IEEE 802.11ac was tested with IEC 61850 electrical automation devices, where an average of 5.4ms and a maximum 10ms was obtained. In [79], the grid control for critical applications via wireless communication networks was investigated, where the throughput and latency performances were compared between IEEE 802.11, IEEE 802.15 and cellular networks. In [80], the throughput, packet loss and latency were analysed in a virtual power plant scenario, where DSL network was considered. In [81], the latency was modelled and measured in wide area power control system, while its impact on the control performance was analysed. In [82], the IEEE 802.15.4 PHY layer and three different MAC protocols including TDMA, CSMA/CA and Master-Slave protocol were tested in a Wireless Networked Control Systems via simulation.

From the above discussions, it can be seen that empirical studies have shown great potential for the application of wireless communication technologies in Smart Grid scenario, especially for the application of IEEE 802.11ac with an average of 5.4ms and a maximum 10ms. But it should be noted that these are application specific and hardware dependent solutions. In Chapter 6, a Software Defined Smart Grid Testbed is to be proposed and implemented, which can achieve an equivalent performance of an average of 9.6ms and maximum of 12ms. The testbed is using OFDM for the PHY layer, while the MAC protocol can be customized to accommodate more sophistical technologies such as the cognitive radio considered in Chapter 6. Note that the testbed is on the software defined radio platform without any optimisation efforts, which means there is still potential room for performance improvement.

2.3.4   Cross Layer Analysis

Layered models such as Open Systems Interconnection (OSI) model and IEEE 802 model isolate the functions between layers. This modular design makes each layer to be standard, which brings many benefits. For example, a network layer using IEEE 802.2 standard is able to work with different MAC and PHY standards, such as Ethernet and IEEE 802.11. This feature enables the researchers and developers to focus on single layers to during analysis or design, where the performances are guaranteed by the standards described by other layers. However, this also makes it hard to perform the QoS analysis. From the discussion in Section 2.3.2, it can be seen that the total delay experienced by the applications is complex. Each layer will contribute to the total delay. Hence the performance analysis within a single layer will be hard to exactly describe the whole case. Besides, due to the layered design, QoS metrics are usually confined to the functions within individual layers. For example, conventional wireless communication channel models are based on the PHY layer, which characterizes the radio signal statistics such as path loss, shadowing and multipath [67]. These metrics are used to estimate the PHY layer performances, such as the symbol error rate (SER), bit error rate (BER), signal to noise ratio (SNR) and data rate. However, delay as one of the most concerned QoS Metric is only used in the network layer, while it is not possible to be analysed within PHY layer.

Existing and emerging Smart Grid applications provide a wide range of services, from metering and billing to grid control. It is a very difficult task to design a universal QoS provisioning mechanism for all Smart Grid communication networks, because the provided application may have totally different QoS performance requirements. The QoS metrics are characterized in different layers. For example, in wireless communication networks, the data rate mainly depends on the MAC and PHY layers, while the delay may come from almost every layer. Hence the cross layer analysis provides a more versatile method to allow more parameters from two or more layers to be optimized for desired performances.

Sensors are basic components to enable the grid monitoring, where wireless sensor networks are the top choices for such cases [83]. There are various cross layer anal-

ysis models available, which combines some or all layers of application, transport, network, MAC and PHY layer [84]. Specifically, there are several works considering Smart Grid applications and their features in the cross layer modelling. In [85], a distributed cross layer cognitive radio sensor network model was proposed for Smart Grid application analysis, which considered routing algorithms and channel access mechanisms. In [86], a delay responsive model based on network and MAC layer was proposed for Smart Grid applications with priorities.

The cross layer analysis is a hot research topic in the communication area. As one of the advantages of Smart Grid is to exploit all available advanced communication technologies, the fruitful results on cross layer QoS studies in various communication networks can be borrowed, such as cognitive radio networks [87], IEEE 802.16 (WiMax) networks [88], OFDM-TDMA and OFDMA Networks [89], multi-hop wireless networks [90] and mobile wireless networks [91, 92]. Among these models, a link layer wireless communication network model named effective capacity has attracted the interests of many researchers, which will be detailed in the next part.

2.3.5   A Review on Effective Capacity

A practical link-layer model for statistical QoS analysis is proposed by Wu and Negi in [4], which is referred as effective capacity theory. It is a dual concept of the effective bandwidth, which is widely used in the wired communication system [5]. The effective capacity is defined as the maximum supported constant bit rate under statistical delay constraints, which is based on the link layer queueing behaviour and the physical fading channel scenarios. Empirical study has shown the validity of this model in IEEE 802.11 wireless networks [93]. The theory of effective capacity describes the statistical relations between four QoS metrics, i.e. data rate, delay, channel fading parameters and the probability of delay violation. It can be seen that these four factors are all highly concerned in Smart Grid application QoS performances. On one hand, data rate and delay are the two major communication performance indexes for various applications. On the other hand, all these four parameters are characterized by the communication system as well as the physical environment under the considered Smart Grid scenarios. Hence it provides a good

potential to integrate the studies in both power system and communication system, which are the two major fundamental supporting pillars for Smart Grid.

In wireless communication networks, the fading effect is a major source of the communication system performance fluctuation. The classical Shannon capacity theory is widely used to analyse the maximum support data rate under certain spectrum bandwidth allocation and SNR affected by the fading channels. The effective capacity theory is developed based on Shannon capacity theory, which extends the model to embrace the network layer queueing effects into considerations. Hence the effective capacity theory can be used to analyse the delay performance under various fading channel conditions, which can be applied to the analysis of specific scenarios. Several fading channel scenarios have been investigated, including Rayleigh [4], Rician [94], Weibull [95], Nakagami-m, generalized K [10], $\eta - \mu$ [6], $\kappa - \mu$ [96] and $\alpha - \mu$ fading channels [97]. There are also studies extended to include other fading effects, such as shadowing effects [7]. Besides, with the development of multi-antenna techniques in recent years, the communication system throughput has been significantly improved. The effective capacity theory is also analysed under multi-antenna system scenarios, such as Multiple Input Single Output (MISO) [10] and Multiple Input Multiple Output (MIMO) [98] systems. When multiple antennas are considered, the correlation between antennas is one of the most important influencing factors. In order to address the correlation effects, there are also studies focusing on the effective capacity analysis over correlation channels, such as correlated Rayleigh [99,100] and correlated Nakagami-m [101, 102] and correlated $\Gamma - \Gamma$ fading channels [103]. From the above discussion, it can be seen that the effective rate has been extensively studied under various fading scenarios as well as different systems with multiple antennas. But it can be also indicated by these studies that, the effective capacity analysis under specific scenarios is a challenging problem, which usually involves multiple integrations of multiple variates and sophisticated mathematical manipulations. This renders the results obtained from certain scenarios hard to extend to other cases. Thus it has stimulated the effective capacity studies to base on more and more general channel fading assumptions, as can be seen from the references listed above. To avoid this integration of Probability Density Function (PDF) of

the fading channel parameter distributions, a unified framework using H transform and Moment Generation Function (MGF) has been proposed by the author [36]. The proposed framework is able to describe a wide range of fading scenarios, including both independent and correlated cases. Details about this framework will be discussed in Chapter 4.

Based on the effective capacity under various fading channels, there have been several QoS provisioning mechanisms proposed to improve the wireless communication system performances. Much efforts have been made on the resource allocation scheme for wireless networks [104], and several scheduler algorithms are designed based on the effective capacity theory, such as joint K&H/RR scheduler [105], reference channel scheduler [106], and optimal power control, dynamic channel allocation scheduler [107] and optimal scheduling algorithm for time division downlinks under the confine of limited capacity and power [108]. Energy-efficient statistical QoS provisioning mechanisms for cellular networks and video applications are studied in [9]. Joint spectrum and power efficiency optimisation for statistical QoS provisioning is studied in both Single-Input and Single-Output (SISO) and Multi-input Multi-output (MIMO) situations [109,110]. Adaptive power and rate cases are considered in [111], and extended to the multichannel scenarios [111]. QoS provisioning in mobile wireless networks is also discussed in [91,112]. In [8], QoS provisioning in cognitive radio networks is extensively researched, which uses effective capacity to predict the maximum throughput under the limitation of buffer violation probabilities. The effective capacity has also been applied to various QoS aware protocols in cellular networks [113] and wireless mobile networks [91,92].

Due to the advantage of effective capacity theory in QoS performance analysis, the author proposed to exploit it in the performance analysis within Smart Grid communication network in [114]. Furthermore, using effective capacity as a joint point between power system and communication system performance analysis, a resource allocation method is proposed for the Smart Grid communication networks. The research is aiming at improving the power system observability performance via the optimal communication resource allocation. This will be detailed in Chapter 5.

2.4   A Review on Smart Grid Testbed

As can be seen in the previous reviews, QoS performance in Smart Grid is a complex research subject. The QoS performance experienced by Smart Grid applications are synthetic results from the deeply coupled communication networks and power systems. Therefore beside analysis from theoretical aspects, a lot of Smart Grid testbeds have been proposed, which can provide a practical Smart Grid environment for QoS performance studies.

The various smart devices within Smart Grid not only carry the power flow within the power system, but also support the bi-directional information flow for monitoring and control purposes. To enable Smart Grid with these features, advanced communication and power system technologies are merging into the system designs. This trend has stimulated the increasing interest in the development of Smart Grid testbeds, which plays an important role before any new concept been actually implemented. The testbeds are able to provide a safe and controllable environment to verify and evaluate the performances for different application layers, such as basic metering, grid monitoring, system operation, fault protection, grid automation and utility markets [115, 116].

Due to this close interaction between physical components, digital elements, people, markets and environment, it is also proposed to use the cyber-physical system to describe the Smart Grid [117]. Accordingly, various Smart Grid testbeds have been proposed to emphasize different aspects of cyber-physical systems [118], which can be simulation based, hardware based or the hybrid of simulation and hardware.

2.4.1   Simulator Based Smart Grid Testbed

Until now, Moore's law [119] is still working. It has predicted and witnessed the boost of computing capacity available for human beings. The exponentially expanding computing capability has also spawned the method of using simulation to analyse or even solve the complex physical problems. This is also true to the power grid, where the optimal power flow, hardware placement and control mechanism can be solved via simulation tools such as Matpower [120]. Matpower is a toolbox based on

Matlab [121] for general purpose power system analysis. There are also stand alone simulation tools, which are specially designed for power system simulation purpose.

Virtual Control System Environment (VCSE) is an OPNET-based platform developed at Sandia National Laboratories, which is focusing on grid's cyber security, especially Supervisory Control And Data Acquisition (SCADA) vulnerabilities associated with energy systems [122].

Virtual Power System Testbed (VPST) is another simulation oriented platform which is focusing on the cyber security aspect of Smart Grid [123]. It exploits PowerWorld [124] to simulate the large scale electrical network and RINSE [125] to simulate the networks.

A testbed for analysing the security of SCADA control systems (TASSCS) was proposed in [126], where the electrical network was simulated via PowerWorld while the networks were simulated via OPNET [127]. This testbed is also focusing on security aspect where attacks on SCADA system was considered.

An intrusion and defence testbed was proposed in [128], which consisted of power system simulation, substation automation, and the SCADA system. In this testbed, the anomaly was specially considered. In the considered distributed scenario, a mitigation strategy was proposed to distribute important information from the vulnerable data agent to other agents.

In [129], a testbed framework SCADASim was proposed based on OMNET++ [130]. The simulation tool provides methods to model and test TCP/IP based SCADA system components, including smart meter and real time schedulers. Four main types attacks could be evaluated, including denial of service, man-in-the-middle, eavesdropping and spoofing. The provided interfaces were able to further integrate external devices.

The testbed developed by Mississippi State University SCADA Security lab and Power and Energy Research Lab [131]. The system was an integration of several power simulator components, including RTDS for power system simulation, MU4000 Analyzer for cyber security vulnerability analysis, PMU for power data acquisition and NI PXI for system control. The system was also used for pedagogy purpose, which was part of some smart grid oriented courses.

A testbed dedicated to the study of Plug-in Hybrid Electric Vehicles (PHEVs) and Plug-in Electric Vehicles (PEVs) was proposed in [132]. Zigbee was considered as the communication protocol between vehicles, while PHEV and PEV charging scenario was considered. The GUI interface was able to provide real time visualization of the charging status.

The testbed described in [133] was specified for the test and evaluation of transmission utilities, regarding real time performances, protection relays, PTPv2 time clocks and artificial network impairments. The transmission network was simulated using RTDS while the IEC 61850 series protocols were investigated.

Mosaid was software simulation testbed framework [134]. It provided standard APIs for the simulations of different levels within distributed renewable energy networks, including control level, scenario level, semantic level and syntactic level [135]. Various test cases were evaluated using this testbed, including electric vehicle charging, 11-bus power system emulation [136] and multivariate power flow analyses [137]. The Mosaid was also used to cooperate with other testbeds or simulation tools to provide co-simulation analysis, such as IPSYS [138], RT-LAB [139] and open source tools including PyPower and PowerFactory [140].

Vottron was an open source testbed platform, which was able to test and evaluate distributed control strategies, integration of DERs and improving EV charging [141]. The platform had been upgraded and derived into many versions to support state-of-the-art distributed control and sensing strategies, including agent-based and transaction-based controls [142].

GridLAB-D was a power system modelling and simulation environment developed by the US Department of Energy [143]. It was an open source software and could be integrated into other simulators for power system analysis and modelling [144]. The GridLAB-D was more mathematical oriented, which was designed for the analysis of power flow, end-use appliance technologies, equipment and controls. Applications such as conservation voltage reduction had been used to demonstrate the use of GridLAB-D testbed [145].

VSCADA was an advanced testbed framework based on the service-oriented architectures for integrated MG modelling, monitoring, and control [146]. The

web services were used to define the interfaces within Microgrid, including geo-referential information interface web service (GISinterfaceWS), real time data acquisition web service (DataAcquisitionWS), generation and storage unit capability assessment (eAssessmentWS), computational web service (ComputationalWS) and data storage web service (DataStorageWS). The testbed was evaluated via interfacing with MATLAB, where the dynamic performance of a MG was analysed under both grid-connected and islanded scenarios.

The Software-Defined Industrial Internet of Things testbed framework was proposed in [147]. The architecture was proposed in the context of Industry 4. 0 [148], where each layer was specified, including physical infrastructure, control and application layers. The information exchange services between different layers were defined and analysed, while data safety, system reliability and technology standardization were addressed.

2.4.2   Hardware Based Smart Grid Testbed

Hardware based Smart Grid testbed focuses on the experiments on real hardware devices, namely hardware-in-the-loop experiments. These testbeds provide the direct performance evaluation of the desired smart grid components. These testbeds provide a real smart grid environment for tests and evaluations. The scale of the testbed ranges from a comprehensive laboratory to a full scale microgrid. Some representative hardware based Smart Grid testbeds are reviewed as follows.

National SCADA Test Bed Program (NSTB) was jointly created in 2003, and it currently involves several national laboratories including Los Alamos National Laboratory, Idaho National Laboratory, Sandia National Laboratories, Lawrence Berkeley National Laboratory, Argonne National Laboratory, Pacific Northwest National Laboratory and Oak Ridge National Laboratory [149]. The NSTB provides 17 testing and research facilities and 61 miles of 138 kV transmission lines and 7 substations [150]. The cooperation between these laboratories and their project partners is aiming at addressing the cyber security challenges within energy delivery systems.

The Consortium for Electric Reliability Technology Solutions (CERTS) micro-

grid testbed was a full-scale testbed built near Columbus, Ohio, which was operated by American Electric Power [151]. The system consisted of four remotely controlled load banks and an induction motor, while twelve 7650 ION meters were deployed throughout the system. Several inverters and generators were tested using this testbed, while various fault and isolation scenarios were evaluated against the designed algorithms.

A hardware-based laboratory smart grid testbed was developed at Energy Systems Research Laboratory, Florida International University [152]. The system consisted of programmable loads up to 35 kW, 36kW renewable energy resources and energy storages. The applications of wide area monitoring (WAM), wide area protection (WAP) and wide area control (WAC) were studied, where corresponding control systems were developed and evaluated [153].

The testbed proposed in [154] was designed for Electric Vehicle control in the Virtual Power Plant scenario. The testbed was implemented as part of Danish EDISON project. The testbed was tested with real regulating power data from Danish Transmission System Operator and shown potential real time response to the power regulating request.

The testbed for microgrid scenario was implemented in Zhejiang University [155]. The integration of multiple microgrids was investigated, where different renewable resources and energy storage systems were considered, including PV Panel, Wind Turbine, BESS and flywheel energy storage [156]. A variation of microgrid configuration was used for different microgrids, where the faults and islanded scenarios were studied.

DeterLab is an open experimental testbed located at University of Southern California Information Sciences Institute (USC/ISI) and University of California, Berkeley [157]. The testbed formed a network consisting of 400 general-purpose computing nodes, where the web based interfaces were developed for cyber security study purpose. The testbed has also been used for teaching purpose involving more than 12 universities and 15 courses.

The testbed hosted at Distributed Energy Control and Communication (DECC) Lab was connected to the ORNL Campus distribution system [158]. The testbed

consisted of various DER devices, including one 50 kW PV system, one 100 kW and one 30 kW microturbine, 24 kW energy storage system and many other smart devices. The system was able to perform on-site device evaluation, including power system components, relays, EV, smart meter, micro grid and communication strategies.

The testbed built on Jeju Island in South Korea was introduced in [159]. The testbed covered the whole islands, and the aim was to make the island carbon neutral and fully sustainable by renewable energy. Due to the scale of this testbed, it was able to support five major research areas, including the smart power grid, smart place, smart transportation, smart renewable and smart electricity service studies.

A microgrid testbed was build at the campus of Illinois Institute of Technology (IIT) in Chicago [160]. The testbed was designed to test and evaluate the microgrid's economic and reliable operation aspects. The on-campus testbed integrated common microgrid components, such as PVs, battery storage, wind turbine, natural gas turbine, Smart meters and PMUs. The microgrid control strategy was developed and evaluated considering the economic aspects, which showed its potential in cutting the energy prices.

Smart energy integration lab (SEIL) was a power hardware-in-the-loop microgrid testbed [161]. The SEIL testbed integrated various hardware components, including remote controller, load banks, battery storage system and real time control and acquisition system. The testbed was designed to investigate DER integration as well as the associated system dynamic performance evaluation and dispatch aspects. It also provided a convenient evaluation environment for DC and AC microgrid configurations [162].

Cyber Physical Smart Grid (CPSG) testbed modelled distribution system, where smart metering and DGs were considered [163]. Various hardware components were integrated into the testbed, including 7 buses, SEL relays, GPS, phase angle control circuit, and capacitor banks. The OpenPDC was used for data visualization purpose, where the distribution network control was also integrated.

The Energy Systems Integration Facility (ESIF) at National Renewable Energy Laboratory (NREL) was able to perform experiment and demonstration of advanced

energy technologies [164]. The facilities were able to support the research at MW scale, where DGs, energy storage systems and their grid integration technologies were considered.

A RFID Sensor Network (RFID-SN) testbed was introduced in [165]. The testbed was based on RFID technologies, where the prototypes were designed and implemented. The evaluation was performed in the Faviganan Smart Grid substation, where the unauthorized access and attack to the substation were performed and analysed.

2.4.3 Hybrid Smart Grid Testbed

Hybrid Smart Grid testbed is a trade-off between simulator based testbed and hardware based testbed. It provides a more practical experimental scenario than simulator based testbed, but the cost is more affordable than hardware based testbed. Here 'hybrid' refers to the testbed prototyping method where part of the system is implemented using hardware devices, while the others are emulated by simulators. Since reproducing different power systems is more expensive than the other subsystems, the hybrid testbed usually exploits dedicated simulators for part or whole power system, while the other subsystems are implemented by hardware devices and interfaced with the power system simulator. One such power system simulator is RTDS, which has spawned a wide range of hybrid testbeds.

In North Carolina State University, an Exo-GENI testbed was implemented [166]. The testbed was built upon RTDS, which simulated the power system operations. The PMUs, GPS, and hardware were connected to the RTDS via interfaces. The distributed time-critical synchrophasor applications including wide area monitoring and control were evaluated using the proposed testbed [167].

In [168], the testbed proposed by North Carolina at Charlotte was introduced. The testbed was built upon RTDS. The IEC 61850 was applied as the communication protocol between power grid components. DC motor and synchronized generator were modelled and evaluated against real hardware devices. The constructed models were used in the testbed, where Phasor Measurement Units were evaluated against dynamic loads in real time.

The PowerCyber testbed at Iowa State University was introduced in [169]. The testbed exploited DIgSILENT PowerFactory and RTDS to simulate the operation of power systems. The testbed cooperated with the Internet-Scale Event and Attack Generation Environment (ISEAGE) testbed for the cyber attack and defence simulations. The testbed was able to perform the evaluation of attacks including malicious breaker trip attack, SCADA Observability DoS attack and Remedial Action Scheme DoS attack, while their cyber-physical impacts were able to be analysed. A resilient model based AGC algorithm was evaluated under data integrity attack using this testbed [170]. The interfacing methods with the proposed testbed were discussed in [171].

The testbed developed by Florida State University was introduced in [172]. This testbed exploits the RTDS to simulate the power system operation in real time. It used a FPGA board and Ethernet switches to interface with some powerful computing platforms, including Mamba board and TS-7800 board. On these computing boards, various distributed control algorithms were able to be evaluated in the controller hardware-in-the-loop method.

The testbed developed at Texas A& M University was based on RTDS and OP-NET [173]. The testbed exploited the real time power system simulation feature of RTDS and the system-in-the-loop feature of OPNET. The LabVIEW Real-Time Module was used to cooperate between RTDS and the OPNET system. Also due to the versatile interfaces provided by RTDS, it showed potential in different configurations of the evaluation cases, where man-in-the-middle attach and its impact on the system was studied. The Wide Area Control was implemented and evaluated using the extended testbed, which was introduced in [174].

The Cyber-Physical Testbed was introduced in [175]. The testbed integrated RTDS and NS-3 to evaluate PMUs and associated infrastructure in a real time manner. It also studied the modelling of the power system communication network in the scenario of different protocols. The testbed had been used to demonstrate Aurora attack impacts, wide area and local voltage stability monitoring applications.

A cybersecurity testbed was proposed for the evaluation of IEC 61850 based systems [176]. The testbed was implemented by layered design, including simulation

level, process level, bay level and substation level. The RTDS was used to model and simulate the power system scenarios. The proposed fuzz testing approach was evaluated using the testbed, which was used to analyse the vulnerabilities of the system components [176]. The testbed was also demonstrated as Intrusion Detection System, where several detection methods were evaluated, including Access-Control Detection (ACD), Protocol Whitelisting Detection, Model-Based Detection (MBD), Multi-Parameter Based Detection (MPD) [177], Protocol-Based Detection (PBD), Anomaly Behaviour Detection (ABD) and GOOSE Detection [178].

A WAMS Cyber-Physical testbed was proposed in [179]. In the architecture of the testbed, the RTDS, PMUs, relays, PDC and software components were connected via network switches. The hardware components were configured and monitored by General Electric (GE) and Schweitzer Engineering Laboratories (SEL) software, while communication network was monitored and analysed using Wireshark and Snort. The testbed was designed for cybersecurity study and power system related data mining. Several cyber attack methods and their impacts on the smart grid system were evaluated and analysed using this testbed, including Aurora Attack, Voltage Collapse Due to a Cyber Attack and Network Based Cyber Attack.

A Remedial Action Scheme (RAS) testbed was proposed in [180]. The testbed exploited the RTDS to emulate the power system and NS-3 to simulate the communication networks. The interface between RTDS and NS-3 was achieved via SEL-PMU and PDC. The decentralized S state estimation and remedial control action for minimum wind curtailment were evaluated using this testbed, where DC power flow and linear programming was used. The scenario of RAS with AC formulation and resiliency to limited cyber failures was considered in [181].

Besides RTDS, there are also other options for the hybrid testbeds, which are reviewed as follows.

ScorePlus was a scalable cyber-physical testbed [182]. It provided the smart grid experiment environment via software emulator and hardware testbed. The software emulator was fulfilled via Smart-Grid Common Open Research Emulator (SCORE) [183] developed based on the open source communication network emulator CORE [184]. The evaluated hardware devices included PV systems, wind tur-

bine, demand simulator and storage simulator. The software and hardware components were interfaced via different controller boards, including Beagle board, TelosW board and Energy board. The test cases include distributed network control and demand response application.

The Network Intrusion Detection System (NIDS) was testbed designed for real time cyber physical security studies [185]. The power system was simulated using Matlab/Simulink, and the control system was emulated by PLCs. The testbed also implemented a network tap to coordinate the communication between its components, where the TCP/IP network was exploited as the communication protocol. The NIDS testbed was able to monitor and visualize the status of the system components, while the network intrusion was detected in real time.

University of South Florida (USF) Smart Grid Power System Lab (SPS) testbed was introduced in [186]. The testbed exploited the Opal-RT [187] to simulate the power network in real time. With SEL relay/PMU device, LabView boards and OSIsofts PI-system data centre, the testbed was able to emulate a SCADA system. The testbed was used to validate the operations of SCADA measurement, communication, control, optimization and dynamic modelling.

The Cyber Physical testbed at Iowa State University was introduced in [188]. The testbed exploited both RTDS and Opal-RT for power system operation simulation, while the communication network was simulated via NS-3. The interface between the power system and communication system was fulfilled via Schweitzer Relays with PMU capability (SEL-421). The open source software Modelica was used for user defined models in power systems, which were evaluated using Opal-RT configurations.

The testbed was implemented based on Schweitzer Engineering Laboratories (SEL) SCADA systems at Joint State University of New York Buffalo State/University at Buffalo Smart Grid Laboratory [189]. The testbed was used to demonstrate eXtensible Messaging and Presence Protocol (XMPP) in a SCADA scenario.

A Multi-Agent System (MAS) was developed as part of West Virginia Super Circuit (WVSC) Smart Grid Demonstration project [190]. The testbed was based on hardware MAS and specialized for the test and evaluation of smart grid control

applications. The power system was simulated via the Analogue Power Simulator (APS) while the MAS was implemented by designed agent modules.

G-ICS (GreEn-ER1 Industrial Control Systems Sandbox) testbed was introduced in [191]. The testbed exploited the commercially available Intelligent Electronic Devices (IEDs) to emulate the operation of various power system utilities, where dedicated microcontroller was implemented to control and monitor the IEDs. The testbed as designed to evaluate the performance of IEC in the power utility automation network scenarios, where false data injection attacks were tested and analysed.

2.4.4   Remarks on Different Testbeds

As listed and reviewed in previous parts, all simulator based, hardware based and hybrid testbeds have attracted a lot of research interests all around the world. Individual testbeds are designed to focus on specific aspect within Smart Grid. This is due to the fact that Smart Grid is an integration of several systems, which makes the research topics covering traditionally separated areas such as power system controls and communication networking. The deviations between these topics make it hard to model or analyse their performances when they are deeply coupled within one system. This is also one of the motivations for the development of different types testbeds, i.e. to gain a perspective understanding of the Smart Grid system with integrated and coupled subsystems.

Due to the different methods in the design of each testbed type, a general comparison between simulator based, hardware based and hybrid Smart Grid testbed can be given as follows.

- *Flexibility:*
  Simulator based Smart Grid testbeds are generally most flexible. Since components are modelled and modularized, the simulators are relatively easy in changing scenarios, testing new hardware models and expanding with new features.

  On the contrary, hardware based Smart Grid testbeds are the least flexible among the three types. It might be not hard for a small scale hardware

testbed to change the considered scenarios, such as lab hosted testbeds. But usually for large scale hardware testbeds, the infrastructure is not feasible to be changed.

Hybrid testbeds are in the middle. During the design, some parts are emulated using simulators, while other parts are implemented in hardware. Thus the flexibility of hybrid testbeds depends on the interfacing method between its software and hardware components.

- *Cost:*

  Simulator based Smart Grid testbeds are relatively least expensive solution in test and evaluation. The cost will be mainly on the software license, component models and program development. If considering the fact that the open source simulators are becoming popular and powerful, the cost for simulator based testbeds can be even less.

  Hardware based Smart Grid testbeds are generally very expensive. This is reasonable since it usually involves infrastructure construction and purchasing hardware devices. As can be indicated from the previous reviews, the large scale hardware testbeds are usually funded by government or cooperated by several partners.

  The cost for hybrid testbeds is generally more than simulator based testbed, but can be significantly less than hardware based testbeds if very large scale experiments are considered. This is because during the design procedure, the costly components, for example generators and energy storages are emulated using simulators.

- *Practicality:*

  Hardware based testbeds are favourited by researchers mainly due to its practicality. The experiments on real devices provide the real responses for analysis. The evaluation results will be most close to the cases when these devices are deployed in the real grid.

  In the contrast, the simulator based testbeds are mainly for theoretically research purpose, where the accuracy of the simulation results is not exactly

that of the real cases. This is rooted in the nature of simulator models, where trade-offs, compromises and approximations have to be made during modelling procedure.

The hybrid methods provide a practicality between the other two. In general cases, the focused parts are implemented in hardware, which provides the accuracy for real world scenarios. The rest of the systems is simulated using simulators, which is less accurate but a trade-off between cost and flexibility.

It should be noticed that actually there are no firmed boundaries among simulator based, hardware based or hybrid smart grid testbeds. As can be seen from the reviews, simulators can be interfaced with hardware, while the hardware based testbeds are possible to implement the software simulator for extensive studies. As for the hybrid testbeds, most of them are designed to be flexible in replacing its software and hardware components with counterparts. This makes each type of testbeds of their own special value, and leaves more choices for dedicated research purposes. For example, simulator based testbeds are great for theoretical oriented studies, where strategies and algorithms are focused. The hardware testbeds provide critical evaluations for real world deployment. In the meantime, the hybrid testbeds can be used for a deep perspective on the system integration.

2.5   Concluding Remarks

In this chapter, Smart Grid was reviewed from the aspect of standardization efforts, renewable penetration and Smart Grid testbeds development. After that, specific focuses were placed on the Smart Grid applications' requirement on the communication system. The QoS requirement was analysed from both power system aspect, including data rate, latency, reliability, security and redundancy. Based on the time performance requirements, the Smart Grid applications were generally categorised into three classes, namely informative information class, important information class and critical information class. Based on the discussion on Smart Grid application QoS requirements, the QoS metrics were analysed from the communication networks aspect. Since delay performance is one of the top interested QoS metrics,

an investigation on the delay sources was performed and discussed. The existing QoS provisioning methods and QoS analysis models were reviewed thereafter, which was discussed from the view of empirical study or theoretical analysis. In the last section, a detailed review on the potential cross layer analysis model named effective capacity theory was performed. This model showed potential in providing a quantified analysis basis for the QoS provisioning mechanisms, which would be detailed in the next chapter.

Chapter 3

Effective Capacity Theory

The investigation on the Smart Grid application QoS requirements indicates that, in order to guarantee and improve the application performances, the QoS provisioning mechanism needs to consider QoS metrics, system set-up and physical scenario influences simultaneously. This requires a cross layer analysis within communication systems. In this chapter, the effective capacity theory is considered, which provide a quantified statistical analysis framework between data rate, latency bound, the probability of latency bound violation and the physical channel fading effects. Besides, the i.n.i.d. Weibull fading channel is considered, which is used to illustrate how to apply the effective capacity analysis in specific fading channel scenarios. In order to illustrate the application of effective capacity theory in the QoS performance analysis in Smart Grid communication networks scenarios, a case study based on various Smart Grid deployment scenarios will be performed at the end of this chapter.

The main contributions of this chapter are listed as follows.

- The effective rate under i.n.i.d. Weibull fading channel scenarios is derived.

- The approximations of the effective rate under i.n.i.d. Weibull fading channel in both low-SNR and high-SNR scenarios are derived.

- The QoS performance analysis is studied using the effective rate theory in the Smart Grid scenario.

The rest of this chapter is organised as follows. To facilitate later derivations, the effective rate theory [4] is introduced in Section 3.1, while the traditional integration and PDF based analysis framework is introduced in Section 3.2. Then the new effective rate representation under i.n.i.d. Weibull fading channel scenario is studied in Section 3.3, while the application of effective rate in general QoS analysis in Smart Grid communication networks is performed in Section 3.4. Finally, concluding remarks are drawn in Section 3.5.

3.1 Effective Capacity Theory

Let $C(t)$ be the instantaneous channel capacity at time t, and assume the asymptotic log-moment generation function of $C(t)$ defined as [192]

$$\Lambda\left(-z\right) = \lim_{t \to \infty} \frac{1}{t} \ln \mathbb{E}[e^{-z \int_0^t C(\tau)d\tau}], \tag{3.1}$$

exists for all $z \geq 0$. Then the effective capacity function $E_C(z)$ is defined as [4]

$$E_C(z) = -\frac{\Lambda\left(-z\right)}{z} = -\lim_{t \to \infty} \frac{1}{zt} \ln \mathbb{E}[e^{-z \int_0^t C d\tau}]. \tag{3.2}$$

Denote $D(t)$ the end-to-end delay experienced by a source packet arriving at time t. For a data source of constant data rate μ, the probability of $D(t)$ exceeding a delay bound $D_{\max}$ satisfies [192]

$$\Pr\left\{D(t) > D_{\max}\right\} \approx e^{-\theta E_C(\theta)D_{\max}}, \tag{3.3}$$

where the QoS exponent θ is defined as the solution of $E_C(\theta) = \mu$. It can be seen that the probability $D(t) > D_{\max}$ can be estimated via the value of θ. It can be proved that the effective capacity function $E_C(z)$ is mono-decreasing with θ. For a real-time communication system, the delay violating the maximum allowed latency bound should be statistically limited to a probability p_0 [4], namely,

$$\Pr\left\{D(t) > D_{\max}\right\} < p_0. \tag{3.4}$$

By (3.4), a minimum required θ_0 can be defined and calculated. In order to guarantee the delay performance, the QoS exponent θ has to satisfy the constraint $\theta > \theta_0$. Moreover, when $\theta_0 \to 0$, the effective capacity approaches the well-known Shannon capacity [98]. Similar to the Shannon capacity, the effective rate is the upper bound for the theoretically achievable performance, i.e. for a desired QoS performance where the latency and its violation probability are known, the maximum available channel capacity can be quantified using the effective rate theory. There has been study showing that the effective rate model fits good to the empirical measurement regarding the channel service delay [93].

3.2 Integration Based Effective Capacity Analysis

According to Shannon capacity theory [14], it can be given as follows,

$$C = B \log_2(1 + \text{SNR}), \tag{3.5}$$

where B is the channel bandwidth and SNR is the instantaneous signal-to-noise ratio at time t.

Further, it is assumed that the process $\{E_C(\theta)\}$ is a stationary and ergodic process, and it is uncorrelated across time frames, then the effective capacity can be derived as follows [4],

$$E_C(\theta) = -\frac{1}{\theta T} \ln \mathbb{E}\{e^{-\theta T C}\} = -\frac{1}{\theta T} \ln \mathbb{E}\{e^{-\theta T B \log_2(1+\text{SNR})}\} \tag{3.6}$$

Additionally, we define the effective rate $R(\theta)$ as follows,

$$R(\theta) \equiv \frac{E_C(\theta)}{B} = -\frac{1}{\theta T B} \ln \mathbb{E}\{e^{-\theta T B \log_2(1+\text{SNR})}\} \tag{3.7}$$

This definition is useful and helps to simplify the derivation procedure of effective capacity under different fading channel condition, as will be detailed in later sections.

In this thesis, a Multiple Input Single Output (MISO) fading channel model is considered, where there are N transmit antennas and only one receive antenna. The channels are assumed to be flat block fading, then the channel input-output relation

can be given as follows,

$$y = \mathbf{h}\mathbf{x} + n_0, \tag{3.8}$$

where $\mathbf{h} \in \mathbb{C}^{1 \times N}$ denotes the MISO channel vector, $\mathbf{x}$ is the transmit signal vector, and n_0 represents the complex additive white Gaussian noise with zero mean and variance N_0. It is assumed that the transmission power is uniformly allocated across the transmit antennas, and the channels are assumed to be arbitrarily correlated and not necessarily identically distributed.

The average transmit SNR is defined as $\rho = \frac{P}{BN_0}$, where P is the average transmit power of the system and B denotes the bandwidth. The channel state information is assumed to be only available at the receiver and the instantaneous channel power gain of the jth channel is defined by $\gamma_j = |h_j|^2$, where h_j is the jth component of the fading vector $\mathbf{h}$. In this part, we consider the maximum ratio transmission scheme, hence the instantaneous channel power gain at the receiver end can be defined by $\gamma_{\text{end}} = \sum_{j=1}^{N} \gamma_j$.

Hence the effective rate can be given by [98]

$$R(\theta) = -\frac{1}{A} \log_2 \mathbb{E} \left\{ \left(1 + \frac{\rho}{N} \gamma_{\text{end}} \right)^{-A} \right\}, \tag{3.9}$$

where $A = \theta T B / \ln 2$. Normally, (3.9) will involve multiple integrations of multivariate functions, since the PDF of $\gamma_{\text{end}} = \sum_{j=1}^{N} \gamma_j$ is described by multivariate random variables in general cases. Hence the effective rate analysis based on (3.9) is referred to integration based effective capacity analysis throughout the thesis. Generally speaking, multiple integrations of multivariate functions are complex in derivation. This aspect will be illustrated in the next section, where the effective capacity analysis is performed under MISO Weibull fading channels.

3.3 Effective Capacity Analysis in Weibull Fading Channels

The performance analysis over fading channels plays an important role in the research of communication systems. IEEE Vehicular Technology Society Committee on Radio Propagation has recommended Nakagami-m and Weibull models for theoretical studies of fading channels [193]. Measurements show that distributions of the small scale fading in many scenarios follow Weibull distributions, such as in fixed-to-walk and mobile-to-mobile channels [194]. It has been also shown that Weibull fading channels can characterise both indoor and outdoor scenarios, such as communication with individuals walking in residential or office buildings, and to fixed stations sending messages to robots in motion in assembly lines and factory environments [195].

The ergodic capacity performance of multiple-input and multiple-output (MIMO) systems over low signal-to-noise ratio (SNR) Weibull fading channels was studied in [196]. In this section, the effective rate over i.n.i.d. Weibull fading channels is studied.

3.3.1 The Weibull Fading Model

Weibull fading can characterize the effect of clusters of multipath waves propagating in the non-homogeneous environment. Assume that $|h_j|$ are i.n.i.d. Weibull random variables (RVs) and denote $\gamma_j = |h_j|^2$. Then γ_j is also distributed as a Weibull random variable. For a single Weibull fading channel, the PDF of γ_j is given by [194]

$$f_{\gamma_j}(z) = \frac{\beta_j}{\omega_j} \left(\frac{z}{\omega_j} \right)^{\beta_j - 1} e^{-\left(\frac{z}{\omega_j} \right)^{\beta_j}},$$
(3.10)

where the shape parameter β_j characterizes the severity of fading, and the scale parameter ω_j characterizes the average power of the fading. As the severity of fading increases, the value of β_j decreases.

3.3.2 Exact Expressions

Let $\gamma_{\text{end}} = \sum_{j=1}^{N} \gamma_j$ denote the sum of N i.n.i.d. Weibull RVs, then the MGF of γ_{end} is given by [197]

$$M_{\gamma_{\text{end}}}(s) = \sum_{l=0}^{\infty} \frac{(\Omega s)^l a_l}{(1 + \Omega s)^{l+N}}, \tag{3.11}$$

where

$$a_l = \sum_{k_1+\cdots+k_N=l} \prod_{j=1}^{N} \sum_{k=0}^{k_j} \frac{(-1)^k}{\Omega^k k!} \binom{k_j}{k} \Gamma(1 + \frac{k}{\beta_j}) \omega_j^{\frac{k}{\beta_j}}, \tag{3.12}$$

$$\Omega = \frac{2}{N} \sum_{j=1}^{N} \Gamma(1 + \frac{1}{\beta_j}) \omega_j^{\frac{1}{\beta_j}}, \tag{3.13}$$

where $\binom{l}{k}$ is binomial coefficients operator defined by $\binom{l}{k} = \frac{\Gamma(l+1)}{\Gamma(k+1)\Gamma(l-k+1)}$ and the operator $\sum_{k_1+\cdots+k_N=l}$ denotes the summation over all possible non-negative integers $k_1, \ldots, k_N$ satisfying the condition of $k_1 + \cdots + k_N = l$. $\Gamma(t)$ is Gamma function defined by $\Gamma(t) = \int_0^{\infty} z^{t-1} e^{-z} dz$.

Theorem 1 *The exact analytical effective rate $R(\rho, \theta)$ over MISO i.n.i.d. Weibull fading channels can be written as*

$$R(\rho, \theta) = \log_2 \frac{\Omega \rho}{N} - \frac{1}{A} \log_2 \left\{ \sum_{l=0}^{\infty} \frac{a_l \Gamma(A+l)}{\Gamma(A)} \times U\left(A+l; A+1-N; \frac{N}{\Omega \rho}\right) \right\}, \tag{3.14}$$

where $U(\cdot)$ is Tricomi hypergeometric function [198, eq. (13.2.5)], a_l and Ω are given in (3.12) and (3.13), respectively.

Proof *Using the MGF defined by $M_{\gamma_{end}}(s) = \mathbb{E}\{e^{-sz}\}$, the effective rate can be given by [199]*

$$R(\rho, \theta) = -\frac{1}{A} \log_2 \frac{1}{\Gamma(A)} \int_0^{\infty} s^{A-1} e^{-s} M_{\gamma_{end}}\left(\frac{\rho s}{N}\right) ds. \tag{3.15}$$

In [197], the MGF $M_{\gamma_{end}}(s)$ is obtained via Laguerre moment and Cauchy residue theorem, which can be generally represented by

$$M_{\gamma_{end}}(s) = \sum_{l=0}^{\infty} m_l(s) \tag{3.16}$$

According to [197], series $\{m_l(s)\}$ is absolutely converge for every s, then there exists a constant K large enough so that $\sum_{l=0}^{\infty} |m_l(s)| \leq K$ for every s. We have

$$\int_0^\infty |s^{A-1} e^{-s} \sum_{l=0}^\infty m_l(s)| ds \leq K \int_0^\infty s^{A-1} e^{-s} ds = K\Gamma(A) < \infty \qquad (3.17)$$

where we have applied $\Gamma(t) = \int_0^\infty x^{t-1} e^{-x} dx$. Then according to Fubini's theorem, the sum and integration operator can be swapped.

Substituting (3.11) into (3.15) and swapping the order of integration and summation using Fubini's theorem, (3.14) can be obtained using the following identity [198, eq. (13.4.4)]

$$\int_0^\infty (1+az)^{-v} z^{q-1} e^{-pz} dz = \Gamma(q) U(q; q+1-v; p/a) / a^q \qquad (3.18)$$

and Kummer's transform $U(a; b; z) = z^{1-b} U(a-b+1; 2-b; z)$ [198, eq. (13.2.40)].

Let $b_l = \Gamma(A+l) U(A+l; A+l-N; N/(\Omega\rho)) / \Gamma(A)$, then we can represent the b_l in the integral form as follows.

$$b_l = \frac{1}{\Gamma(A)} \int_0^\infty e^{-\frac{Nt}{\Omega\rho}} t^{A-1} (1+t)^{-N} (\frac{t}{1+t})^l dt \qquad (3.19)$$

As all integrals are all positive, it is clear that $b_l > 0$. The partial differential of b_l with respect to l can be given as follows.

$$\frac{\partial b_l}{\partial l} = \frac{1}{\Gamma(A)} \int_0^\infty e^{-\frac{Nt}{\Omega\rho}} t^{A-1} (1+t)^{-N} (\frac{t}{1+t})^l \ln \frac{t}{1+t} dt \qquad (3.20)$$

Since the integral of $\frac{\partial b_l}{\partial l}$ is negative, it can be seen that the general term b_l is positive, monotonically decreasing with respect to l and upper bounded by b_0. Because the series $\{a_l\}$ converges as proved in [197], the convergence of (3.14) follows using the Abel's criterion. Note that Tricomi U function is a built-in function in numerical software such as Matlab and Maple, which means (3.14) can be conveniently evaluated. As highlighted in [197] [200], small l (e.g $l \leq 50$) shows a good approximation to the exact value.

Corollary 1 *For i.i.d. Rayleigh situations, if let $\beta_j=1$, $\omega_j=\omega$, the effective rate expression* (3.14) *can be simplified to*

$$R\left(\rho,\theta\right)=\log_2\frac{\omega\rho}{N}-\frac{1}{A}\log_2 U\left(A;A+1-N;\frac{N}{\omega\rho}\right). \tag{3.21}$$

Proof *Substituting $\beta_j=1$, $\omega_j=\omega$ to* (3.14) *and using binomial coefficient identities [198, eq. (26.3.3-4)]*, (3.21) *follows.*

Note that this result coincides with [100, eq. (11)], which implies the accuracy of (3.14) in Theorem 1.

3.3.3 Approximation Analysis

This part will derive closed-form approximations of the effective rate in both high-SNR and low-SNR regimes. These approximations reduce the computational complexity and provide a straightforward way to understand the parameters' impact on the system performance.

It is assumed that the joint PDF $f_{\gamma_{\text{end}}}(z)$ can be parameterized as a polynomial around the origin. Note that this assumption can be readily applied to any fading distributions with known MGF [201]. Specifically, $f_{\gamma_{\text{end}}}(z)$ and $M_{\gamma_{\text{end}}}(s)$ satisfy the asymptotic parametrization assumption as follows [201]

$$\begin{cases} f_{\gamma_{\text{end}}}(z) \stackrel{z\to 0}{=} \dfrac{mz^{n-1}}{\Gamma(n)} \\ M_{\gamma_{\text{end}}}(s) \stackrel{|s|\to+\infty}{=} m|s|^{-n} \end{cases} \tag{3.22}$$

where the parameters m and n can be obtained via the MGF of the sum of MISO i.n.i.d. Weibull RVs, which leads to the following theorem.

Theorem 2 *For MISO i.n.i.d. Weibull fading channels in high-SNR regimes, the effective rate can be approximated by*

$$R(\rho,\theta)\approx-\frac{1}{A}\log_2\frac{(N\bar{\omega})^{N\bar{\beta}}\prod_{j=1}^{N}\omega_j^{-\beta_j}}{\Gamma(N\bar{\beta}+1)}{}_2F_1(A,N\bar{\beta};N\bar{\beta}+1;-\rho\bar{\omega}). \tag{3.23}$$

where $\bar{\beta}=\frac{1}{N}\sum_{j=1}^{N}\beta_j$ and $\bar{\omega}=\frac{1}{N}\sum_{j=1}^{N}\omega_j$ are the average shape parameter and scale

parameter, and $_2F_1(\cdot)$ is the hypergeometric function [198, eq.(15.1.1)].

Proof *Using the definition of expectation, the integral in (3.9) can be truncated by $Q = \sum_{j=1}^{N} \omega_j$, which captures the major part of the PDF of the sum of Weibull random variables [197]. Then the truncation error for the integration can be given by $E(Q) = \int_{Q}^{\infty} (1 + \frac{\rho z}{N})^{-A} f_{\gamma_{end}}(z) dz$. It can be proved that $(1 + \frac{\rho z}{N})^{-A}$ is monotonically decreasing with respect to ρ, then $E(Q)$ is upper bounded by $(1 + \frac{\rho Q}{N})^{-A}$. Hence $\lim_{\rho \to 0} E(Q) = 0$. Then using the relation $M_{\gamma_{end}}(s) = \prod_{j=1}^{N} M_{\gamma_j}(s)$, [197, eq. (19)] and [202], when $|s| \to \infty$, the following expansion of $M_{\gamma_{end}}(s) = s^{-N\bar{\beta}} \prod_{j=1}^{N} \omega_j^{-\beta_j}$ can be obtained. Using the assumptions in (3.22) and [198, eq. (3.194.1)], (3.23) can be obtained.*

Note that the hypergeometric function $_2F_1(\cdot)$ is also a built-in function in numerical software such as Matlab and Maple. It is much easier to evaluate the closed-form (3.23) compared to (3.14). It can be seen that the effective rate in high-SNR regime is mainly related to the averaged shape parameter and scale parameter, which means the impact of fading on the communication system has been averaged.

In many communication networks, such as cellular networks, systems often operate in low-SNR situations [203]. Hence it is beneficial to derive an approximation of (3.14) in the low-SNR regime. As explained in [203] [204], low-SNR regimes are approached not only when a given data rate is transmitted through a very large bandwidth, but when a given bandwidth is used to transmit a very small data rate. Hence the capacity analysis should be better conducted using the transmitted normalized energy per information bit $\frac{E_b}{N_0}$ rather than the average SNR ρ. Following the same method in [196] and [98], the effective rate in the low-SNR regime can be approximated by

$$R\left(\frac{E_b}{N_0}, \theta\right) \approx S_0 \log_2\left(\frac{\frac{E_b}{N_0}}{\left(\frac{E_b}{N_0}\right)_{\min}}\right), \tag{3.24}$$

where S_0 denotes the capacity slope in bits/s/Hz/(3dB) and $\left(\frac{E_b}{N_0}\right)_{\min}$ is the minimum energy per information bit required to reliably convey any positive rate, which are

given by [203]

$$
\begin{cases}
\left(\dfrac{E_b}{N_0} \right)_{\min} = \lim_{\rho \to 0} \dfrac{\rho}{R(\rho, \theta)} = \dfrac{1}{R'(0, \theta)} \\[2ex]
S_0 = -\dfrac{2\left[R'(0,\theta)\right]^2 \ln 2}{R''(0,\theta)}
\end{cases}
\tag{3.25}
$$

where $R'(0,\theta)$ and $R''(0,\theta)$ denote the first and second order partial derivatives with respect to ρ evaluated at $\rho=0$.

Theorem 3 *The effective rate over MISO i.n.i.d. Weibull fading channels in low-SNR regimes can be approximated by* (3.24), *with the metrics given by*

$$
\left(\frac{E_b}{N_0} \right)_{min} = \frac{2\ln 2}{\Omega} = \frac{N \ln 2}{\sum\limits_{j=1}^{N} \Gamma\left(1 + \frac{1}{\beta_j}\right) \omega_j^{\frac{1}{\beta_j}}},
\tag{3.26}
$$

$$
S_0 = \frac{2}{1 + (A+1)\dfrac{\sum_{j=1}^{N} \omega_j^{\frac{2}{\beta_j}} \left\{ \Gamma\left(1 + \frac{2}{\beta_j}\right) - \left[\Gamma\left(1 + \frac{1}{\beta_j}\right)\right]^2 \right\}}{\left[\sum_{j=1}^{N} \Gamma\left(1 + \frac{1}{\beta_j}\right) \omega_j^{\frac{1}{\beta_j}}\right]^2}}.
\tag{3.27}
$$

Proof   *When $\rho \to 0$, the Tricomi function has the Poincare-Type expansion as $U(a; b; z) \approx z^{-a} \sum_{n=0}^{\infty} (a)_n (a - b + 1)_n (-z)^{-n} / n!$ [198], where $(a)_n$ is the Pochhammer operator given by $(a)_n = a(a+1)\cdots(a+n-1)$ and $(a)_0 = 1$. By taking $\rho \to 0$ and following the rules of limitation, $R'(0,\theta) = \frac{\Omega}{2\ln 2}$ and $R''(0,\theta) = -\frac{\Omega^2}{4\ln 2} - \frac{A+1}{N^2 \ln 2} \sum_{j=1}^{N} \left[\mathbb{E}\left(\gamma_j^2\right) - (\mathbb{E}\gamma_j)^2 \right]$ can be obtained. Substituting these results into* (3.25), *both* (3.26) *and* (3.27) *can be obtained.*

Note that the capacity slope S_0 has a reverse relationship with the parameter $A = \theta TB/\ln 2$. Hence with the same increase of E_b/N_0, the transmission with more relaxed QoS requirement will have a higher upper bound of the supported rate. It can be inferred that, the increase of the bandwidth or the QoS requirement will result in a lower effective rate, if the same fading channel conditions and E_b/N_0 are assumed. Note that $\left(\frac{E_b}{N_0} \right)_{\min}$, S_0 and (3.24) are all in the closed-form, which means the low-SNR approximation (3.24) is easier to compute compared to (3.14).

3.3.4   Numerical Results

In this section, numerical simulations are presented to verify the proposed effective rate analysis in Section III. Channel fading parameters are assumed and listed in Table 3.1 [197]. Without loss of generality, the bandwidth $B=1$ and the duration of a time block $T=1$ are assumed [96].
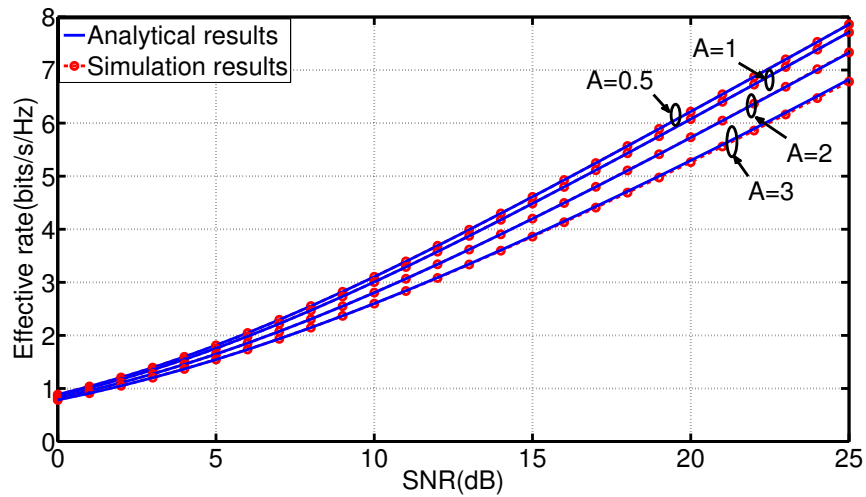
Figure 3.1: Analytical and simulated effective rate versus the average SNR over MISO i.n.i.d. Weibull fading channels with $N = 2$.

As the QoS exponent θ increases, the delay constraints become more stringent, which is corresponding to the increase of A. It is illustrated in Fig. 3.1 that analytical results agree with the simulation results. Also under the same channel fading conditions, the overall effective rate decreases as the delay constraints increase.

High-SNR approximation results and simulation results are compared in Fig. 3.2, where $A = 2$ is assumed. It can be seen that the high-SNR approximation results agree with the simulation results in different i.n.i.d. scenarios. When the average SNR ρ is relatively high, e.g. above 10 dB, the high-SNR approximation results fit

Table 3.1: Parameters for different i.n.i.d. Weibull fading scenarios

Scenario	Parameters
$N=1$	$\omega_1=1$, $\beta_1=1$
$N=2$	$\omega_1=1$, $\beta_1=1$, $\omega_2=1$, $\beta_2=2$
$N=3$	$\omega_1=1$, $\beta_1=1$, $\omega_2=1$, $\beta_2=2$, $\omega_3=1$, $\beta_3=3$
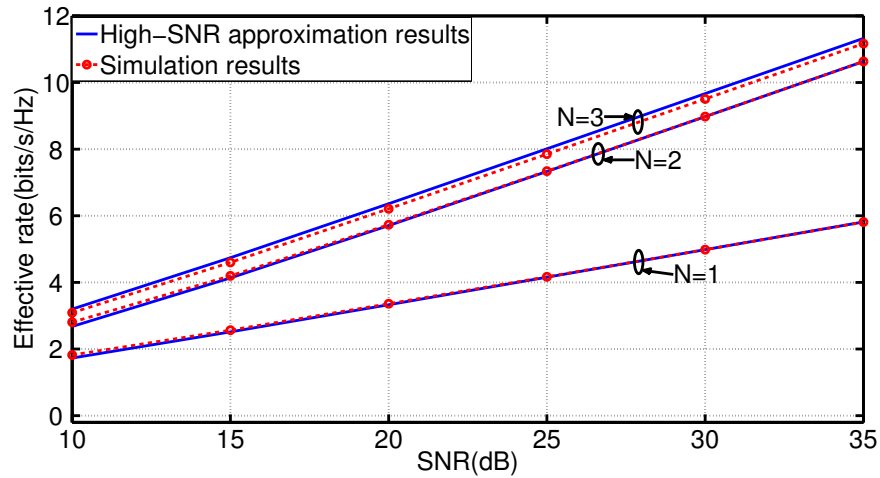
Figure 3.2: High-SNR approximated and simulated effective rate versus the average SNR over i.n.i.d. Weibull fading channels with different N.

well with the simulation results. As $\rho \to \infty$, in theory the high-SNR approximation will approach the exact simulation results, and accordingly the approximation error will approximate 0. But the convergence speed may vary with different system parameters and channel conditions, such as the QoS exponent and fading severity.
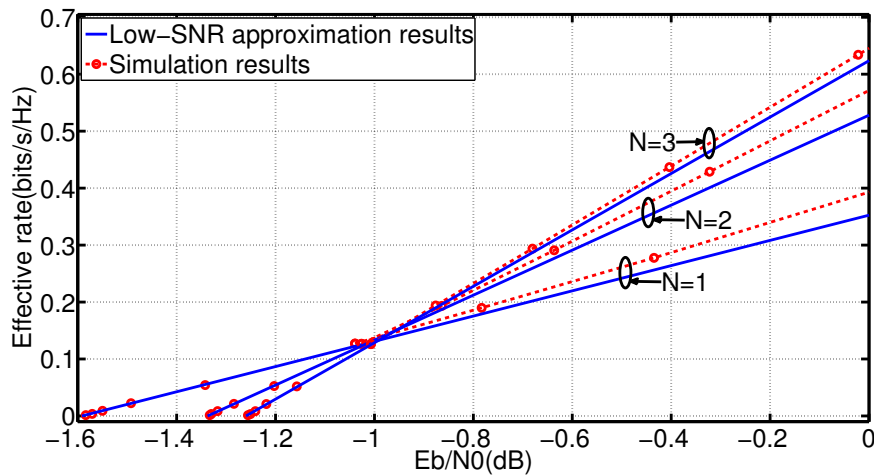
Figure 3.3: Low-SNR approximated and simulated effective rate versus E_b/N_0 over i.n.i.d. Weibull fading channels with different N.

In low-SNR regimes, it is shown in Fig. 3.3 that the proposed low-SNR approximation results agree with the simulation results in different i.n.i.d. scenarios, where $A = 1$ is assumed. From both Fig. 3.2 and Fig. 3.3, it can be inferred that with the increase of the antenna numbers N, the effective rate of the system also increases.

As the shape parameter β_j describes the fading severity of the channel, the channels with larger fading severity contribute less to the total effective rate under the same QoS requirements. It is noteworthy that the simulated channel follows Rayleigh fading in the case of $N = 1$, and these simulation results coincide with the results of [96].

3.3.5 Remarks

In this section, new analytical expressions for the effective rate over i.n.i.d. Weibull fading channels were derived. Closed-form approximations in high-SNR and low-SNR situations were also given for reducing computational complexity. The convergence of these proposed expressions was studied. Numerical results verified these analyses and approximations. It was found that tighter QoS requirement resulted in lower effective rate. The channel with larger fading severity contributed less to the overall effective rate. These results extended and complemented previous work on the effective rate analysis over different fading channels.

3.4 Effective Capacity Analysis of Smart Grid Communication Networks

Smart grid represents a significant new technology for improving the efficiency, reliability and economics of the production, transmission and distribution of electricity that helps reduce carbon emissions. Communication networks become a key to achieving smart grid benefits due to their capability of delivering data and control signals. However, there does not exist a unified approach to quantify how well a communication network supports smart grid applications. In this section, effective capacity is exploited as a good candidate to quantitatively measure how well the communication network supports smart grid applications, regardless of specific network technologies. Case studies using the effective capacity are given and analysed by simulations in different smart grid application scenarios.

The typical smart grid application scenarios involve industrial, residential and

Table 3.2: Parameter Setup

Channel Environment	Channel Parameters	Communication requirements
Industrial building	Rician K=5.1dB	Source Rate 60~100kbps,
Residential building	Rayleigh	D_{max}=10ms,Delay violation
Office	Rician K=-6.8dB	probability $10^{-2} \sim 10^{-5}$
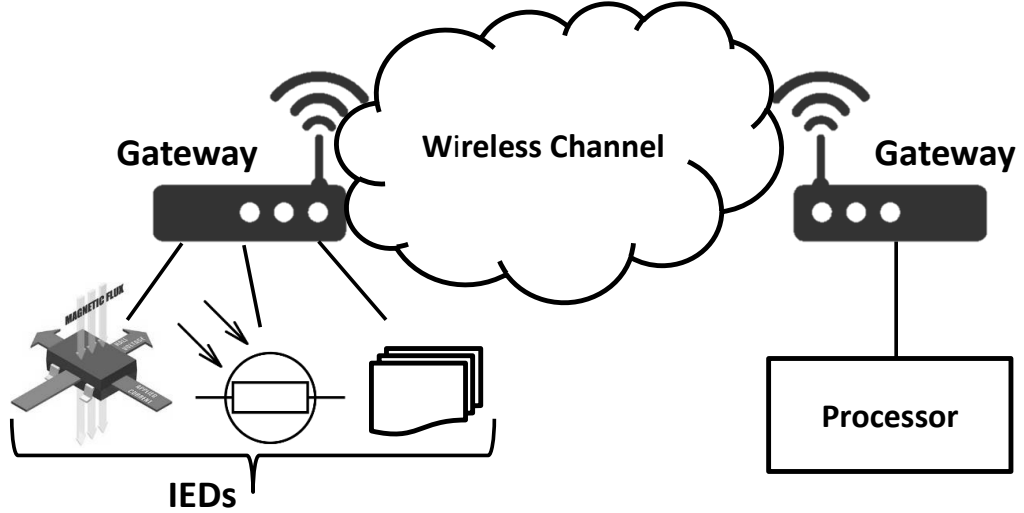
Figure 3.4: The Wireless Communication System Model

office environment. In this part, we consider smart grid applications in these environments. The considered system model is shown in Fig. 3.4, where the data from several intelligent electronic devices (IEDs) (or sensors) are aggregated at the gateway and transmitted using wireless technologies. In the case of industrial environment, a typical application is the raw data collection from IEDs, where the data consist of continuous streams of synchronized samples from each IED, and interleaved with data from other IEDs. The delay requirement for this type of application is 10ms, and the delay violation probability may range from 10^{-2} to 10^{-5} depending on the specific functions [25]. The channel can be modelled by Rician model with the estimate of mean random/specular power ratio (K) of 5.1dB [205]. This is a typical situation where light-of-sight (LOS) is expected due to the open architecture and significant reflection in an industrial environment. As for the residential and office environment, the application of non-intrusive load monitoring is considered. A delay of 10ms with a delay violation probability ranging from 10^{-2} to 10^{-5} is considered. Rayleigh channel model is used for the residential environment, where there is usually no LOS path between the transceivers. For an office building

environment, a Rician model is applied while the typical K parameter is chosen as -6.8dB [206]. For the convenience of discussion, a data rate ranging from 60 to 100 kbps is considered. The parameters used are summarized in Table 3.2. Besides, we assume that the queueing delay is dominant, where other delay components such as propagation delay are negligible. Moreover, Doppler effect is not considered since the transceivers in the smart grid are fixed to a position. An assumption is made that Shannon's capacity can be approached by the throughput of the system, in order to perform an analysis in a general way that might work with different MAC and PHY layers.
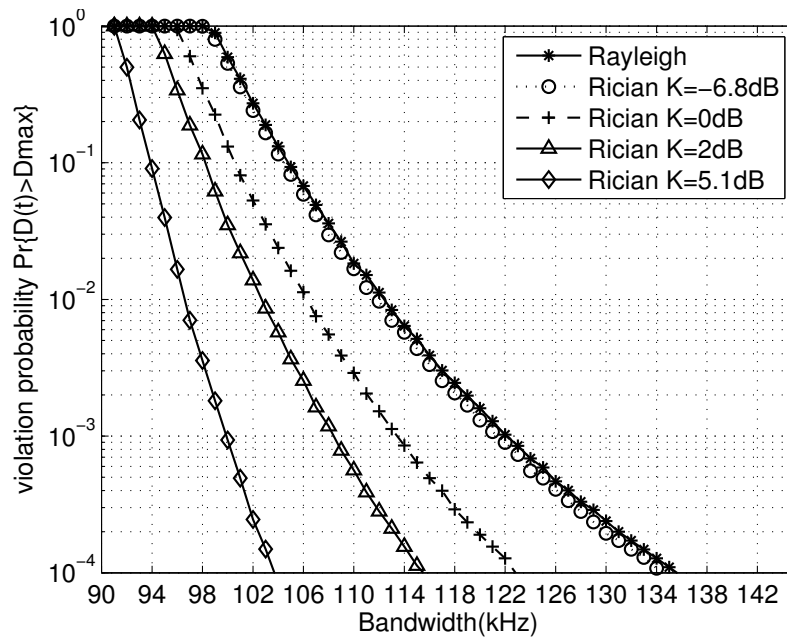
Figure 3.5: Delay violation probability under different bandwidths and temporal fading channels, average SNR=0dB

First, the resource allocation is considered. Before each transmission, the amount of resource required to support the application's QoS requirement is calculated and reserved. In most algorithms, the resource allocation is static. Once an application is admitted, the total reserved resource would be kept for the whole transmission procedure. Therefore the amount of resource assigned and reserved for the application would be critical to guarantee the application's QoS requirement. We consider the bandwidth allocation cases, which is to provide the application with a source data rate of 85kbps and a maximum delay bound of 10ms under different channel
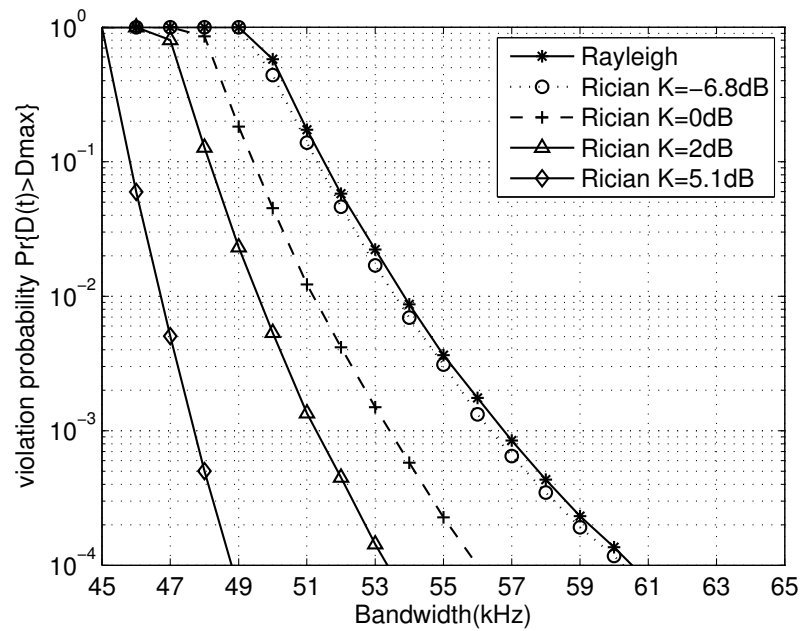
Figure 3.6: Delay violation probability under different bandwidths and temporal fading channels, average SNR=5dB

conditions. It can be seen from Fig. 3.5-3.6 that the residential situation (Rayleigh fading), is the worst case which needs a wider bandwidth to support the same data rate transmission for the same delay performance. Office environment with weak LOS component, which is corresponding to the Rician model with K=-6.8dB, has almost the same performance with the Rayleigh fading. As the LOS component gets stronger, which is corresponding to the increase of K, the bandwidth needed to guarantee the desired violation probability (e.g. 0.01% for some delay-sensitive application) under specific average signal-to-noise ratio condition also decreases.
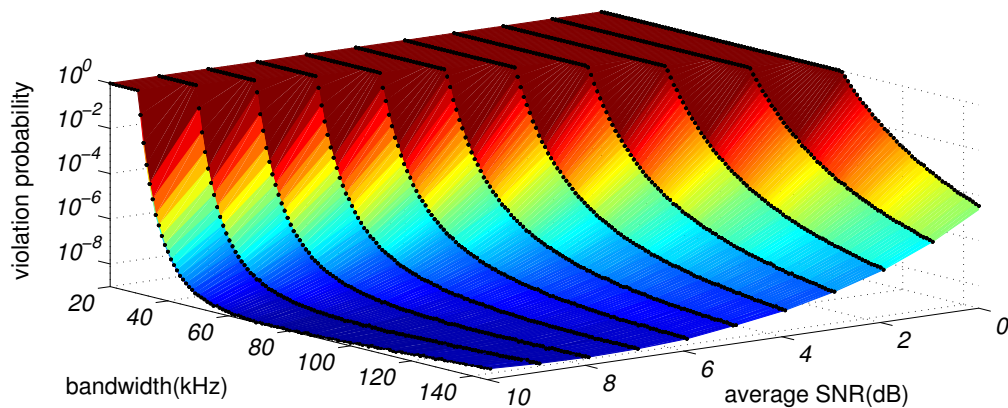
Figure 3.7: Delay violation probability under different bandwidths with average SNR from 0dB to 10dB in Rayleigh fading channel

A more detailed bandwidth required to support the application varying with the
average SNR is shown in Fig.3.7. It indicates that in relatively low SNR situations
(e.g. 0-10dB), the required bandwidth to support the same data rate for the delay
performance increases significantly along with the drop of the average SNR. This
makes sense since the Shannon capacity will decrease along with the drop of the
average SNR under a fixed bandwidth. But a further calculation in Table 3.3 shows
that the extra bandwidth needed to get the same delay performance along with the
decrease of the average SNR also increases in an exponential way. If only assigned
with the bandwidth using average SNR information, it will violate the delay bound
in a probability of 100%. This gives a direct sense of the importance to consider
channel fading statistical characteristics in resource allocation mechanisms.
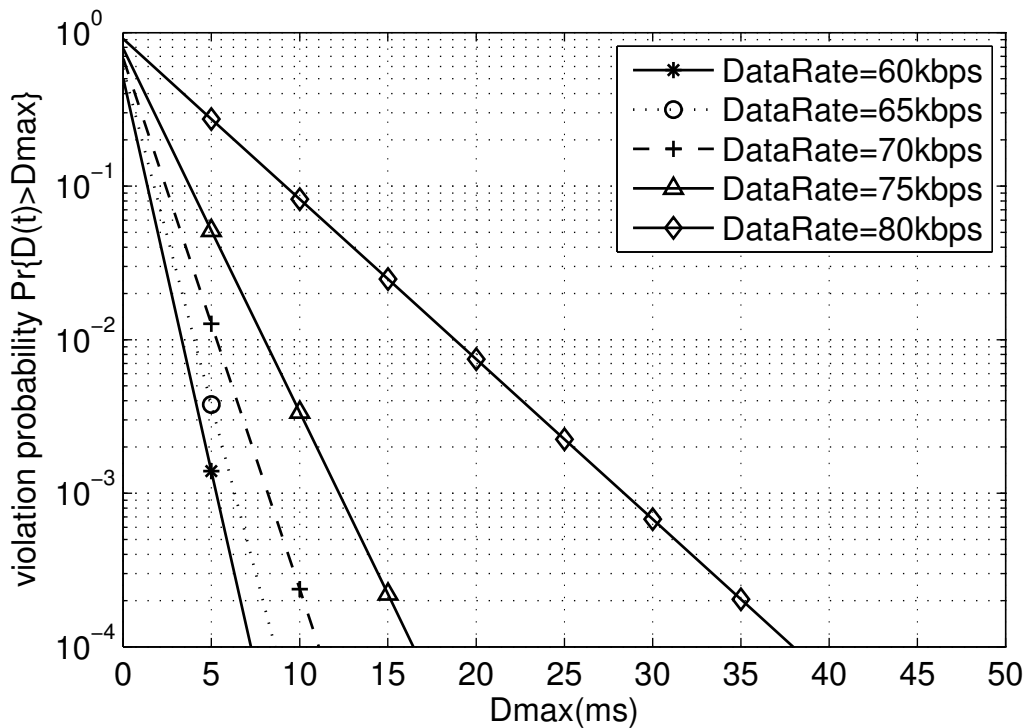
Figure 3.8: Delay violation probability under different data rates and delay bounds,
Rayleigh fading channel

Real channel capacity will vary randomly with time, which means that a guaran-
tee of 100% that the transmission will not violate the upper delay bound is almost
impossible. Indeed the increase of redundant bandwidth would certainly improve
the delay bound violation performance. However, it can also be inferred from the
Fig. 3.5-3.6 that the bandwidth increased exponentially while the delay-violation

probability approaches zero, i.e. a 100% guarantee of transmission within the delay bound, which is unrealistic due to the limited bandwidth in practice. Hence the admission control and resource allocation algorithms should assign resources, e.g. bandwidth, according to the delay bound and the reliability requirement of the application. A typical example is the system exploiting Orthogonal Frequency-Division Multiple Access (OFDMA), which is already used in many standards such as IEEE802.16 (WiMAX) and 3GPP LTE. The subsets of sub-carriers in OFDMA can be mapped to the bandwidth allocation problem.
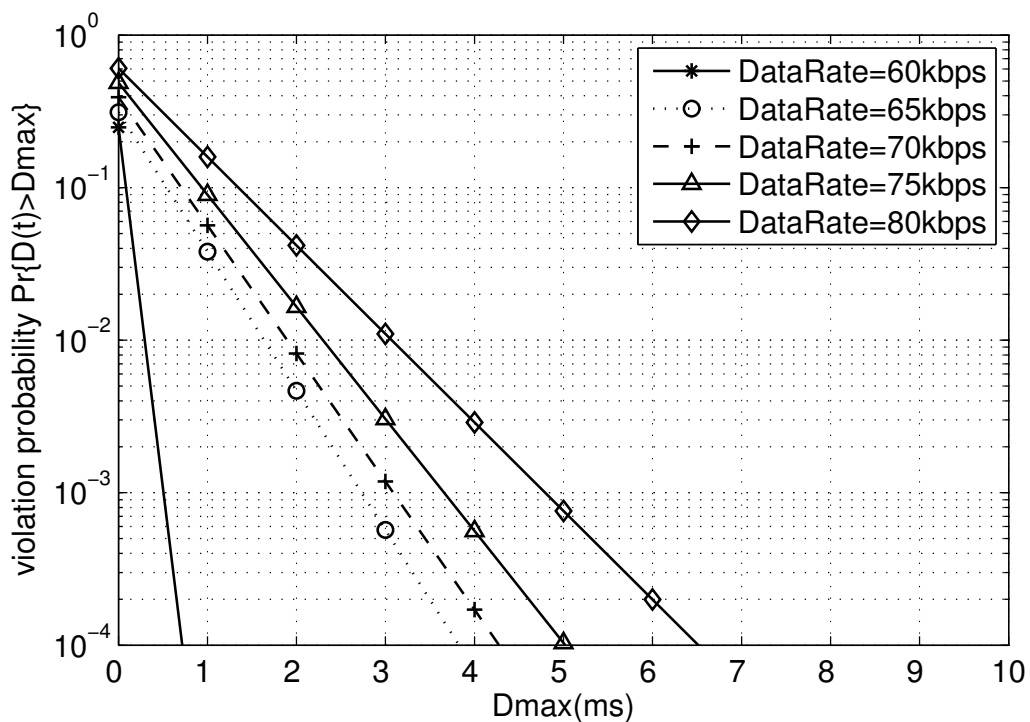
Figure 3.9: Delay violation probability under different data rates and delay bounds, Rician fading channel K=5.1dB

Second, the admission control is considered. Whenever a new request for transmission is launched, the admission control algorithm would check the availability of the request. That means the available resources have to be evaluated and mapped to the required QoS metrics to see if or not the application can be admitted. As for delay-sensitive applications, not only the available throughput of the system is of matter, but also the estimated delay and the violation probability is essential. Take the video surveillance as an example, video frames would be useless and discarded if certain delay bound is exceeded. Moreover, for most control command, the delay

performance is crucial, where a delay violation might even result in a disaster. Thus
in the design of the admission control algorithm, delay and violation probability
should be included in the QoS metrics to be estimated with the available resources.
A scenario that the source data rate as well as the associated delay bound and re-
liability can be supported when a channel capacity of 100kbps is available under
an average SNR of 5dB and different temporal fading channels is considered. The
Rician model with K=5.1dB for industrial environment and Rayleigh model for the
residential scenario are presented in Fig. 3.8 and 3.9. It is worth noticing that D_{max}
associated to a source data rate is the lower bound. For example, with an average
SNR of 5dB and Rayleigh fading channel as shown in 3.8, it can be predicted that an
application with a data rate of 80kbps and a delay bound requirement no less than
37ms would be guaranteed by 99.99%, which can be used as criteria for admissions.
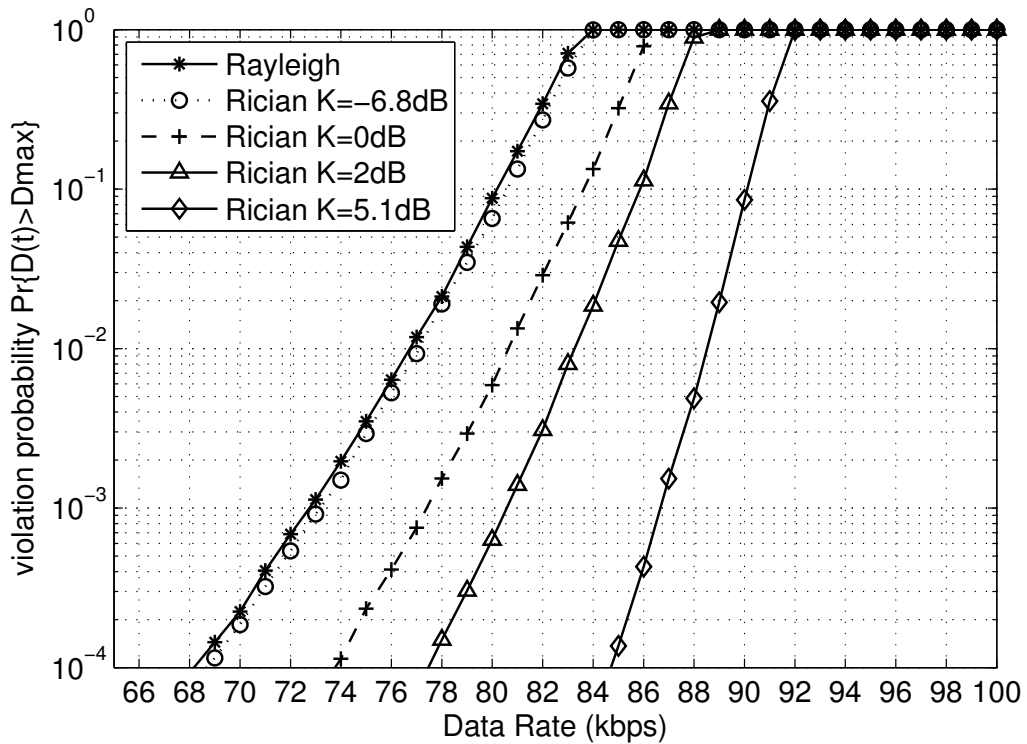
Figure 3.10: Delay violation probability under different data rates and temporal
fading channels

Another situation is considered when variable source data rate is achievable.
Communication under tough environment is involved in smart grid. Resources might
be strictly confined and valued, yet the applications are still delay sensitive. Also in

practice, even deployed within a close geographical location, the channel condition for different transceivers would still be heterogeneous. For example the channel between one pair of transceivers might be Rayleigh fading with an average SNR of 5dB yet the other is Rician fading with an average SNR of 0dB. The variable data rate can be achieved by many methods, for example a feedback control of a tunable Analog-to-Digital Converter (ADC) at the data source, or by an Adaptive Modulation and Coding (AMC) at the transmitter. An example of an application with a delay bound requirement of 10ms under different temporal fading models with an average SNR of 5dB is illustrated in Fig. 3.10. It can be indicated in Fig. 3.10 that the delay bound violation probability decays exponentially with the decrease of the source data rate, but for the same conditions other than temporal fading statistical characters, the maximum supported data rate is different. In such cases, if the source data rate can be adapted based on the prediction of delay bound violation under current and past channel condition of the transceivers along the path, a trade-off can be obtained between the information quality and the delay performance, or even enable some delay-sensitive applications which would not be admitted with a high data rate. For example, an application with a delay bound of 10ms, and delay violation probability of 0.1%, it might not be admitted (i.e. blocked) with a data rate of 78kbps, but it can expect an even lower delay violation probability of 0.01% with a drop (e.g. using AMC) of data rate to 74kbps as shown in Fig. 3.10.

Table 3.3: Extra bandwidth under different average SNR

Average SNR(SNR_{avg})	0	2	4	6	8	10
bandwidth for SNR_{avg}(kHz)	85	62	47	37	30	25
bandwidth for pr=10^{-4}(kHz)	136	96	70	53	42	33
extra bandwidth(kHz)	51	34	23	16	12	8

Smart grid has a wide range of applications covering different scenarios, leading to different QoS requirements. Delay-sensitive applications often exist, hence the delay and the probability of delay bound violation should also be considered in the QoS metrics. This chapter proposes to use effective capacity to evaluate the support level of communication networks to the smart grid applications. Examples as well as simulations with measured statistical channel model in common smart

grid application scenarios including industrial, residential and office environment are used to verify the effective capacity concept. In the future, we will focus on integrating the effective capacity into the admission control and resource allocations algorithms for heterogeneous networks in smart grid systems.

3.5 Concluding Remarks

In this chapter, the effective capacity theory was first introduced. Then the integration based effective analysis method was discussed, where an application of such framework in the analysis of i.n.i.d. Weibull fading channel was illustrated. Besides, both analytical and asymptotic results were derived, while the simulation results supported the correctness of the obtained results.

It could be also indicated from the illustrated example that this integration based method has several drawbacks. Firstly, this framework was defined in integration representation. The framework could be applied to a wide range of fading scenarios, but each of them needed further efforts to obtain the required results for performance evaluation. Secondly, the analysis procedure highly depended on the specific mathematical models of the fading channels. Hence a different scenario might lead to a totally different derivation procedure. Thirdly, the derivation procedure involved frequent sophisticated mathematical manipulations. This complicated the individual cases by coupling with the former two reasons. These issues will be addressed via a MGF and H transform based framework in the next chapter.

In addition, a case study on Smart Grid communication networks was performed, where several deployment scenarios were discussed. It was shown by extensive simulations that effective capacity theory could be used to provide a quantified analysis between the interested Smart Grid QoS metrics, such as delay performance, data rate and channel fading effects.

Chapter 4

Unified Framework for the Effective Rate Analysis of Wireless Communication Systems over MISO Fading Channels

When evaluating the maximum achievable bit rate of a wireless system over fading channels, Shannon's channel capacity is the most important performance metric. It has also been widely adopted as the basis of performance analysis as well as mechanism design. However, many emerging applications are real-time applications, for example voice over IP, interactive video and most of the smart grid applications. For these real-time applications, not only throughput, but also delay should be considered as one of the quality of service (QoS) requirements. Thus the effective rate theory (or effective capacity) has been proposed by Wu and Negi [4], which bridges the gap between statistical QoS guarantees and the maximum achievable transmission rate. Since then it has been widely used as a powerful analytical tool and QoS provisioning metric in different scenarios.

The approaches studied in Chapter 3 can be categorized as probability density function (PDF) based method, since the analyses highly rely on the exact or approximated PDF of the signal-to-noise ratio (SNR). However, the joint PDF is unavailable for many fading channels and it is often very hard, if not impossible, to

obtain the exact PDF for further analysis. This fact results in the situation that the PDF based effective rate analyses are generally studied in a case-by-case way. To address aforementioned issues, this chapter proposes a moment generating function (MGF) based framework for the effective rate analysis over MISO fading channels using H transform representation. Moreover, in this chapter we use the H transform and multivariate Fox's H function to present the effective rate over both i.n.i.d. and correlated fading channels, which further simplify the analysis and provide a more general analytical framework. The major contributions of this chapter are listed as follows:

- A MGF based framework is proposed for analysing the effective rate over arbitrary correlated and not necessarily identical MISO fading channels using H transform representation. Due to the properties of H transform, the cumbersome mathematical calculation involving integration operation can be simplified.

- H transform involving multivariate Fox's H function is investigated. As many important metrics in wireless communication systems can be represented by H transform and the statistical properties of multiple fading channels may be characterized using multivariate Fox's H functions, the obtained results are also valuable in the analysis of other metrics in the multiple channel conditions. Also to the authors' best knowledge, this work is the first to deal with multiple channel problems within the H transform framework.

- Effective rate over both i.n.i.d. and correlated channel scenarios are studied. The exact analytical expressions of effective rate over i.n.i.d. MISO hyper Fox's H fading channels and arbitrary correlated generalized K fading channels are given. The effective rates over various practical fading channels are readily available by simply substituting corresponding parameters, such as generalized K and Weibull/Gamma fading channels, which avoids the case-by-case study in these fading scenarios.

- Asymptotic approximations are provided for the effective rate analysis over MISO fading channels, where the truncation error and the discretization error

are studied. Using this approximation, the proposed effective rate expressions over i.n.i.d. MISO hyper Fox's _H_ fading channels can be accurately estimated in a unified and closed-form framework.

The rest of this chapter is organised as follows. In Section 4.1, the Fox's _H_ function and _H_ transform related theories are studied. Then the MGF based effective rate analysis framework is proposed in Section 4.2. Based on the proposed framework, the exact and asymptotic analysis over MISO fading channels are performed in Section 4.3 and Section 4.4, respectively. Numerical results are presented in Section 4.5, and the conclusions are drawn in Section 4.6.

4.1 Fox's _H_ Function and _H_ Transform

In the statistical system performance analysis, it usually uses a random variable to describe the interested parameters' statistical characteristics. Typical examples are the various channel fading effects, such as multipath fading effect and shadowing effect. These random variables describing fading effects can be empirically modelled for different application scenarios.For example, it has been verified that fading models such as Rayleigh, Weibull and Nakagami-m fit well to the empirical multipath fading measurements, while the log-normal and gamma distribution can characterize the shadowing effect in many practical scenarios. The theoretical study using random variables can provide an analytical framework that describes the system's general statistical performance, while the application of specific fading models can give a good estimation of the performance we can expect. Hence similar to other science and engineering subjects, the statistical study has provided a theoretical tool in the system design, as well as a deeper understanding of the various parameters' influence on the system performance. On one hand, the statistical distribution models have facilitated the theoretical analysis. In practical scenarios, the fading effects may result from the superposition of different fading effects. This composite fading effect can be described by the composition of the random variables for these fading effects. On the other hand, statistical analysis will usually involve the integration or differential of these random variables. The algebra combination of random variables

is even more challenging. Since this is a common problem in engineering studies, there has been a series efforts in addressing this issue. One important result is the Fox's *H* function proposed by Fox in [207]. Based on the Fox's *H* function, the *H* variate and *H* transform have been also been proposed, which will be detailed as follows.

4.1.1 Univariate Fox's *H* Function

The Fox's *H* function is a generalized function, which involves Meijer *G* function and many other functions that can not be represented by Meijer *G*-function as special cases. It has been shown that *H* function can provide general, deep, and useful results directly applicable to various problems of engineering, physical, biological and many other disciplines [202]. Besides, the Fox's *H* function has been a build-in function in numerical software such as Matlab and Mathematics, which is not hard to evaluate.

Definition 1 (Fox's *H* function [202]) *The Fox's H function $H_{p,q}^{m,n}[\cdot]$, or univariate Fox's H function in order to distinguish from multivariate Fox's H function, can be defined by a single Mellin-Barnes type of contour integral as [202, Ch. 1.2]*

$$H[s, \mathbf{O}, \mathbf{P}] = u H_{p,q}^{m,n} \left[vs \left| \begin{matrix} \mathbf{c}, \mathbf{C} \\ \mathbf{d}, \mathbf{D} \end{matrix} \right. \right] = \frac{u}{2\pi i} \oint_{\mathcal{L}} \Phi(z) (vs)^z dz, \tag{4.1}$$

where $i = \sqrt{-1}$, $s \neq 0$ and $\mathcal{L}$ is a suitable contour. The following notation is used for simplicity,

$$\begin{cases} \mathbf{O} = (m, n, p, q) \\ \mathbf{P} = (u, v, \mathbf{c}, \mathbf{d}, \mathbf{C}, \mathbf{D}) \end{cases} \tag{4.2}$$

where $\mathbf{c} = (\dot{\mathbf{c}}, \ddot{\mathbf{c}})$, $\mathbf{d} = (\dot{\mathbf{d}}, \ddot{\mathbf{d}})$, $\mathbf{C} = (\dot{\mathbf{C}}, \ddot{\mathbf{C}})$ and $\mathbf{D} = (\dot{\mathbf{D}}, \ddot{\mathbf{D}})$, with $\dot{\mathbf{c}} = (c_1, \ldots, c_n)$, $\ddot{\mathbf{c}} = (c_{n+1}, \ldots, c_p)$, $\dot{\mathbf{d}} = (d_1, \ldots, d_m)$, $\ddot{\mathbf{d}} = (d_{m+1}, \ldots, d_q)$, $\dot{\mathbf{C}} = (C_1, \ldots, C_n)$, $\ddot{\mathbf{C}} = (C_{n+1}, \ldots, C_p)$, $\dot{\mathbf{D}} = (D_1, \ldots, D_m)$ and $\ddot{\mathbf{D}} = (D_{m+1}, \ldots, D_q)$. Also

$$\Phi(z) = \frac{\prod_{j=1}^{m} \Gamma(d_j - D_j z) \prod_{j=1}^{n} \Gamma(1 - c_j + C_j z)}{\prod_{j=n+1}^{p} \Gamma(c_j - C_j z) \prod_{j=m+1}^{q} \Gamma(1 - d_j + D_j z)}. \tag{4.3}$$

Some frequently used parameter sequences have been summarized in Table 4.1.

Table 4.1: Frequently Used Order and Parameter Sequences

Symbols	Order and Parameter Sequences
$\mathbf{O}_{\mathrm{MGF}}$	$(1, 0, 0, 1)$
$\mathbf{P}_{\mathrm{MGF}}$	$(1, 1, \text{---}, 0, \text{---}, 1)$
$\mathbf{O}_{\mathrm{ER}}$	$(1, 0, 0, 1)$
$\mathbf{P}_{\mathrm{ER}}$	$(1, 1, \text{---}, A - 1, \text{---}, 1)$
$\mathbf{O}_f$	(m, n, p, q)
$\mathbf{P}_f$	$(u, v, \mathbf{c}, \mathbf{d}, \mathbf{C}, \mathbf{D})$
$\mathbf{O}_\phi$	$(n + 1, m, q, p + 1)$
$\mathbf{P}_\phi$	$(u/v, 1/v, 1 - \mathbf{d} - \mathbf{D}, (0, 1 - \mathbf{c} - \mathbf{C}), \mathbf{D}, (1, \mathbf{C}))$

One of the most important properties of H function is that, it can describe a wide range of functions by its standardized parameters. This makes the application of H function as integral kernels very versatile, which includes the classical Fourier, Laplace, Mellin, Stielgjes and Hankel transform, as special cases [1, 202]. Furthermore, due to the H preserving property, the integration or differential operation involving H function has the potential to be further simplified by the algebra manipulations of the parameters. Typical operations include convolution operation, Mellin operation, scaling operation, and elementary operation, which are detailed in Table 4.2.

Although the definition of H function seems to be complex, the practical usage is not that hard, where sophisticated mathematical knowledge is not required [208]. In communication systems, it is a common problem that the definition of certain metrics are in integral forms, where no closed form is available. A typical example is the error function in bit error rate analysis. This makes the analysis based on these metrics hard in mathematical manipulations. In such cases, a versatile function like H function is very attractive, which thanks to the conversion of complex mathematical manipulations to the parameter operations above.

4.1.2 Multivariate Fox's *H* Function

If we use different random variables to describe individual fading effects, then the superposition of these fading effects will involve the composite of these random variables. For some special cases, it can be simplified, for example when the individual

Table 4.2: Unary and binary operations on the order and parameter sequences of Fox's H function [1]

Operation	Symbol	Order or parameter sequence
Scaling	$\mathbf{P}\lvert\alpha\rangle$	$(\frac{u}{\alpha},\frac{v}{\alpha},\mathbf{c},\mathbf{d},\mathbf{C},\mathbf{D})$
Conjugate	$\langle\eta\rvert\mathbf{P}$	$(\frac{u}{v^\eta},v,\mathbf{c}+\eta\mathbf{C},\mathbf{d}+\eta\mathbf{D},\mathbf{C},\mathbf{D})$
Elementary	$\langle\alpha,\beta,\eta\rvert\mathbf{P}$	$(\frac{u}{(\alpha v)^{\beta\eta}},(\alpha v)^{\beta\eta},\mathbf{c}+\beta\eta\mathbf{C},\mathbf{d}+\beta\eta\mathbf{D},\beta\mathbf{C},\beta\mathbf{D})$
Differential	$\partial^l\mathbf{O}$	$(m+1,n,p+1,q+1)$
	$\partial^l\mathbf{P}$	$(uv^l,v,(\mathbf{c}-l\mathbf{C},-l),(0,\mathbf{d}-l\mathbf{D}),(\mathbf{C},1),(1,\mathbf{D}))$
Inverse	$\mathbf{O}^{-1}$	(n,m,q,p)
	$\mathbf{P}^{-1}$	$(u,\frac{1}{v},\mathbf{1}_q-\mathbf{d},\mathbf{1}_p-\mathbf{c},\mathbf{D},\mathbf{C})$
Mellin	$\mathbf{O}_1\boxdot\mathbf{O}_2$	$(m_1+n_2,m_2+n_1,p_1+q_2,p_2+q_1)$
	$\mathbf{P}_1\boxdot\mathbf{P}_2$	$(\frac{u_1u_2}{v_2},\frac{v_1}{v_2},\mathbf{c}',\mathbf{d}',\mathbf{C}',\mathbf{D}')$
		$\begin{cases}\mathbf{c}'=(\dot{\mathbf{c}}_1,\mathbf{1}_{q_2}-\mathbf{d}_2-\mathbf{D}_2,\ddot{\mathbf{c}}_1)\\\mathbf{d}'=(\dot{\mathbf{d}}_1,\mathbf{1}_{p_2}-\mathbf{c}_2-\mathbf{C}_2,\ddot{\mathbf{d}}_1)\\\mathbf{C}'=(\dot{\mathbf{C}}_1,\mathbf{D}_2,\ddot{\mathbf{C}}_1)\\\mathbf{D}'=(\dot{\mathbf{D}}_1,\mathbf{C}_2,\ddot{\mathbf{D}}_1)\end{cases}$
Convolution	$\mathbf{O}_1\boxplus\mathbf{O}_2$	$(m_1+m_2,n_1+n_2,p_1+p_2,q_1+q_2)$
	$\mathbf{P}_1\boxplus\mathbf{P}_2$	$(u_1u_2,v_1v_2,\mathbf{c}',\mathbf{d}',\mathbf{C}',\mathbf{D}')$
		$\begin{cases}\mathbf{c}'=(\dot{\mathbf{c}}_1,\mathbf{c}_2,\ddot{\mathbf{c}}_1)\\\mathbf{d}'=(\dot{\mathbf{d}}_1,\mathbf{d}_2,\ddot{\mathbf{d}}_1)\\\mathbf{C}'=(\dot{\mathbf{C}}_1,\mathbf{C}_2,\ddot{\mathbf{C}}_1)\\\mathbf{D}'=(\dot{\mathbf{D}}_1,\mathbf{D}_2,\ddot{\mathbf{D}}_1)\end{cases}$

variates are independent of each other. For most cases, it will generally require using the multivariate random variables. The multivariate H function provides a potential way to characterize the superposition of multiple random variables, which can be defined based on the univariate Fox's H function.

Definition 2 (Multivariate Fox's *H* function [202]) *The operator* $H^{0,n_0;m_1,n_1;\dots;m_N,n_N}_{p_0,q_0;p_1,q_1;\dots;p_N,q_N}[\cdot]$ *is Fox's H function of N variables, or multivariate Fox's H function for simplicity, which can be defined in terms of multiple Mellin-Barnes type contour integrals as follows*

$$H^{0,n_0}_{p_0,q_0}\left[\begin{array}{l}(a_j;A_j^{(1)},\dots,A_j^{(N)})_{1,p_0}\\(b_j;B_j^{(1)},\dots,B_j^{(N)})_{1,q_0}\end{array}:(s_j,\mathbf{O}_j,\mathbf{P}_j)_{1,N}\right] \qquad (4.4)$$

$$=\frac{u_1\cdots u_N}{(2\pi i)^N}\int_{\mathcal{L}_1}\cdot\cdot\int_{\mathcal{L}_N}\Psi(\boldsymbol{\zeta})\left\{\prod_{j=1}^N\Phi_j(\zeta_j)(v_js_j)^{\zeta_j}\right\}d\zeta_1\cdot\cdot d\zeta_N, \qquad (4.5)$$

where

$$\Psi(\boldsymbol{\zeta}) = \frac{\prod\limits_{j=1}^{n_0} \Gamma(1 - a_j + \sum\limits_{\ell=1}^{N} A_j^{(\ell)} \zeta_\ell)}{\prod\limits_{j=n_0+1}^{p_0} \Gamma(a_j - \sum\limits_{\ell=1}^{N} A_j^{(\ell)} \zeta_\ell) \prod\limits_{j=1}^{q_0} \Gamma(1 - b_j + \sum\limits_{\ell=1}^{N} B_j^{(\ell)} \zeta_\ell)}, \tag{4.6}$$

$$\Phi_j(\zeta_j) = \frac{\prod\limits_{\ell=1}^{m_j} \Gamma(d_\ell^{(j)} - D_\ell^{(j)} \zeta_j) \prod\limits_{\ell=1}^{n_j} \Gamma(1 - c_\ell^{(j)} + C_\ell^{(j)} \zeta_j)}{\prod\limits_{\ell=n_j+1}^{p_j} \Gamma(c_\ell^{(j)} - C_\ell^{(j)} \zeta_j) \prod\limits_{\ell=m_j+1}^{q_j} \Gamma(1 - d_\ell^{(j)} + D_\ell^{(j)} \zeta_j)}, \tag{4.7}$$

whereas $\mathcal{L}_j$ is the suitable contours in the ζ_j-plane. $(a_j; A_j^{(1)}, \ldots, A_j^{(N)})_{1,p_0}$ abbreviates p_0-parameter array $(a_1; A_1^{(1)}, \ldots, A_1^{(N)}), \ldots, (a_{p_0}; A_{p_0}^{(1)}, \ldots, A_{p_0}^{(N)})$, and $(s_j, \mathbf{O}_j, \mathbf{P}_j)_{1,N}$ abbreviates N-parameter array $\{s_1, \mathbf{O}_1, \mathbf{P}_1; \cdots; s_N, \mathbf{O}_N, \mathbf{P}_N\}$, where $\mathbf{O}_j = (m_j, n_j, p_j, q_j)$ and $\mathbf{P}_j = (u_j, v_j, \mathbf{c}^{(j)}, \mathbf{d}^{(j)}, \mathbf{C}^{(j)}, \mathbf{D}^{(j)})$, whereas $\mathbf{c}^{(j)}$ abbreviates p_j-parameter array $(c_1^{(j)}, \ldots, c_{p_j}^{(j)})$. Other abbreviations follow the same way. See [202] for more related details.

The multivariate Fox's *H* function is a kind of versatile function, which includes or relates to a wide range of generalized functions, such as multivariate Lauricella hypergeometric functions [209], Laguerre polynomials [210] and univariate Fox's *H* function [211]. These hypergeometric functions with one or more variables are frequently encountered and used in many research areas, including communications [1], engineering [212], computing sciences [213], applied mathematics [214], and physics [215].

Specially, when $n_0 = p_0 = q_0 = 0$, the multivariate Fox's *H* function breaks up into the product of N univariate Fox's *H* functions as [202, eq.(A.13)]

$$H_{0,0}^{0,0} \left[\begin{array}{c} - \\ - \end{array} : (s_j, \mathbf{O}_j, \mathbf{P}_j)_{1,N} \right] = \prod_{j=1}^{N} H \left[s_j, \mathbf{O}_j, \mathbf{P}_j \right]. \tag{4.8}$$

A special case satisfies the above condition is that all variables are independent of each other. This assumption is widely applied in communication studies where multiple variables are considered, such as in multiple antenna systems and a composition of fading effects.

4.1.3 *H* Transform

H transforms are integral transforms involving *H* function as kernels, which include many integral transforms, such as the classical Fourier, Laplace, Mellin, Stielgjes and Hankel transform, as special cases [1, 202]. We first recall the definition of *H* transforms in the following lemma, which will be extensively used in the later part.

Definition 3 (*H* transform [1]) *The H transform of a function $f(t)$ with Fox's H kernel of the order sequence $\boldsymbol{O} = (m, n, p, q)$ and the parameter sequence $\boldsymbol{P} = (u, v, \mathbf{c}, \mathbf{d}, \mathbf{C}, \mathbf{D})$, is defined by [1]*

$$\mathbb{H}\left\{f(z), \mathbf{O}, \mathbf{P}\right\}(s) = \mathbb{H}_{p,q}^{m,n}\left\{f(z), \mathbf{P}\right\}(s) = u \int_0^\infty H_{p,q}^{m,n}\left[vsz \left| \begin{matrix} \mathbf{c}, \mathbf{C} \\ \mathbf{d}, \mathbf{D} \end{matrix} \right.\right] f(z)dz, \quad (4.9)$$

provided that the integral converges absolutely and $s > 0$.

As will be shown in the following sections, the effective rate can be written in the *H* transform format in a very compact and clear way, which enables further analysis in the i.n.i.d. MISO fading channel conditions.

If the integral is an *H* function, then it has been proved that the *H* transform defined in (4.9), i.e. the integration of the product of two *H* functions, is an *H* function, which can be conveniently expressed by the following lemma.

Definition 4 (Mellin Operation [1]) *Let $f(z) = H[z, \mathbf{O}_2, \mathbf{P}_2]$, then the H transform of $f(z)$ is again Fox's H function whose parameter sequence is given by the Mellin operation between the parameter sequences of the kernel and $f(z)$, that is,*

$$\mathbb{H}\left\{f(z), \mathbf{O}_1, \mathbf{P}_1\right\}(s) = H\left[s, \mathbf{O}_1 \boxdot \mathbf{O}_2, \mathbf{P}_1 \boxdot \mathbf{P}_2\right], \quad (4.10)$$

where $\mathbf{O}_1 \boxdot \mathbf{O}_2$ and $\mathbf{P}_1 \boxdot \mathbf{P}_2$ denote the Mellin operation given in Table 4.2.

As will be shown in the following analysis, Lemma 4 provides a fruitful equation that can be used as a tool to derive the MGF based effective rate expression directly from the PDF based effective rate expression. By applying Lemma 4, the integration operation of the product of two *H* function has been simplified to the basic algebraic

manipulations of the parameters. Also it should be highlighted that if the overall MGF function can be expressed by a single H function, the effective rate can be easily obtained by directly applying Lemma 4.

4.1.4 H Variates

H distribution is defined based on the definition of H function, which includes a wide range of well-known distributions as special cases, such as gamma, Rayleigh, Weibull, Maxwell, beta, chi-square and F distributions [216, Ch. 6.3.4]. The definition of H variate is recalled in the following lemma.

Definition 5 (H variate [1, 217]) *A nonnegative random variable X is said to have an H distribution with the order sequence $\boldsymbol{O}=(m, n, p, q)$ and the parameter sequence $\boldsymbol{P}=(u, v, \boldsymbol{c}, \boldsymbol{d}, \boldsymbol{C}, \boldsymbol{D})$, denoted by $X \sim H(\mathbf{O}, \mathbf{P})$ or simply $X \sim H_{p,q}^{m,n}(\mathbf{P})$, if its PDF is given by*

$$f_X(x){=}H[x, \mathbf{O}, \mathbf{P}]{=}uH_{p,q}^{m,n}\left[vx\left|\begin{matrix}\mathbf{c}, \mathbf{C}\\ \mathbf{d}, \mathbf{D}\end{matrix}\right.\right], \quad (x \geq 0). \tag{4.11}$$

with the set of parameters satisfying a distributional structure such that $f_X(x) \geq 0$ for all $x \in \mathbb{R}_+$ and $\mathbb{H}\{1, \mathbf{O}, \mathbf{P}\}(1){=}1$. The MGF of the Fox's H variate X can be given by

$$\begin{aligned}\phi_X(s){=}&\mathbb{H}\{H[x, \mathbf{O}, \mathbf{P}], \mathbf{O}_{MGF}, \mathbf{P}_{MGF}\}(s),\\ {=}&H[s, \mathbf{O}_{MGF}\boxdot\mathbf{O}, \mathbf{P}_{MGF}\boxdot\mathbf{P}],\end{aligned} \tag{4.12}$$

where

$$\begin{cases}\mathbf{O}_{MGF} = (1, 0, 0, 1),\\ \mathbf{P}_{MGF} = (1, 1, -, 0, -, 1).\end{cases} \tag{4.13}$$

The necessary conditions for the H variates to be a density function have been extensively studied in [1, 208, 218, 219], these conditions are assumed to be satisfied.

The H variate has a very important and useful property, i.e. the so called the H preserving property [220], which is that the products, quotients and powers of independent H variables are again H variables [208, 219]. It should also be noticed that there are studies successfully modelled the various fading channel models in a

generalized fading model, which exploits the H variables as the basis, such as the H fading model [1] and hyper H fading [2], which will be detailed in Section 4.3.

4.1.5   Hyper Fox's H Fading Model

The hyper Fox's H fading model [2] uses the sum of several H variates to exactly represent or approximate a very wide range of different fading distribution models, including Rayleigh, Weibull, Nakagami-m, Weibull/Gamma and generalized K fading models. For a full list of special cases, interested readers are referred to [2]. By matching the parameters, effective rates over various i.n.i.d. MISO fading channels are readily available, which will further simplify the effective rate analysis under such conditions.

Let γ_j be a random variable following the hyper Fox's H fading distribution, then its PDF is given by [2]

$$f_j(\gamma) = \sum_{k=1}^{K_j} H[\gamma, \mathbf{O}_{f_{j,k}}, \mathbf{P}_{f_{j,k}}], \tag{4.14}$$

where

$$\begin{cases} \mathbf{O}_{f_{j,k}} = (m_{j,k}, n_{j,k}, p_{j,k}, q_{j,k}) \\ \mathbf{P}_{f_{j,k}} = (u_{j,k}, v_{j,k}, \mathbf{c}_{j,k}, \mathbf{d}_{j,k}, \mathbf{C}_{j,k}, \mathbf{D}_{j,k}) \end{cases} \tag{4.15}$$

defined over $\gamma \geq 0$ and the subscripts of $m_{j,k}$ denote that this parameter is associated to the kth parameter set of the PDF $f_j(\gamma)$, where $k \in (1, 2, \ldots, K_j)$. Same notation rule applies to the other parameters. The notations K_j, $\mathbf{O}_{f_{j,k}}$ and $\mathbf{P}_{f_{j,k}}$ are the parameters satisfying a distributional structure such that $f_j(\gamma) \geq 0$ for all $\gamma \geq 0$ and $\int_0^\infty f_j(\gamma)d\gamma = 1$ [2]. The necessary condition for the Fox's H function in (4.14) to be a density function can be given by [1, 217, 219]

$$\begin{cases} c_j + C_j < 1, \forall j = 1, 2, \ldots, n \\ -\dfrac{d_j}{D_j} < 1, \forall j = 1, 2, \ldots, m \end{cases} \tag{4.16}$$

The MGF ϕ_j can be obtained by using H transform defined in (4.9) as [1]

$$\phi_j(s) = \sum_{k=1}^{K_j} H[s, \mathbf{O}_{\phi_{j,k}}, \mathbf{P}_{\phi_{j,k}}],\tag{4.17}$$

where the parameter sequences of the MGF can be calculated by

$$\begin{cases} \mathbf{O}_{\phi_{j,k}} = \mathbf{O}_{\mathrm{MGF}} \boxdot \mathbf{O}_{f_{j,k}} \equiv (n_{j,k}+1, m_{j,k}, q_{j,k}, p_{j,k}+1) \\ \mathbf{P}_{\phi_{j,k}} = \mathbf{P}_{\mathrm{MGF}} \boxdot \mathbf{P}_{f_{j,k}} \\ \quad \equiv \left(\dfrac{u_{j,k}}{v_{j,k}}, \dfrac{1}{v_{j,k}}, \mathbf{1}_{q_{j,k}} - \mathbf{d}_{j,k} - \mathbf{D}_{j,k}, (0, \mathbf{1}_{p_{j,k}} - \mathbf{c}_{j,k} - \mathbf{C}_{j,k}), \mathbf{D}_{j,k}, (1, \mathbf{C}_{j,k})\right) \end{cases}\tag{4.18}$$

where $\mathbf{O}_{\mathrm{MGF}} = (1, 0, 0, 1)$ and $\mathbf{P}_{\mathrm{MGF}} = (1, 1, \text{—}, 0, \text{—}, 1)$ as given in Table 4.1. The Mellin operation $\boxdot$ is defined in Table 4.2, which is a typical operation in H transform. Mellin operation is very useful since when the integration kernel is fixed, for example in the case of deriving MGF from PDF, it uses basic arithmetic manipulation of parameters to replace the integration operation procedure.

Typical multipath fading and composite fading models can be directly obtained by changing parameters sequences in hyper Fox's H fading model, which are listed in Table 4.3

Table 4.3: Typical multipath fading and composite fading parameters [1] [2]

Fading Model	Order Sequence $\mathbf{O} = (m, n, p, q)$	Parameter sequence $\mathbf{P} = (u, v, \mathbf{c}, \mathbf{d}, \mathbf{C}, \mathbf{D})$
One-sided Gaussian	(1,0,0,1)	$\left(\frac{1}{2\sqrt{\pi}}, \frac{1}{2}, -, -\frac{1}{2}, -, 1 \right)$
Maxweil	(1,0,0,1)	$\left(\frac{3}{\sqrt{\pi}}, \frac{3}{2}, -, \frac{1}{2}, -, 1 \right)$
Rayleigh	(1,0,0,1)	$(1, 1, -, 0, -, 1)$
Nakagami-m	(1,0,0,1)	$\left(\frac{m}{\Gamma(m)}, m, -, m - 1, -, 1 \right)$
Weibull	(1,0,0,1)	$\left(\Gamma\left(1 + \frac{2}{\beta}\right), \Gamma\left(1 + \frac{2}{\beta}\right), -, 1 - \frac{2}{\beta}, -, \frac{2}{\beta} \right)$
$\alpha - \mu$(Stacy)	(1,0,0,1)	$\left(\frac{\Gamma(\mu + \frac{2}{\alpha})}{\Gamma(\mu)^2}, \frac{\Gamma(\mu + 2/\alpha)}{\Gamma(\mu)}, -, \mu - \frac{2}{\alpha}, -, \frac{2}{\alpha} \right)$
$N*$Nakagami-m	$(N,0,0,N)$	$\left(\prod_{i=1}^{N} \frac{m_i}{\Gamma(m_i)}, \prod_{i=1}^{N} m_i, -, (m_1 - 1, \ldots, m_N - 1), -, \mathbf{1}_N \right)$
Generalized Gamma	(1,0,0,1)	$\left(\frac{\beta}{\Gamma(m)}, \beta, -, m - \frac{1}{\xi}, -, \frac{1}{\xi} \right)$
K-fading	(2,0,0,2)	$\left(\frac{\sqrt{v}}{\Gamma(v)}, \sqrt{v}, -, (v - \frac{1}{2}, \frac{1}{2}, -, \frac{1}{2}\mathbf{1}_2) \right)$
Generalized K-fading	(2,0,0,2)	$\left(\frac{m_1 m_2}{\Gamma(m_1)\Gamma(m_2)}, -, (m_1 - 1, m_2 - 1), -, \mathbf{1}_2 \right)$
Weibull/Gamma	(2,0,0,2)	$\left(\frac{v\Gamma(1 + \frac{2}{\beta})}{\Gamma(v)}, v\Gamma(1 + \frac{2}{\beta}), -, (v - 1, 1 - \frac{2}{\beta}), -, (1, \frac{2}{\beta}) \right)$
Extended Generalized Gamma	(2,0,0,2)	$\left(\frac{\beta_1 \beta_2}{\Gamma(m_1)\Gamma(m_2)}, \beta_1 \beta_2, -, (m_1 - \frac{1}{\xi_1}, m_2 - \frac{1}{\xi_2}), -, (\frac{1}{\xi_1}, \frac{1}{\xi_2}) \right)$

4.2 MGF Based Effective Rate Analysis Framework

Although effective rate theory is very attractive in modelling the cross layer behaviour within the communication system, the study on individual fading channels is still very challenging. One of the main reason is that the analysis will involve multiple integrations of multivariate functions. It has been shown in the previous section that traditional PDF and integration based method requires delicate mathematical techniques and transforms between equalities. This common problem can be addressed via a general framework based on the MGF and H transform representation, which will be detailed as follows.

4.2.1 System Model

In this chapter, a MISO fading channel model is considered, where there are N transmit antennas and only one receive antenna as shown in Fig. 4.1. MISO fading scenarios are common in practice, which can also characterise the MIMO keyhole. The channels are assumed to be flat block fading, then the channel input-output relation can be written as

$$y = \mathbf{h}\mathbf{x} + n_0, \tag{4.19}$$

where $\mathbf{h} \in \mathbb{C}^{1 \times N}$ denotes the MISO channel vector, $\mathbf{x}$ is the transmit signal vector, and n_0 represents the complex additive white Gaussian noise with zero mean and variance N_0. It is assumed that the transmission power is uniformly allocated across the transmit antennas, and the channels are assumed to be arbitrarily correlated and not necessarily identically distributed.

The average transmit SNR is defined as $\rho = \frac{P}{BN_0}$, where P is the average transmit power of the system and B denotes the bandwidth. The channel state information is assumed to be only available at the receiver and the instantaneous channel power gain of the jth channel is defined by $\gamma_j = |h_j|^2$, where h_j is the jth component of the fading vector $\mathbf{h}$. In this part, we consider the maximum ratio transmission scheme, hence the instantaneous channel power gain at the receiver end can be

Figure 4.1: MISO system model.

defined by $\gamma_{\mathrm{end}} = \sum_{j=1}^{N} \gamma_j$. The joint MGF ϕ_{end} is defined by $\phi_{\mathrm{end}}(s) = \mathbb{E}\{e^{-s\sum_{j=1}^{N}\gamma_j}\}$. Specifically, if the channels are independent with each other, then the joint MGF $\phi_{\mathrm{end}}(s)$ can be expressed by the product of the MGF of individual channel's power gain as

$$\phi_{\mathrm{end}}(s) = \prod_{j=1}^{N} \phi_j(s), \tag{4.20}$$

where $\phi_j(s)$ is defined by $\phi_j(s) = \int_0^\infty e^{-s\gamma} f_j(\gamma) d\gamma$ and $f_j(\gamma)$ is the PDF of the jth channel's power gain.

4.2.2 Effective Rate Analysis Framework Based on MGF and H Transform

Effective rate is the maximum constant rate that a fading channel can support under statistical delay constraints, which can be written as [4]

$$R(\theta) = -\frac{1}{\theta TB} \ln \mathbb{E}\left\{e^{-\theta TC}\right\}, \quad \theta \neq 0, \tag{4.21}$$

where C represents the system's throughput during a single time block and T denotes the duration of a time block. The QoS exponent θ is given by [4]

$$\theta = -\lim_{z \to \infty} \frac{\ln \Pr\{L > z\}}{z}, \tag{4.22}$$

where L is the equilibrium queue-length of the buffer at the transmitter. When z is large, the buffer violation probability can be approximated by $\Pr\{L \geq z\} \approx e^{-\theta z}$. Correspondingly, if we denote the steady-state delay at the buffer by D_{delay}, then the probability of D_{delay} exceeding the maximum allowed delay $d_{\max}$ can be given by $\Pr\{D_{\text{delay}} \geq d_{\max}\} \approx e^{-\theta \delta d_{\max}}$, where δ is determined by the characters of the queueing system [98]. Hence the minimum required QoS exponent θ_0 is decided by the delay constraints, and in order to guarantee the delay performance, the QoS exponent θ has to satisfy the constraint $\theta \geq \theta_0$. Moreover, when $\theta_0 \to 0$, the effective rate approaches the Shannon's capacity [98].

When the transmitter sends uncorrelated circularly symmetric zero-mean complex Gaussian signals, the effective rate can be written as [98]

$$R(\theta) = -\frac{1}{A} \log_2 \mathbb{E}\left\{ \left(1 + \frac{\rho}{N}\gamma_{\text{end}}\right)^{-A} \right\}, \tag{4.23}$$

where $A = \theta T B / \ln 2$. Normally, (4.23) will involve multiple integrationss of multivariate functions, since the PDF of $\gamma_{\text{end}} = \sum_{j=1}^{N} \gamma_j$ is described by multivariate random variables in general cases. Yet by using the MGF instead of PDF and applying the H transform theory, the effective rate can be derived as follows.

Theorem 4 *The effective rate over arbitrary correlated and not necessarily identically distributed MISO fading channels can be given by*

$$R(\theta) = -\frac{1}{A} \log_2 \frac{1}{\Gamma(A)} \mathbb{H}\left\{ \phi_{\text{end}}(\frac{\rho s}{N}), \mathbf{O}_{\text{ER}}, \mathbf{P}_{\text{ER}} \right\}(1) \tag{4.24}$$

$$\equiv -\frac{1}{A} \log_2 \frac{N}{\rho \Gamma(A)} \mathbb{H}\left\{ \phi_{\text{end}}(s), \mathbf{O}_{\text{ER}}, \mathbf{P}_{\text{ER}} \right\}\left(\frac{N}{\rho}\right) \tag{4.25}$$

where $\mathbf{O}_{\text{ER}} = (1, 0, 0, 1)$ and $\mathbf{P}_{\text{ER}} = (1, 1, -, A-1, -, 1)$.

Proof *Using [1, eq.(28)] with the identity of [202, eq.(1.39)], [202, eq.(1.43)] and*

[202, eq.(2.22)] we have

$$H_{1,1}^{1,1}\left[\frac{\rho\sum_{j=1}^{N}\gamma_j}{N}\left|\begin{matrix}1-A,1\\0,1\end{matrix}\right.\right]=\int_0^\infty H_{0,1}^{1,0}\left[s\left|\begin{matrix}-\\A-1,1\end{matrix}\right.\right]H_{0,1}^{1,0}\left[\frac{\rho s\sum_{j=1}^{N}\gamma_j}{N}\left|\begin{matrix}-\\0,1\end{matrix}\right.\right]ds. \quad (4.26)$$

Substituting [202, eq.(1.43)] into (4.23) *and using* (4.26) *as well as [1, eq.(62)], the following equation can be obtained*

$$R(\theta)=-\frac{1}{A}\log_2\frac{1}{\Gamma(A)}\int_0^\infty H_{0,1}^{1,0}\left[s\left|\begin{matrix}-\\A-1,1\end{matrix}\right.\right]\phi_{end}\left(\frac{\rho s}{N}\right)ds. \quad (4.27)$$

Then use the definition of H transform (4.9), (4.24) *can be achieved. By changing the integral variate, an alternative form can be obtained as* (4.25).

Remark: The integral form of the effective rate of MISO fading channels can be obtained by using H transform definition and substituting the identity of $e^{-s}s^{A-1} = H_{0,1}^{1,0}\left[s\left|\begin{matrix}-\\(A-1,1)\end{matrix}\right.\right]$ [202, eq.(2.22)] into (4.24), which can be written as

$$R(\theta)=-\frac{1}{A}\log_2\frac{1}{\Gamma(A)}\int_0^\infty e^{-s}s^{A-1}\phi_{\text{end}}(\frac{\rho s}{N})ds. \quad (4.28)$$

Using the fact that $0 \leq \phi_{\text{end}}(s) \leq 1$, the integral can be proved to be absolutely converge. Hence the H transform in (4.24) and (4.25) exist.

We highlight that (4.24) and its equivalent (4.25) in H transform form are more attractive than the integral form in (4.28). On one hand, the MGF of most commonly used fading distributions can be written in Fox's H function format [2], which facilitates the application of Theorem 4. On the other hand, we can interpret the effective rate as the H transform of the PDF or MGF of the power gain by the parameter sequence $\mathbf{O}_{\text{ER}}$ and $\mathbf{P}_{\text{ER}}$ with some more manipulations. It has been studied in [1] that many important metrics such as ergodic capacity, error probability, error exponent can be expressed in similar H transform format with corresponding parameter sequences. Note that one merit of H transform is that the manipulation of parameter sequences only involves very basic arithmetic operations, hence the H transform representation can provide a unified, systematic and simple framework

for wireless performance analysis such as effective rate. In addition, in Section 4.3, we will show that for deriving MGF from the known PDF or analysing effective rate over SISO, i.n.i.d. and correlated scenarios, H transform is a very useful analysing tool.

In addition, compared to the PDF based approach, the MGF based approach has many advantages. First, the PDF based approach can be viewed as a special case of the MGF based approach. This is due to the fact that in the PDF based approach, the joint PDF has to be obtained in advance of further analysis. When the joint PDF is available, by using the relationship of PDF and MGF, it can be proved that the PDF based approach is involved in the case of $N = 1$ in the proposed MGF based approach. Second, in the i.n.i.d. scenarios, the joint MGF can be calculated by the product of the individual channels' MGF, which enables the analyses where the PDF based approach has difficulties [96, 221]. This feature makes the analysis more flexible and applicable to different and complex channel conditions.

4.3 Exact Effective Capacity Analysis over MISO Fading Channels

In this section, we will investigate the effective rate over specific i.n.i.d. and correlated channels. For the i.n.i.d. scenario, the effective rate over i.n.i.d. hyper Fox's H fading channels is derived, while the arbitrary correlated generalized K fading channels are considered for the correlated scenario.

4.3.1 Effective Rate over i.n.i.d. MISO Hyper Fox's H Fading Channels

As the derivation will involve the H transform of multivariate H function, we introduce the following lemma, which enables us to analyse the effective rate over i.n.i.d. MISO fading channels.

Lemma 1 *The H transform of the product of Fox's H functions can be given by*

$$\mathbb{H}\left\{\prod_{j=1}^{N} H\left[z, \mathbf{O}_j, \mathbf{P}_j\right], \mathbf{O}_{R'}, \mathbf{P}_{R'}\right\}(s) = s^{-\eta} H_{1,0}^{0,1}\left[\begin{array}{c} (1-\eta, \mathbf{1}_N) : \left(\dfrac{1}{s}, \mathbf{O}_j, \mathbf{P}_j\right)_{1,N} \\ -- \end{array}\right], \quad (4.29)$$

where $\mathbf{O}_{R'} = (1, 0, 0, 1)$, $\mathbf{P}_{R'} = (s^{1-\eta}, 1, --, \eta-1, --, 1)$, $s > 0$ *and* $\eta \geq 0$. *The short notation of multivariate Fox's H function* $H_{p_0, q_0}^{0, n_0}[\cdot]$ *is defined by* (4.4). *Specially, when* $N = 1$, (4.29) *reduces to*

$$\mathbb{H}\left\{u H_{p,q}^{m,n}\left[vz \left|\begin{array}{c} \mathbf{c}, \mathbf{C} \\ \mathbf{d}, \mathbf{D} \end{array}\right.\right], \mathbf{O}_{R'}, \mathbf{P}_{R'}\right\}(s) = u s^{-\eta} H_{p+1,q}^{m,n+1}\left[\dfrac{v}{s}\left|\begin{array}{c} (1-\eta, \mathbf{c}), (1, \mathbf{C}) \\ \mathbf{d}, \mathbf{D} \end{array}\right.\right]. \quad (4.30)$$

Proof *Using [222, eq.(2.1)] and the H transform definition* (4.9), (4.29) *can be obtained. Applying* (4.1), (4.30) *can be obtained. See [222] for details.*

It is straightforward that the H transform parameter $\mathbf{O}_{\mathrm{ER}}$ and $\mathbf{P}_{\mathrm{ER}}$ in Theorem 4 are special cases of $\mathbf{O}_{R'}$ and $\mathbf{P}_{R'}$ in Lemma 1. Hence with the MGF representation of γ_j and Lemma 1, the effective rate over i.n.i.d. MISO hyper Fox's H fading channel can be given by the following theorem.

Theorem 5 *If N channels of the MISO systems are mutually independent but not necessarily identical distributed and the instantaneous channel power gain γ_j of each channel follows hyper Fox's H fading, then the effective rate over i.n.i.d. MISO hyper Fox's H fading channels can be written as*

$$R(\theta) = -\dfrac{1}{A} \log_2 \dfrac{1}{\Gamma(A)} \sum_{k_1=1}^{K_1} \cdots \sum_{k_N=1}^{K_N} H_{1,0}^{0,1}\left[\begin{array}{c} (1-A, \mathbf{1}_N) : \left(\dfrac{\rho}{N}, \mathbf{O}_{\phi_{j,k_j}}, \mathbf{P}_{\phi_{j,k_j}}\right)_{1,N} \\ -- \end{array}\right]. \quad (4.31)$$

where $A = \frac{\theta T B}{\ln 2}$. *The notations K_j, $\mathbf{O}_{f_{j,k}}$ and $\mathbf{P}_{f_{j,k}}$ are the parameters satisfying a distributional structure such that $f_j(\gamma) \geq 0$ for all $\gamma \geq 0$ and $\int_0^\infty f_j(\gamma)d\gamma = 1$ [2].*

Proof *Substituting both* (4.17) *and* (4.20) *into Theorem 4, then using Lemma 1,* (4.31) *can be obtained.*

Remark: Theorem 5 is a good example of how to apply Theorem 4 to estimate the i.n.i.d. fading channels in a general way. As will be illustrated in 4.3.2, the equa-

tion (4.31) can be much simplified in some special cases and estimated thereafter. However, as presented in Section 4.4, the equation (4.31) using multivariate Fox's H function can be evaluated uniformly without the need for further reduction or simplification, which simplifies the analysis and calculation procedure in a general way.

Although many parameters have been used to describe the hyper Fox's H fading model, according to [2], most commonly used fading channels have very simple parameters. Another interesting observation is that the parameter sequences in (4.31) are the parameter sequences of the involved MGF functions without changes. By substituting corresponding parameters in specific channel scenarios, Theorem 5 is directly applicable to the analysis of effective rate over various i.n.i.d. fading channel conditions. In addition, the multivariate Fox's H function is a mathematical traceable function. There are studies on the property [209], reduction [223], expansion [224] and integrations [225] involving multivariate Fox's H functions, which can be used for the simplification in special cases and derivation in applications. Interested readers can refer to the references therein for further details.

4.3.2   Special Cases of i.n.i.d. Hyper Fox's H Fading Channels

We now investigate the effective rate over three special fading channels, namely i.n.i.d. Fox's H fading channels, i.i.d. Nakagami-m fading channels and SISO hyper Fox's H channel. On one hand, the scenarios considered in these special cases are very practical and widely used in the study of wireless system performance. On the other, these special cases give examples of how to apply the proposed theorems under specific channel conditions.

I.n.i.d. Fox's H fading channels

Fox's H fading model can be included as a special case in the hyper Fox's H fading model, which can characterize the fluctuations of the signal envelope due to mul-

tipath fading superimposed on shadowing variations [1]. Typical fading models describing both small-scale and large-scale fading effects, such as Rayleigh/lognormal, Nakagami-m/lognormal and Weibull/Gamma fading, are all special cases of the Fox's H fading model. This model is extensively used in the research of fading channels due to its clear physical meaning [1, 226]. Every fading effect in the Fox's H fading is defined based on the Fox's H variate, which uses the Fox's H function to describe the PDF of the random variate. Hence when defining a Fox's H variate, it only needs to define its parameter sequences in the format of $X \sim H(\mathbf{O}, \mathbf{P})$. For simplicity, the Fox's H function, Fox's H transform and their associated operation functions are exploited. These operations are all basic manipulations of the parameter sequences, which is beneficial in compositing different fading effects as well as deriving MGF from PDF as shown below.

For a single channel labelled with j (j=1,2,...,N), let the non-negative random variable Z_j and X_j be Fox's H variates [226] and describe the multipath fading effect and shadowing effect, such that $Z_j \sim H(\mathbf{O}_{Z_j}, \mathbf{P}_{Z_j})$ and $X_j \sim H(\mathbf{O}_{X_j}, \mathbf{P}_{X_j})$ [1].

If the multipath fading and shadowing effects are statistically independent, then the instantaneous channel power gain γ_j is again Fox's H variate $\gamma_j \sim H(\mathbf{O}_{f_j}, \mathbf{P}_{f_j})$, where $\mathbf{O}_{f_j} = \mathbf{O}_{Z_j} \boxplus \mathbf{O}_{X_j}$ and $\mathbf{P}_{f_j} = \langle 1, 2, -\frac{1}{2} | \mathbf{P}_{Z_j} \boxplus \mathbf{P}_{X_j}$. The elementary operation $\langle \cdot | \mathbf{P}$ and convolution operation $\boxplus$ are defined in Table 4.2.

The MGF of the instantaneous channel power gain γ_j can be written as

$$\phi_j(s) = H[s, \mathbf{O}_{\phi_j}, \mathbf{P}_{\phi_j}], \tag{4.32}$$

with

$$\begin{cases} \mathbf{O}_{\phi_j} = & \mathbf{O}_{\text{MGF}} \boxdot \mathbf{O}_{f_j} \\ \mathbf{P}_{\phi_j} = & \mathbf{P}_{\text{MGF}} \boxdot \mathbf{P}_{f_j} \end{cases} \tag{4.33}$$

where Mellin operation $\boxdot$ is defined in Table 4.2. Note the MGF of Fox's H fading model is represented by only one Fox's H function, it coincides as a special case of hyper Fox's H fading model with the parameter $K_j = 1$ in (4.14). Then the effective

rate over i.n.i.d. MISO Fox's H fading channels can be given by

$$R(\theta) = -\frac{1}{A} \log_2 \frac{1}{\Gamma(A)} H_{1,0}^{0,1} \left[\begin{array}{c} (1-A, \mathbf{1}_N) : \left(\frac{\rho}{N}, \mathbf{O}_{\phi_j}, \mathbf{P}_{\phi_j} \right)_{1,N} \\ -\!- \end{array} \right], \qquad (4.34)$$

where $\mathbf{O}_{\phi_j}$ and $\mathbf{P}_{\phi_j}$ are defined in (4.33).

This special case gives a good example of how to derive the effective rate from the known fading parameters of the specific fading channel via the proposed method and H transform operations. It should also be noticed that although several H transform operations are used in the deriving procedure, they only involve some basic arithmetic manipulations of the parameters, such as addition, subtraction, multiplication, division, sequence changes of the parameters as well as the combination of such operations. One can readily obtain the more familiar yet tedious representation by expanding these operations described in Table 4.2.

I.i.d. Nakagami-m fading channels

Nakagami-m fading model is one of the most widely used fading models in the performance analysis of wireless communication systems, which includes one-sided Gaussian and Rayleigh fading model as special cases. It has been recommended by IEEE Vehicular Technology Society Committee on Radio Propagation for theoretical studies of fading channels [193]. For a single channel, if the instantaneous channel power gain follows the Nakagami-m distribution, then $\gamma_j \sim H(\mathbf{O}_j, \mathbf{P}_j)$, where $\mathbf{O}_j = (1, 0, 0, 1)$ and $\mathbf{P}_j = (\frac{\hat{m}}{\Gamma(\hat{m})}, \hat{m}, -\!-, \hat{m}-1, -\!-, 1)$ [1]. The symbol $\hat{m}$ denotes the parameter associated to Nakagami-m fading model. Using (4.32), the MGF can be given by

$$\phi_j(s) = H[s, \mathbf{O}_{\phi_j}, \mathbf{P}_{\phi_j}], \qquad (4.35)$$

where $\mathbf{O}_{\phi_j} = (1, 1, 1, 1)$ and $\mathbf{P}_{\phi_j} = (\frac{1}{\Gamma(\hat{m})}, \frac{1}{\hat{m}}, 1-\hat{m}, 0, 1, 1)$. Substituting these parameters into Theorem 5 as well as the relation connecting generalized Lauricella function and multivariate Fox's H function [202, A.31], then using the reduction formulae for the multivariate hypergeometric function [227, eq.(14)], the effective rate expres-

sion can be simply represented by generalized hypergeometric functions $_pF_q[\cdot]$ [198, eq.(16.2.1)] as follows

$$R(\theta) = -\frac{1}{A} \log_2 {}_2F_0\left[A, \hat{m}N, -\frac{\rho}{\hat{m}N}\right]. \tag{4.36}$$

Note that using the identity of [198, eq.(13.6.21)], the expression given in (4.36) coincides with [10, eq.(7)], which supports the validation of our derivation.

SISO hyper Fox's H fading channel

SISO fading channel is included as a special case of i.n.i.d. channel, where only one channel is considered, i.e. $N = 1$. Under SISO hyper Fox's H fading channel condition, the MGF can be expressed by the sum of univariate Fox's H functions as $\phi_{\text{end}}(s) = \sum_{k=1}^{K} H[s, \mathbf{O}_{\phi_k}, \mathbf{P}_{\phi_k}]$, where $\mathbf{O}_{\phi_k} = (m_{\phi_k}, n_{\phi_k}, p_{\phi_k}, q_{\phi_k})$ and $\mathbf{P}_{\phi_k} = (u_{\phi_k}, v_{\phi_k}, \mathbf{c}_{\phi_k}, \mathbf{d}_{\phi_k}, \mathbf{C}_{\phi_k}, \mathbf{D}_{\phi_k})$. In this case, using (4.24) in Theorem 1 and (4.30) in Lemma 1, the effective rate expression can be directly given by

$$R(\theta) = -\frac{1}{A} \log_2 \sum_{k=1}^{K} \frac{u_{\phi_k}}{\Gamma(A)} H^{m_{\phi_k}, n_{\phi_k}+1}_{p_{\phi_k}+1, q_{\phi_k}} \left[\frac{v_{\phi_k}}{\rho}\left|\begin{matrix}(1-A, \mathbf{c}_{\phi_k}), (1, \mathbf{C}_{\phi_k})\\ \mathbf{d}_{\phi_k}, \mathbf{D}_{\phi_k}\end{matrix}\right.\right]. \tag{4.37}$$

Note that (4.37) can be also obtained by substituting $N = 1$ into (4.31). It can be verified that (4.37) coincides with [199, eq.(7)], which supports the validation of the derivation. Also in this special case, the effective rate representation in (4.37) only involves univariate Fox's H functions.

4.3.3   Effective Rate over Arbitrary Correlated Generalized K Fading Channels

If the transmit antennas are sufficiently separated in space, it is reasonable to assume independence between the received signals from different antennas. Yet this assumption may be crude for some systems, where the correlation between antennas is a more practical scenario. Hence in this part, we investigate the effective rate over the arbitrary correlated generalized K fading channels.

Generalized K fading model has been first introduced in [228] to model the intensity of radiatio scattered with a non-uniform phase distribution (weak-scatterer regime), which accounts for the composite effect of Nakagami-m multipath fading and gamma shadowing. Here we assume the multipath fading effect and shadowing effect are independent of each other, which are represented by random variable ω_j and ξ_j, respectively. Let $\gamma_j = \xi_j \omega_j$ with $j = 1, 2, \ldots, N$ and assume $\xi_j (j = 1, 2, \ldots, N)$ are i.i.d. Gamma-distributed random variables with parameter m_1, while $\omega_j (j = 1, 2, \ldots, N)$ are identically distributed with arbitrary correlation matrix $\boldsymbol{\Sigma}$ and parameter m_2. The elements of the correlation matrix are given by $\Sigma_{i,j} = 1$ for $i = j$ and $\Sigma_{i,j} = r_{i,j}$ for $i \neq j$, where $0 \leq r_{i,j} < 1$ is the correlation coefficient between channel i and j. Using [103, eq.(9)] as well as the relation between Meijer's G function and Fox's H function [202, eq.(1.112)], the joint MGF of $\boldsymbol{\gamma} = [\gamma_1, \gamma_2, \ldots, \gamma_N]$ can be given by

$$\phi_{\boldsymbol{\gamma}}(s) = \frac{\det|\mathbf{W}|^{m_1}}{\Gamma(m_1)[\Gamma(m_2)]^N} \sum_{k_1, k_2, \ldots, k_{N-1}=0}^{\infty} \left(\prod_{l=1}^{N-1} \frac{|p_{l,l+1}|^{2k_l}}{k_l! \Gamma(m_1 + k_l)} \right) \prod_{j=1}^{N} \mathbf{H}[s, \mathbf{O}_j, \mathbf{P}_j], \quad (4.38)$$

where $\mathbf{O}_j = (1, 2, 2, 1)$ and $\mathbf{P}_j = (p_{j,j}^{-m_1-\alpha_j}, \frac{1}{p_{j,j} m_1 m_2}, (1 - m_1 - \alpha_j, 1 - m_2), 0, (1, 1), 1)$ with $\alpha_j = k_1$ for $j = 1$, $\alpha_j = k_{N-1}$ for $j = N$ and $\alpha_j = k_{j-1} + k_j$ for $j = 2, 3, \ldots, N-1$. $\mathbf{W}$ is the inverse of $\boldsymbol{\Sigma}$, whose elements are denoted by $p_{i,j}$. By substituting (4.38) into Theorem 4 and applying Lemma 2, the effective rate of generalized K fading channels with arbitrary correlation matrix can be given by

$$R(\theta) = -\frac{1}{A} \log_2 \frac{\det|\mathbf{W}|^{m_1}}{\Gamma(A)\Gamma(m_1)[\Gamma(m_2)]^N} \sum_{k_1, k_2, \ldots, k_{N-1}=0}^{\infty} \left(\prod_{l=1}^{N-1} \frac{|p_{l,l+1}|^{2k_l}}{k_l! \Gamma(m_1 + k_l)} \times \right. \quad (4.39)$$
$$\left. H_{1,0}^{0,1} \left[\begin{matrix} (1-A, \mathbf{1}_N) : \left(\frac{\rho}{N}, \mathbf{O}_j, \mathbf{P}_j \right)_{1,N} \\ — \end{matrix} \right] \right).$$

Note that if γ_j are independent with each other, then $\mathbf{W} = \mathbf{I}$ and (4.39) reduces to the case of i.i.d. generalized K fading channels as

$$R(\theta) = -\frac{1}{A} \log_2 \frac{1}{\Gamma(A)[\Gamma(m_1)\Gamma(m_2)]^N} H_{1,0}^{0,1} \left[\begin{matrix} (1-A, \mathbf{1}_N) : \left(\frac{\rho}{N}, \mathbf{O}_j, \mathbf{P}_j \right)_{1,N} \\ — \end{matrix} \right] \quad (4.40)$$

where the operator sequence reduces to $\mathbf{O}_j = (1, 2, 2, 1)$ and $\mathbf{P}_j = (1, \frac{1}{m_1 m_2}, (1 - m_1, 1 - m_2), 0, (1, 1), 1)$.

4.4 Asymptotic Effective Rate Analysis over MISO Fading Channels

By substituting the parameters corresponding to the individual channels, we can obtain the analytical expression for the effective rate over hyper Fox's H fading channels through Theorem 5. The numerical calculations for the general form of multivariate H function is not available in software such as Matlab. Thus in this section, we propose a simple asymptotic approximation method, which provides an easy way to evaluate the representations presented in Section 4.3. The derived asymptotic approximations also provide a useful tool for other studies where multivariate functions are involved.

We commence on the following lemma.

Lemma 2 *If let* $E(Q) = \int_Q^\infty f(z)dz$ *denote the truncation error and* $E(M) = \int_0^Q f(z)dz - \sum_{\ell=0}^M f(\ell)$ *denote the discretization error, then for* $0 \ll Q \ll M$ *the following relation can be obtained*

$$
\mathbb{H}\left\{\phi_{\text{end}}(\frac{\rho s}{N}), \mathbf{O}_{ER}, \mathbf{P}_{ER}\right\}(1) \equiv \int_0^\infty e^{-s} s^{A-1} \phi(\frac{\rho s}{N}) ds
$$
$$
= \left(\frac{Q}{M}\right)^A \sum_{\ell=1}^M \ell^{A-1} e^{-\frac{\ell Q}{M}} \phi\left(\frac{\ell Q \rho}{MN}\right) + E(Q) + E(M),
$$

(4.41)

where $\mathbf{O}_{ER} = (1, 0, 0, 1)$ *and* $\mathbf{P}_{ER} = (1, 1, —, A-1, —, 1)$ *are effective rate parameter sequences defined in Theorem 4. The truncation error* $E(Q)$ *and discretization error* $E(M)$ *can be given by*

$$
E(Q) = \int_Q^\infty e^{-s} s^{A-1} \phi(\frac{\rho s}{N}) ds,
$$

(4.42)

$$
E(M) = -\frac{Q^3}{12M^2} \frac{\partial^2 e^{-s} s^{A-1} \phi(\frac{\rho s}{N})}{\partial s^2}\bigg|_{s=\xi}, \quad 0 < \xi < Q,
$$

(4.43)

and

$$\lim_{Q \to \infty} E(Q) = 0, \lim_{M \to \infty} E(M) = 0. \tag{4.44}$$

Proof *Using the H transform definition* (4.9)*, the integration form can be obtained. First we prove that the integration can be truncated. Use the fact* $\frac{\partial \phi(s)}{\partial s} < 0$ *for* $s \in [0, \infty)$*, the truncation error* $E(Q)$ *can be upper bounded by*

$$E(Q) = \int_Q^\infty e^{-s} s^{A-1} \phi_{\text{end}}(\frac{s}{N}) ds \leq \Gamma(A, Q), \tag{4.45}$$

where $\Gamma(A, Q)$ *is the incomplete gamma function [229, eq.(8.350.2)]. Since the integrands in* (4.45) *are all positive for* $s \in [0, \infty)$*, then* $E(Q) \geq 0$*. Apply the Trapezoidal rules [198, eq.(3.5.2)] to evaluate the finite integration, then* (4.41) *and* (4.43) *can be obtained. Follow the limitation rules, we get* (4.44)*.*

By applying Lemma 2, the multivariate Fox's H function involved in the effective rate calculation can be approximated using the following theorem.

Theorem 6 *The special series multivariate Fox's H function can be approximated by*

$$H_{1,0}^{0,1} \left[\begin{matrix} (1-\eta, \mathbf{1}_N) \\ \text{---} \end{matrix} : \left(\frac{\rho}{N}, \mathbf{O}_j, \mathbf{P}_j \right)_{1,N} \right] \approx \left(\frac{Q}{M} \right)^\eta \sum_{\ell=1}^M \ell^{\eta-1} e^{-\frac{\ell Q}{M}} \prod_{j=1}^N H \left[\frac{\ell Q \rho}{MN}, \mathbf{O}_j, \mathbf{P}_j \right], \tag{4.46}$$

providing that each $H[s, \mathbf{O}_j, \mathbf{P}_j]$ *satisfies the convergence conditions of MGF functions,* $\eta \geq 0$ *and* $0 \ll Q \ll M$*.*

Proof *Applying Lemma 2 to Lemma 1,* (4.46) *can be obtained.*

Remark: Theorem 6 shows that the special multivariate Fox's H function can be evaluated by the product of univariate Fox's H functions, where there are already methods for the evaluation of univariate Fox's H function in numerical software like Matlab. It should be noticed that although we limit the conditions of each univariate Fox's H function involved in (4.46) to be satisfying the MGF functions' convergence conditions, in fact the conditions can be further relaxed, for example when each

univariate Fox's H function approaches 0 as $s \to \infty$ and the second partials are bounded for all non-negative real number s.

Hence in this way, we can get the general approximation formula for the MGF based approach in the following theorem.

Theorem 7 *The effective rate over arbitrary correlated and not necessarily identical MISO fading channels can be approximated by the finite summation of the MGF as the following equation*

$$R(\theta) \approx \frac{\log_2 \Gamma(A)}{A} - \frac{1}{A} \log_2 \left(\frac{Q}{M} \right)^A \sum_{\ell=1}^{M} \ell^{A-1} e^{-\frac{\ell Q}{M}} \phi_{\text{end}}(\frac{\ell Q \rho}{MN}), \qquad (4.47)$$

where $0 \ll Q \ll M$ and the truncation error as well as the discretization error is given by (4.42) and (4.43).

Proof *Substituting (4.41) into (4.28) and after some simple algebra manipulation, the desired result can be obtained.*

Compared to the exact representation (6) proposed in Theorem 1, the approximated representation (31) in Theorem 4 is also very attractive. This representation only involves the summation of finite terms, which may help to reduce the computational complexity at the cost of accuracy. But as shown in Section 4.5, the asymptotic approximation converges quickly since the exponential fading form is involved, where $Q = 15$ and $\frac{M}{Q} = 300$ provides a good fit to both analytical and simulation results.

Remark: Applying Theorem 6, the effective rate of i.n.i.d. MISO hyper Fox's H fading channels given by (4.31) in Theorem 5 can be approximated as

$$R(\theta) \approx - \frac{1}{A} \log_2 \frac{1}{\Gamma(A)} \sum_{k_1=1}^{K_1} \cdots \sum_{k_N=1}^{K_N} \left(\frac{Q}{M} \right)^A \sum_{\ell=1}^{M} \ell^{A-1} e^{-\frac{\ell Q}{M}} \prod_{j=1}^{N} H \left[\frac{\ell Q \rho}{MN}, \mathbf{O}_{\phi_{j,k_j}}, \mathbf{P}_{\phi_{j,k_j}} \right].$$
$$(4.48)$$

4.5 Numerical Results

In order to verify the proposed MGF approach and approximation method in this section, simulations under different fading scenarios are carried out, where the pa-

rameters are listed in Table 4.4. Without loss of generality, the duration of a time block $T = 1$ ms and the bandwidth of the system $B = 1$ kHz have been assumed. For each simulated scenario, we use Monte Carlo method and 10^7 trails for simulating each channel condition with unit power. Since the parameters in hyper Fox's H fading model have physical meanings only when specific fading models are considered, generalized K fading model and Weibull/Gamma fading model have been used as examples to validate the proposed MGF method, which are all special cases of hyper Fox's H fading model. These two fading models are very practical, which can characterize large scale and small scale fading effect simultaneously, and include many practical fading models as special cases, such as Rayleigh, Nakagami-m and Weibull fading model. These two fading models have been proved to fit measurements in various channel conditions and extensively used in the study of wireless communication systems [228, 230].

For a single channel, the instantaneous channel power gain parameter sequences for generalized K fading model can be given by [1, Table IX] $\mathbf{O}_\gamma = (2, 0, 0, 2)$ and $\mathbf{P}_\gamma = (\frac{\hat{m}}{\psi\Gamma(\hat{m})\Gamma(1/\psi)}, \frac{\hat{m}}{\psi}, —, (\hat{m} - 1, \frac{1}{\psi} - 1), —, \mathbf{1}_2)$, where multipath fading severity parameter $\hat{m} \geq \frac{1}{2}$ and shadowing figure $\psi \in [0, 2]$. Especially, when $\psi = 0$, the generalized K fading reduces to the Nakagami-m fading. The instantaneous channel power gain parameter sequences for Weibull/Gamma fading model are [1, Table IX] $\mathbf{O}_\gamma = (2, 0, 0, 2)$ and $\mathbf{P}_\gamma = (\frac{\Gamma(1+2/\beta)}{\psi\Gamma(1/\psi)}, \frac{\Gamma(1+2/\beta)}{\psi}, —, (\frac{1}{\psi} - 1, 1 - \frac{2}{\beta}), —, (1, \frac{2}{\beta}))$, where the fading severity parameter $\beta > 0$ and shadowing figure $\psi \geq 0$. This model reduces to Weibull fading when $\psi = 0$ and includes K fading as a special case when $\beta = 2$. The exact analytical effective rate representation for i.n.i.d. conditions can be directly obtained by substituting the above parameters into the proposed MGF based approach in Theorem 5. The univariate Fox's H function is evaluated using the method proposed in [231]. When multivariate Fox's H functions are involved, they are estimated using the proposed approximation method in Theorem 6 while the analytical values are evaluated using the numerical method in [232].

The i.i.d. conditions are special cases in i.n.i.d. conditions. In order to verify the proposed approximation methods with existing results, the analytical results are estimated using [10, eq.(53)] and the parameters used in [10] are exploited. When

Table 4.4: Parameters for different fading scenarios

| Scenarios		Fading Model	Parameters
SISO	$N=1$	Weibull/Gamma	$\beta=3, \; \psi=1$
I.i.d.	$N=9$	Generalized K	$\hat{m}=2, \psi=\frac{1}{1.45}$
I.n.i.d.	$N=2$	Weibull/Gamma	$\beta=3, \; \psi=1$
		Weibull/Gamma	$\beta=2, \; \psi=0.5$
	$N=3$	Weibull/Gamma	$\beta=3, \; \psi=1$
		Weibull/Gamma	$\beta=2, \; \psi=0.5$
		Generalized K	$\hat{m}=2, \psi=0.5$
Correlated	$N=2$	Correlated generalized K	$\hat{m}=1, \psi=1$ r=0, 0.5, 0.8
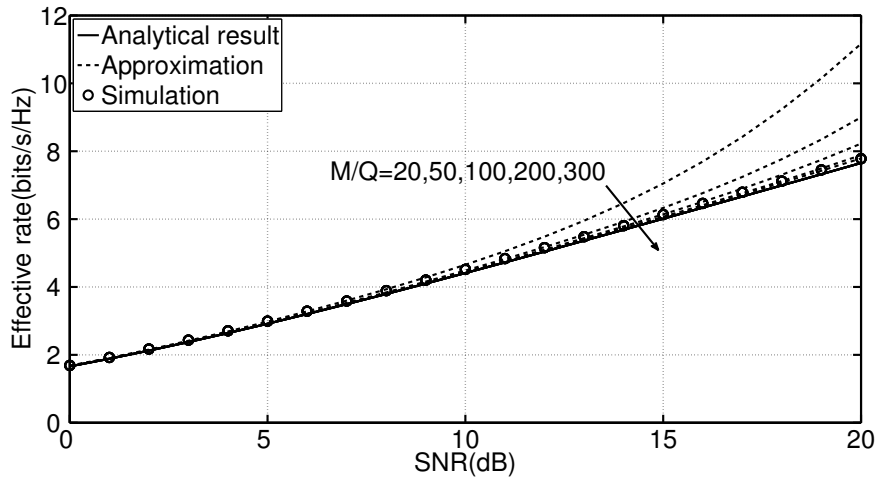
Figure 4.2: Effective rate using different discretization and truncation ratio $\frac{M}{Q}$ compared with analytical results and simulation results in i.i.d. generalized K fading scenario.

approximating the effective rate using (4.47) in Theorem 7, the truncation parameter Q can be chosen by a small number in practice, which is due to the fact that the estimated integration involving exponential fading terms. From the simulation experiments, we find that $Q = 15$ is good enough for the estimation purpose, where a further increase of the value of Q will not give more accurate results. By increasing the ratio of the discretization parameter M and the truncation parameter Q, the approximation approaches the exact value, as shown in Fig. 4.2. It is shown that when $M/Q \geq 200$, the approximations are tight with the simulation as well as analytical results, which supports the validation of the proposed approximation method. In the following part, M/Q is selected as 300 as default, which gives good accuracy as well as low computational complexity.
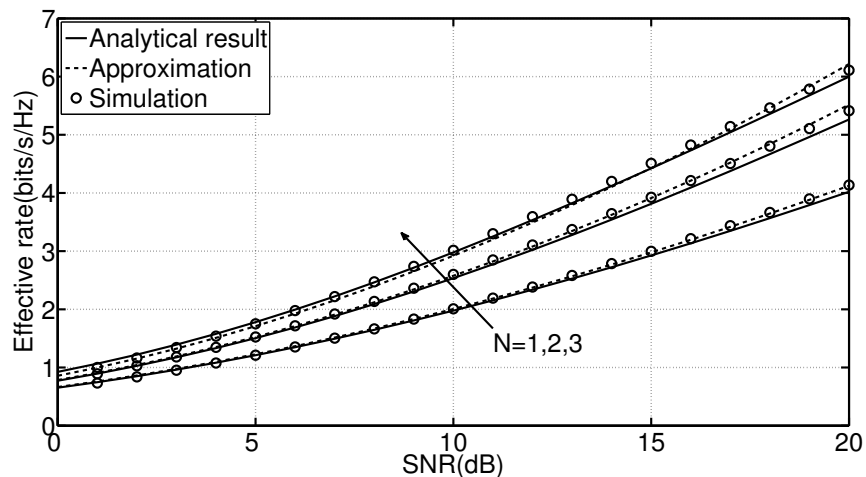

Figure 4.3: Effective rate over SISO and i.n.i.d. MISO fading channels, where parameters for each channel are listed in Table 4.4.

In order to test the performance of the proposed methods under i.n.i.d. MISO fading channel conditions, different fading parameters and channel numbers are used, which are detailed in Table 4.4. For different scenarios, it is shown in Fig. 4.3 that the approximations are sufficiently tight across a wide range of SNR (in this case from 0 to 20 dB) under different scenarios. Since the effective rate over i.n.i.d. MISO fading channels can be estimated based on the product of the individual channel's MGF as presented in Theorem 7, the proposed MGF based approach is flexible and easy to extend.

Effective rate under different QoS exponent θ is the most interested parameter
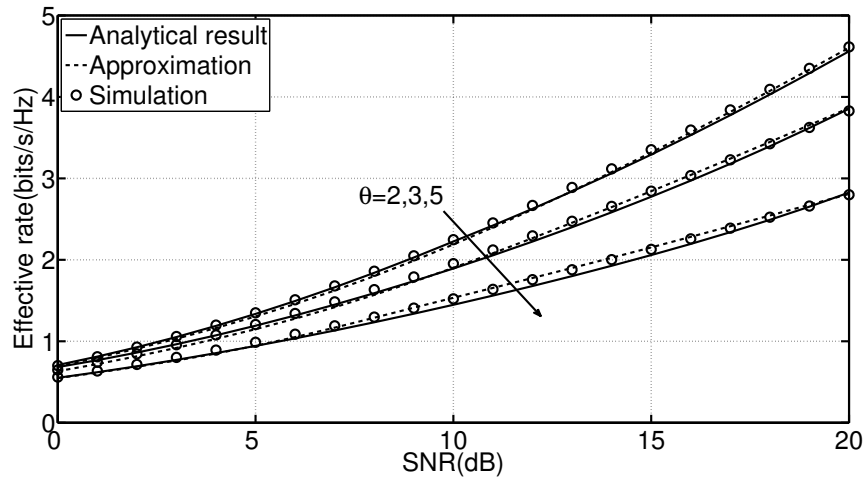
Figure 4.4: Effective rate under different QoS exponent θ in i.n.i.d. Weibull/Gamma fading channels with $N = 2$.

in the applications, since it can be used as a metric in the QoS provisioning schemes. Larger QoS exponent θ corresponds to tighter delay constraint. As shown in Fig. 4.4, the maximum available data rate drops with the increase of QoS exponent θ, in order to guarantee the system's delay performance. Also when the SNR gets higher, the same increase of θ results in a greater drop of the effective rate.
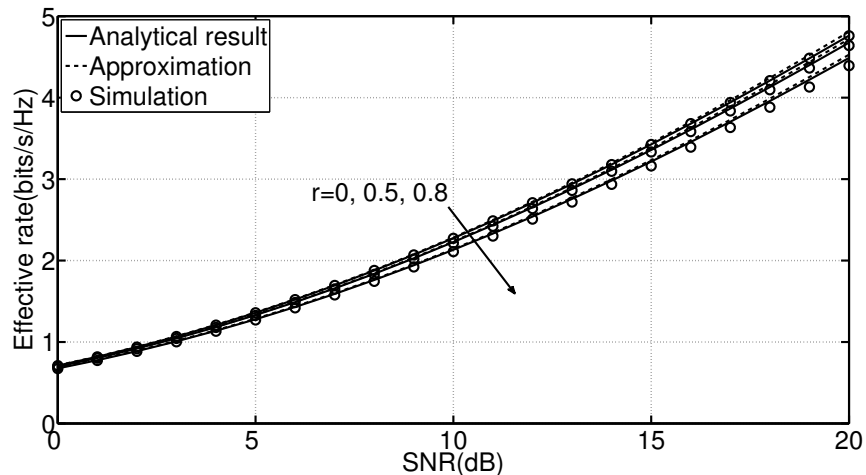
Figure 4.5: Effective rate under correlated generalized K fading channel with different correlation coefficients $r = 0, 0.5, 0.8$ and $N = 2$, where approximation results are compared to analytical results and simulation results.

Furthermore, the effective rate over correlated generalized K fading channels is investigated, whose channel fading parameters are given in Table 4.4. It is shown

in Fig. 4.5 that the effective rate reduces as the correlation coefficient r increases from 0 to 0.8, where the case of $r = 0$ corresponds to i.i.d. generalized K fading channels.

4.6 Concluding Remarks

In this chapter, a new MGF based approach for the effective rate analysis over arbitrary correlated and not necessarily identical MISO fading channels using H transform representation has been proposed. The proposed framework has simplified the representation and analyses of effective rate in a unified way. The effective rate over i.n.i.d. hyper Fox's H fading channels as well as arbitrary correlated generalized K fading channels has been investigated, which has given good demonstrations on the application of the proposed MGF based approaches. Based on these results, the effective rate over many practical fading channels can be obtained by simply substituting the corresponding parameters instead of the cumbersome case-by-case integration procedure.

In addition, approximations have been given for the MGF based effective rate representation as well as the effective rate representation over i.n.i.d. MISO hyper Fox's H fading channels, where both the truncation error and discretization error have been studied. These results have been illustrated readily applicable to practical fading channels, such as Weibull/Gamma and generalized K fading channels. The simulations have been used to show the validation and accuracy of the proposed analytical and approximation methods. These results have extended and complemented the existing research of effective rate analysis.

We highlight that, as various metrics in wireless communication networks can be represented in similar H transform format and multivariate Fox's H functions have the possibility to characterize the statistical properties of both independent and correlated channels, the obtained results will be also valuable to the performance analyses of other statistical metrics in wireless systems.

Chapter 5

On Statistical Power Grid Observability Performance under Communication Constraints

Phasor Measurement Units (PMUs) can provide real-time power grid measurements via advanced power system and communication technologies, which improves the performance of power grid monitoring and control [233]. The PMUs are usually installed at selected buses in the power grid, which can provide measurements of both voltage and current phasor at that bus. At the same time, PMUs also form a communication network, which is synchronised by the Global Positioning Satellite (GPS). From the aspect of power grid observability, PMUs are not only the basis of various smart grid applications, but also an important component for the guarantee of normal power system operation. It has been proposed that maintaining certain degrees of observability redundancy will be beneficial in case of PMU failures.

In this chapter, the power system observability performance under communication constraints is studied. The major contributions are the following,

- We propose a model to account for the power grid observability performance under constraint communication resources, which considers both power system and wireless communication system aspects.

- We propose to assess the performance of the power system that deploys PMUs

connected with wireless links affected by fading in statistical terms rather than in deterministic terms.

- We propose three algorithms to improve the power grid observability performance via the optimal communication resource allocation, which are system observability redundancy algorithm, bus observability sensitivity algorithm and grid observable probability algorithm.

The rest of this chapter is structured as follows. In Section 5.1, the PMU based power system observability has been briefly reviewed, while the power system observability under communication constraints is studied and modelled in Section 5.2. Effective capacity theory is studied in Section 5.3, which provides a communication system cross layer analysis framework to fill the research gap between the statistical power system observability performance analysis and the constraint communication resources. Then three power system observability performance improvement algorithms are proposed in Section 5.4, while case studies are performed in Section 5.5. Finally, conclusions are drawn in Section 5.6.

5.1 PMUs Based Power System Observability

The deployment of PMUs has enabled many potential real-time applications, such as state estimation, adaptive relaying and voltage instability enhancement. Compared to traditional measurement methods, PMUs are more versatile and they can provide more timely information about the power grid. A typical IEEE 14 bus power system is illustrated in Fig. 5.1. When a PMU is installed at a bus in the power grid, it can provide the phasor voltage of that bus and all or part of the outgoing current phasor information on the branches connected to that bus. This is determined by the measuring terminal configuration of the PMUs. In this chapter, it is assumed that a PMU will measure the bus voltage phasor and all connected branch current phasors.

For an N bus power system, let the vector $\mathbf{X} = \{x_1, x_2, \ldots, x_N\}^T$ denote the
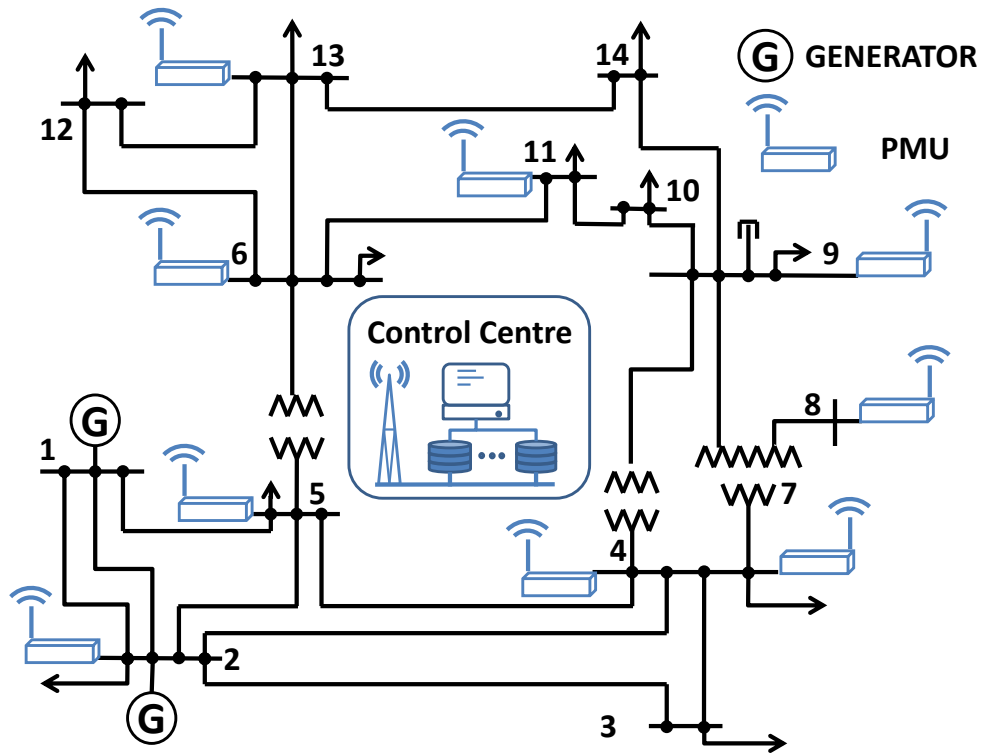
Figure 5.1: IEEE 14 bus power system with 9 PMUs.

PMU installation vector, where $(\cdot)^T$ is transpose operator. Its elements are given by

$$x_i = \begin{cases} 1, & \text{if a PMU is installed at bus } i, \\ 0, & \text{otherwise.} \end{cases} \tag{5.1}$$

In addition, we assume that there are K PMUs in total, which are labelled as PMU_k, where $k = 1, 2, \ldots, K$ and $K \leq N$. It is easy to verify that $K = \sum_{i=1}^{N} x_i$.

For a given power grid, it is assumed that the topology of the grid network is a prior. That is, the elements of binary network connectivity matrix $\mathbf{H}$ are known and given by

$$h_{ij} = \begin{cases} 1, & \text{if bus } i \text{ and } j \text{ are connected or } i = j, \\ 0, & \text{otherwise.} \end{cases} \tag{5.2}$$

A bus will be observable if at least one PMU is placed on that bus or any bus

incident to it [234]. Hence, we can define the bus observability vector **b** as

$$\mathbf{b} = \mathbf{HX},\tag{5.3}$$

where each element b_i in the bus observability vector **b** indicates the number of PMUs connected to or located at bus i, we have

$$b_i = \sum_{j=1}^{N} h_{ij}x_j.\tag{5.4}$$

From (5.4), we see that the power grid will be observable if $\mathbf{b} \geq \mathbf{1}_N$, i.e. $b_i \geq 1, \forall i$. If $b_i = 0$ for some i, the associated bus will not be observable. It can be seen that this grid observability model considers both power grid topology and PMU installation features. In the next section, a modified model will be proposed with the consideration of communication constraints.

A further discussion on the physical meanings on the observability is provided here. The observability is a different metric to evaluate the power system performance other than probability. By (5.3) and (5.4), it is clear that the observability is defined based on expectation other than probability.

To be more specific and to help understand the meaning of observability as well as redundancy, a simple example is given as follows. Bus i is being observed by two PMUs, namely PMU_A and PMU_B, while bus j is being observed by one PMU PMU_C. Then the following definition can be obtained, where the probability of bus i being observed can be given by

$$Pob_i = \Pr\{A \cup B\} = \Pr\{A\} + \Pr\{B\} - \Pr\{A\} * \Pr\{B\},\tag{5.5}$$

where $\Pr\{A\}$ and $\Pr\{B\}$ denote the probability that bus i can be observed by PMU_A and PMU_B, respectively. Also in the (5.5), it is assumed that $\Pr\{A\}$ and $\Pr\{B\}$ are independent. Similarly, the probability of bus j being observed can be given by

$$Pob_j = \Pr\{C\}.\tag{5.6}$$

where $\Pr\{C\}$ denote the probability that bus j can be observed by PMU_C

Here two cases are considered. The first case is all PMUs are able to provide 100% success in communication, which leads to the following results by applying probability analysis,

$$Pob_i = 1 + 1 - 1 \times 1 = 1, \text{ and } Pob_j = 1. \tag{5.7}$$

Another case is that $\Pr\{A\} = 0.8$, $\Pr\{B\} = 0.5$ and $\Pr\{C\} = 0.9$, which leads to the following results by applying probability analysis,

$$Pob_i = 0.8 + 0.5 - 0.8 \times 0.5 = 0.9, \text{ and } Pob_j = 0.9. \tag{5.8}$$

It can be seen that under these two discussed cases, both bus i and j have exactly the same probability of being observed, but apparently the probability fails to indicate which is better.

Hence instead, the notion of observability is used as an alternative metric of probability, which is defined in (5.3). It is clear that the redundancy is essentially defined based on expectation instead of probability. So the expected observability for bus i is given by

$$\begin{aligned} b_i =& 2 \times \Pr\{A\} \times \Pr\{B\} + 1 \times \Pr\{A\} \times (1 - \Pr\{B\}) \\ &+ 1 \times (1 - \Pr\{A\}) \times \Pr\{B\} + 0 \times (1 - \Pr\{A\}) \times (1 - \Pr\{B\}) \\ =& 2, \end{aligned} \tag{5.9}$$

while for bus j, the expected observability can be given as follows,

$$b_j = 1 \times \Pr\{C\} + 0 \times (1 - \Pr\{C\}) = 1. \tag{5.10}$$

And similarly, in the second case, it can be obtained that

$$b_i = 1.3 \text{ and } b_j = 0.9. \tag{5.11}$$

Please note that the physical meaning of the value b_i is that, from the statistical

viewpoint, the bus i is being observed by a number of b_i PMUs. It is from this aspect that the redundancy is helpful to improve the power system's observability performance. Hence in the sense of mathematical expectations, the observability indicates that bus i in both cases can be observed by more PMUs than the bus j.

A further notice on the difference between observability and probability can be given from the information provided by the PMU measurements. In the probability framework, for example in the above cases, the scenario that both PMUs provide measurements is treated the same as the case where only one PMU provides measurements. But actually the extra PMU information can not only provide a redundancy for the observability, but also protect the power grids from data injection attacks [235].

Hence as a concluding remark, the observability and probability are two metrics focusing on different aspects of performance, just like the expectation and probability in mathematics. They both have their advantages and disadvantages in the performance analysis. In this study, the focus is placed on the observability performance from the angle of redundancy.

5.2 Grid Observability under Communication Constraints

In practical power systems, the system statuses, such as currents, voltages and angles, would vary with time. Hence the real-time grid status monitoring of the power grid has a stringent latency requirement. To maintain real-time performance, each measurement from the PMUs will be valid within a delay bound $D_{\max}$. If the measurement packages have been delayed longer than $D_{\max}$, then these measurements can not be used, which results in a compromised power grid status monitoring performance. The latency has many contributors, such as processing overheads and transmission delays, which are usually fixed values for a considered scenario. However, within wireless communication systems, the latency resulting from the channel fading effect usually varies with time and it is hard to bound. In ideal cases, the communication systems should be designed to provide a 100 percent guarantee that

the communication delay d_k of PMU_k is smaller than $D_{\max}$. However, in practice, it has been identified that it is not feasible to provide a deterministic delay bound for the communication system in most fading channel environment [112]. Hence instead, we consider the probability $0 \leq p_k \leq 1$ to guarantee the communication delay within a certain maximum allowed bound $D_{\max}$, that is

$$\Pr\{d_k \leq D_{\max}\} = p_k. \tag{5.12}$$

Based on this, we can provide a statistical measure for the communication performance and the power system performance. It should be noted that in Section V, we will show that providing 100% statistical guarantee is not cost effective. However, the power system performance under ideal communication scenarios can be approached via a trade-off between power system and communication system performances, which will be detailed in Section 5.4.

Furthermore, the diagonal probability matrix $\mathbf{\Lambda}_P = \text{diag}\{P_1, P_2, \ldots, P_N\}$ is defined, whose elements are given by

$$P_i = \begin{cases} p_k, & \text{if } \text{PMU}_k \text{ installed at bus } i, \\ 0, & \text{otherwise.} \end{cases} \tag{5.13}$$

For the real-time grid monitoring, if the latency of the measurements from a certain PMU exceeds $D_{\max}$, then this information will not be used. In this chapter, power grid observability vector $\bar{\mathbf{b}}$ under statistical latency guarantee can be defined as follows

$$\bar{\mathbf{b}} = \mathbf{H}\mathbf{\Lambda}_Q\mathbf{X}, \tag{5.14}$$

where $\mathbf{\Lambda}_Q$ denotes the diagonal communication constraint matrix, which is defined by

$$\mathbf{\Lambda}_Q = \text{diag}\{Q_1, Q_2, \ldots, Q_N\}, \tag{5.15}$$

where Q_i, $i = 1, 2, \ldots, N$, is a binary random variable, which can be given by

$$\begin{cases} \Pr\{Q_i = 1\} = P_i, \\ \Pr\{Q_i = 0\} = 1 - P_i. \end{cases} \tag{5.16}$$

Therefore, the observability vector $\bar{\mathbf{b}}$ is a vector of random variables. In this chapter, we focus on the observability compromised by communication performance fluctuation, where the fluctuation is due to communication channel fading effect. PMUs are installed at selected buses, which are physically and geographically separated. Hence without loss of generality, it is assumed that random variables Q_i are independent of each other. Therefore we can get the following proposition.

Theorem 1 *The expected power grid observability vector* $\tilde{\mathbf{b}}$ *is given by*

$$\tilde{\mathbf{b}} = \mathbf{H}\boldsymbol{\Lambda}_P\mathbf{X}. \tag{5.17}$$

Proof *Since* $\mathbf{H}$ *and* $\mathbf{X}$ *are known as a prior, we have* $\tilde{\mathbf{b}} = \mathbb{E}\{\bar{\mathbf{b}}\} = \mathbf{H}\mathbb{E}\{\boldsymbol{\Lambda}_Q\}\mathbf{X}$. *By using* $\mathbb{E}\{Q_i\} = P_i$ *and* (5.13), *we can get* (5.17).

The physical meaning of each element $\tilde{b}_i, i = 1, 2, \ldots, N$ of the expected grid observability $\tilde{\mathbf{b}}$ is that, the bus status information is available from an average of $\tilde{b}_i$ PMUs connected to the bus i. If any element $\tilde{b}_i$ is smaller than 1, then it means that the observability of this bus will not be guaranteed in a statistical view, and the power grid is vulnerable to the loss of the observability of that bus.

From the power system's aspect, a full observability of the system only requires all bus observability to be one. Any extra information about that bus can be regarded as observability redundancy to that bus. It will be beneficial to use the observability redundancy to cope with possible PMU failures. In this chapter, three different algorithms are proposed to improve the observability performance, which will be detailed in Section 5.4.

From (5.14) and (5.17), it can be proved that the power grid observability vector $\bar{\mathbf{b}}$ as well as the expected power grid observability $\tilde{\mathbf{b}}$ will be enhanced if the p_k for all PMUs are kept to be as close to 1 as possible. However, in practical systems,

the communication system has a limited total bandwidth B^{th}. This can be defined as a constraint for the bandwidth B_k assigned to each PMU_k, that is

$$\sum_{k=1}^{K} B_k \leq B^{\text{th}}. \tag{5.18}$$

It can be seen that the communication constraint only confines the total available bandwidth resources to each PMU, while it is the probability p_k that is directly related to the observability performance. Besides, the throughput of wireless communication system is time varying due to channel fading effect. This channel fading effect on the physical layer performance will also influence the upper layers, which will result in the latencies experienced by PMUs based applications. This research gap requires a cross-layer analysis within the communication system, which will be done in the next section.

5.3 Cross Layer Statistical Delay Analysis

In communication systems, Shannon channel capacity is one of the most important performance indexes, which defines the maximum achievable rate for a given channel. According to Shannon channel capacity theorem, the capacity for a given channel is determined by channel bandwidth B and signal-to-noise ratio (SNR), which can be given as follows,

$$C = B \log_2(1 + \text{SNR}). \tag{5.19}$$

The variation of instant SNR will affect the instant system throughput in the physical layer, and then results in delay at the link layer. One major source for the SNR fluctuation is channel fading, which is characterized by the physical wireless communication channel. Yet the delay aspect is not considered in the formulation above. For real-time services, such as the considered PMU based system in this chapter, we require a bounded delay. If a received PMU measurement packet violates its delay bound, it will not be used and this may compromise the overall performance. It is hard or infeasible to provide a deterministic delay bound, which is due to the

fact that the channel fading attenuation varies with time [112]. Hence instead, we aim to provide a statistical delay bound guarantee for the power system. In this chapter, effective capacity (rate) theory is adopted, which models the cross layer relation between the link layer behaviour and the physical channel statistical characteristics [4].

Effective capacity is the dual concept of effective bandwidth [5], and it is defined as the maximum constant rate that a fading channel can support under statistical delay constraints. The effective capacity function can be written as [36]

$$R(\theta, B) = -\frac{1}{\theta T} \ln \mathbb{E}\left\{e^{-\theta T C}\right\}, \tag{5.20}$$

where C denotes the instantaneous Shannon channel capacity with block transmission of duration T. The parameter θ is called QoS exponent, which is a non-negative value. The minimum required QoS exponent θ_0 is the value that makes the effective capacity equal to the source rate. In order to guarantee the delay performance, the QoS exponent θ has to satisfy the constraint $\theta \geq \theta_0$. Moreover, when $\theta_0 \to 0$, the effective capacity approaches Shannon's capacity [98].

For PMU_k, its effective capacity can be given as

$$R_k(\theta_k, B_k) = -\frac{1}{\theta_k T} \ln \mathbb{E}_{\gamma_k}\{e^{-\theta_k T B_k \log_2(1+\rho_k \gamma_k)}\}, \tag{5.21}$$

where ρ_k is the average transmit SNR, which is decided by the transmit power of the communication system. The parameter γ_k is the instantaneous channel power gain, which is determined by the fading channel characteristics.

With the definition of effective capacity and applying queuing theory, the probability of d_k not exceeding $D_{\max}$ can be given by [4]

$$\Pr\{d_k \leq D_{\max}\} = p_k = 1 - e^{-\theta_k R_k(\theta_k, B_k) D_{\max}}. \tag{5.22}$$

In this chapter, we assume that the measurement from PMU_k generates a constant source rate R_k^{th}. To avoid the system being unstable, the effective capacity of the wireless communication channel has to be no smaller than the source rate R_k^{th},

that is

$$R_k(\theta_k, B_k) \geq R_k^{\text{th}}. \tag{5.23}$$

By using (5.21)-(5.23), effective capacity theory provides a cross layer analysis framework for the study between channel fading effect, delay bound and its associated delay bound violation probability. This probability is the same one defined in (5.12), which affects power system observability performance. Hence the communication constraints' influence on the power system observability performance can be characterized via the effective capacity theory. Based on this, we can provide algorithms to improve the power system performance via the optimal communication resource allocation.

In Section 5.4, the effective capacity theory will be exploited as an analysis tool for improving the power grid observability performance. To facilitate the discussions in Section 5.4, we first introduce the properties of effective capacity R_k here.

Lemma 3 *The effective capacity defined in (5.21) has the following properties*

$$\frac{\partial R_k(\theta_k, B_k)}{\partial \theta_k} \leq 0 \quad and \quad \frac{\partial R_k(\theta_k, B_k)}{\partial B_k} \geq 0, \forall k \tag{5.24}$$

and $R_k(\theta_k, B_k)$ is concave in B_k and θ_k.

Proof *(5.24) can be obtained by applying the partial differential to $R_k(\theta_k, B_k)$. Then using Holder's inequality [198, eq.(1.7.5)], it can be proved that R_k defined in (5.21) is concave in B_k and θ_k. A more detailed proof can be found in [112, 236].*

In theoretical communication system analysis, Shannon capacity defined in (5.19) is usually used to calculate the minimum required bandwidth, which is denoted as $B_{\min}^{\text{th}}$ in this chapter. For a practical system, the allocated bandwidth B^{th} has to be larger than $B_{\min}^{\text{th}}$, in order to have better latency performance. If the total bandwidth is below $B_{\min}^{\text{th}}$, it is for sure that the throughput of the communication system is less than the rate of the PMU measurement messages, which will lead to communication failure. Hence throughout this chapter, it is assumed that $B^{\text{th}} > B_{\min}^{\text{th}}$ has been enforced. Then with the properties of the effective capacity R_k, we can prove the convexity of probability p_k as follows.

Theorem 2 *The probability p_k defined in (5.22) is convex in B_k and θ_k.*

Proof *Using Lemma 3 and the convex function properties, the convexity of p_k defined in (5.22) can be obtained.*

The probability p_k is the bridge between the observability analysis (5.17) and the communication constraints defined in (5.18). Furthermore, the convexity property of p_k will be useful in finding the optimal communication system configuration for the power system observability performance, as will be shown in the next section.

5.4 Power Grid Observability Driven Resource Allocation Algorithms

In power systems, the real-time measurements from PMUs are fundamental to the monitoring of power grid status. Based on these measurements, real-time applications such as voltage stability enhancement and demand side management can be therefore enabled. Hence it is very important to guarantee the observability of buses. In this section, three algorithms are proposed to optimize the power grid observability performance under communication constraints, which are aiming at different power system performance metrics, that are, the system observability redundancy, bus observability sensitivity and power grid observable probability.

5.4.1 System Observability Redundancy (SOR) Algorithm

The grid observability is of great importance to the grid control or planning services, therefore the loss of bus status observability can result in serious consequences. The deployment of PMUs can provide real-time power grid status measurements, which improves the power grid observability compared to traditional methods via power flow. But the installation of PMUs will involve vast investment, which will increase the cost of the power grid operation. In fact, when a PMU is installed at a bus, it can provide information about all buses incident to this bus besides the installed bus itself [234]. By taking advantage of this feature, the PMU installation places can be selected to achieve a trade-off between cost and power grid observability [237]. With

power grid topology as a prior, it is not necessary to have PMUs installed at every bus, while we are still able to provide a desired degree of observability redundancy. Here we consider system observability redundancy r as the main metric, which is defined as follows,

$$r = \mathbf{1}_N^T(\tilde{\mathbf{b}} - \mathbf{1}_N) \equiv \mathbf{1}_N^T \mathbf{H}\boldsymbol{\Lambda}_P \mathbf{X} - N. \tag{5.25}$$

The metric r gives an evaluation of the overall power network observability redundancy. For a power grid with PMU installation places as a prior, the metric r is upper bounded by the case with ideal communication. For a compromised communication system under resource constraints, a larger value of r means that more PMUs are expected to be available to provide measurements from a statistical view. In this part, we focus on the problem of increasing system observability redundancy under communication constraints, namely the maximization of r defined in (5.25), which can be formulated as follows,

$$\max_{B_k, p_k} \quad \mathbf{1}_N^T \mathbf{H}\boldsymbol{\Lambda}_P \mathbf{X} - N \tag{5.26}$$

$$\text{s.t.} \quad \sum_{k=1}^{K} B_k \leq B^{\text{th}}, \tag{5.27}$$

$$R_k(\theta_k, B_k) \geq R_k^{\text{th}}, k = 1, 2, \ldots, K. \tag{5.28}$$

By exploiting the effective capacity theory discussed in Section 5.3, the maximization of the grid observability redundancy under communication constraints defined by (5.26) - (5.27) can be formulated as follows,

$$\begin{aligned}
\max_{B_k, p_k} \quad & \mathbf{1}_N^T \mathbf{H}\boldsymbol{\Lambda}_P \mathbf{X} \\
\text{s.t.} \quad & R_k(\theta_k, B_k) \geq R_k^{\text{th}}, k = 1, 2, \ldots, K, \\
& p_k = 1 - e^{-\theta_k R_k(\theta_k, B_k) D_{\max}}, k = 1, 2, \ldots, K, \\
& R_k(\theta_k, B_k) = -\frac{1}{\theta_k T} \ln \mathbb{E}_{\gamma_k}\{e^{-\theta_k T B_k \log_2(1+\rho_k \gamma_k)}\}, \\
& \sum_{k=1}^{K} B_k \leq B^{\text{th}},
\end{aligned} \tag{5.29}$$

where (5.26) has been simplified to (5.29), which is due to the fact that the power grid bus number N is constant. The optimal observability redundancy is always achievable with valid B^{th}, which can be given using the following proposition.

Theorem 3 *The power grid observability redundancy r defined in (5.25) is convex in $\mathbf{B} = \{B_1, \ldots, B_K\}^T$ and $\boldsymbol{\theta} = \{\theta_1, \ldots, \theta_K\}^T$, and a feasible solution to the problem (5.29) always exists with every $B^{th} > B^{th}_{min}$.*

Proof *The objective's summation form can be given by $\sum_{i=1}^{N} \sum_{k=1}^{K} h_{ik} p_k$. The convexity of the redundancy r and the constraints in (5.29) follows Lemma 3 and the convexity of p_k proved in Proposition 2. The solution existence follows the fact that the domain formed by all possible $\mathbf{B}$ is compact.*

It can be seen that the effective capacity theory bridges not only the cross layer analysis of the communication system, but also the theoretical analysis of the power system jointly with the communication system. This cross layer and cross system model enables the performance optimization of both systems, as illustrated in (5.29).

5.4.2 Bus Observability Sensitivity (BOS) Algorithm

The bus with the least expected observability within the whole grid is most vulnerable to unobservability. Hence the least bus observability can reflect the power grid's sensitivity to losing bus observability. In this chapter, we define the bus observability sensitivity as $\min_i \tilde{b}_i$, that is the least observability among all buses.

It can be seen that, the buses with small observability values can be viewed as the bottlenecks to the whole power grid's observability. From a statistical view, these buses have more influence on the whole power grid's observability. Therefore, the power grid observability performance can be improved by maximizing $\min_i \tilde{b}_i$ as follows,

$$
\begin{aligned}
&\max_{B_k, p_k} \quad \min_i \tilde{b}_i \\
&\text{s.t.} \quad R_k(\theta_k, B_k) \geq R_k^{\text{th}}, k = 1, 2, \ldots, K, \\
&\qquad p_k = 1 - e^{-\theta_k R_k(\theta_k, B_k) D_{\max}}, k = 1, 2, \ldots, K, \\
&\qquad R_k(\theta_k, B_k) = -\frac{1}{\theta_k T} \ln \mathbb{E}_{\gamma_k} \{ e^{-\theta_k T B_k \log_2(1+\rho_k \gamma_k)} \}, \\
&\qquad \sum_{k=1}^{K} B_k \leq B^{\text{th}}.
\end{aligned}
\tag{5.30}
$$

Besides, it can be shown that, the maximization of the power grid observability according to the strategy above is feasible, as stated by the following proposition.

Theorem 4 *A feasible solution to the power gird observable probability algorithm defined in* (5.30) *always exist with every* $B^{th} > B_{min}^{th}$.

Proof *The desired results can be obtained by using the convexity of* p_k *in Proposition 2 and minimax theorem [238].*

We see that the value of $\min_i \tilde{b}_i$ can also reflect the power grid's reliability to the observability loss of individual buses. With a larger value of $\min_i \tilde{b}_i$, the power grid is less sensitive to the compromised observability, which improves the power system's reliability, at least from the observability point of view.

5.4.3 Grid Observable Probability (GOP) Algorithm

Whether the whole power grid is observable or not is determined by the observability of every power grid bus. Hence besides considering the expected observability based algorithms proposed in Section 5.4.1 and 5.4.2, another algorithm is proposed in this part. The aim is to provide a desired probability for the observability of individual buses. This problem can be formulated by the optimization of the probability that each bus's observability is above a desired level, which can be given as follows,

$$
\begin{aligned}
\max_{B_k, p_k} \quad & \Pr\{\bar{\mathbf{b}} \geq \boldsymbol{\lambda}\} \\
\text{s.t.} \quad & R_k(\theta_k, B_k) \geq R_k^{\text{th}}, k = 1, 2, \ldots, K, \\
& p_k = 1 - e^{-\theta_k R_k(\theta_k, B_k) D_{\max}}, k = 1, 2, \ldots, K, \\
& R_k(\theta_k, B_k) = -\frac{1}{\theta_k T} \ln \mathbb{E}_{\gamma_k}\{e^{-\theta_k T B_k \log_2(1+\rho_k \gamma_k)}\}, \\
& \sum_{k=1}^{K} B_k \leq B^{\text{th}}.
\end{aligned}
\tag{5.31}
$$

where $\bar{\mathbf{b}} \geq \boldsymbol{\lambda}$ is the vector inequality which is true only if all elements of $\bar{\mathbf{b}}$ are greater than their counterparts in $\boldsymbol{\lambda}$.

The physical meaning of the desired observability level vector $\boldsymbol{\lambda}$ can be given as follows. For the case when $\boldsymbol{\lambda} = \mathbf{1}_N$, the problem defined in (5.31) reduces to a statistical guarantee that every bus is observable. For more general cases where $\boldsymbol{\lambda} \geq \mathbf{1}_N$ and $\boldsymbol{\lambda} \neq \mathbf{1}_N$, the algorithm defined in (5.31) provides a desired statistical observability level for individual buses. It should be noted that $\boldsymbol{\lambda}$ is upper bounded by $\boldsymbol{\lambda}_{\max}$, which can be calculated under an ideal communication assumption.

Here we define the solution to the problem of $\bar{\mathbf{b}} \geq \boldsymbol{\lambda}$ by the diagonal matrix $\boldsymbol{\alpha}_m$, and all the solutions form a set $\{\boldsymbol{\alpha}_m\}$, where $m = 1, 2, \ldots, M$. Then we can further simplify the problem defined in (5.31) as follows,

$$
\Pr\{\bar{\mathbf{b}} \geq \boldsymbol{\lambda}\} \equiv \Pr\{\mathbf{H}\boldsymbol{\Lambda}_Q\mathbf{X} \geq \boldsymbol{\lambda}\} = \sum_{m=1}^{M} \Pr\{\boldsymbol{\Lambda}_Q = \boldsymbol{\alpha}_m\}.
\tag{5.32}
$$

Similar to the SOR algorithm discussed in Section 5.4.1, the optimal communication resource allocation for the maximization of the power grid observable probability is feasible, which can be given by the following proposition.

Theorem 5 *The power gird observable probability defined in* (5.31) *is convex in* $\mathbf{B}$ *and* $\boldsymbol{\theta}$, *and a feasible solution always exists with* $\boldsymbol{\lambda} \leq \boldsymbol{\lambda}_{max}$ *and* $B^{th} > B_{min}^{th}$.

Proof *The desired results can be obtained following similar arguments in Proposition 3.*

Note that each solution $\boldsymbol{\alpha}_m$ consists of only binary elements, namely 0 and 1. Hence when the PMU installation buses are known as a prior, the solution

set $\{\boldsymbol{\alpha}_m\}$ is readily available. Besides, if the measurements for some buses are critical information or critical to the whole power grid's observability, we impose such buses to offer higher desired observability levels, which can be achieved by assigning corresponding elements in the parameter $\boldsymbol{\lambda}$.

Since the three algorithms are convex, the optimal solution can be obtained using numerical methods, such as the fmincon(̇) function provided in Matlab. The complexity of the algorithm depends on the dimensions of the solution space, which consists of the allocated bandwidth to each PMU.

5.5   Case Studies

In this section, the three proposed algorithms in Section 5.4, namely the System Observability Redundancy (SOR) algorithm, Bus Observability Sensitivity (BOS) algorithm, Grid Observable Probability (GOP) algorithm, are verified using two case studies, namely IEEE 14 bus power system test case and IEEE 30 bus power system test case, as illustrated in Fig. 5.1 and Fig. 5.6, respectively. These two test cases have been extensively used as standard test cases to verify power system performances [239] [234].

Here we apply the primary and backup (P&B) method [237] for the PMU installation. The objective of P&B method is to provide the power grid with two independent PMU sets. Either the primary and backup set is capable to provide a full observability of the whole power grid. This provides the power grid with redundancy, where the whole grid is still observable when multiple PMUs fail within only one set. Without loss of generality, it is assumed that all PMUs generate measurement packages at the rate of 60kbps and the maximum allowed latency bound for these measurement packages is set to be 10ms [25] [240].

Besides, the control centre is assumed to be located at the centre of the power grid. The average SNR ρ_k between the control centre and PMU_k are assumed to be related to their distances, which are in the range of 10-15dB in IEEE 14 bus case and 7-12dB in IEEE 30 bus case. It is assumed that all PMU transceivers use unit transmit power. In order to capture the effect of time varying fading effect, Rayleigh

fading has been considered in this chapter, where Monte Carlo method is used to simulate the fading channels. Under such conditions, the effective capacity under Rayleigh fading channels can be given by [36]

$$R_k(\theta_k, B_k) = -\frac{1}{\theta_k T} \ln {}_2F_0[\frac{\theta_k B_k T}{\ln 2}, 1, -\rho_k],\qquad(5.33)$$

where ${}_2F_0[\cdot]$ is the generalized hypergeometric function [198, eq.(16.2.1)].

In case of PMU communication system failure, a redundancy bandwidth is always allocated to that PMU transceiver. We adopt the bandwidth allocation algorithm similar to [76] as default algorithm, where required bandwidth for the PMUs is calculated using Shannon capacity (5.19) and the extra bandwidth will be evenly divided and allocated to each PMU. In our proposed algorithms, the total bandwidth is allocated according to the optimal solution of (5.29), (5.30) and (5.31). For the GOP algorithm, the desired statistical observability level is assumed to be $\boldsymbol{\lambda} = \mathbf{1}_N$. Since the problems are nonlinear optimization problems, the Matlab optimization toolbox is used to find the optimal bandwidth allocation solution.

Table 5.1: PMU configuration

Case	PMU Number	Bus Index
IEEE 14 bus	9	2,4,5,6,7,8,9,11,13
IEEE 30 bus	21	1,3,5,7,8,9,10,11,12,13,15,17, 18,19,22,24,25,26,27,28,29

5.5.1 IEEE 14 Bus Case Study

Table 5.2: Average bus observability with a total of 159kHz bandwidth.

	Average Bus Observability														Red.	Sen.	Pr.
	1	2	3	4	5	6	7	8	9	10	11	12	13	14			
Default	1.004	1.740	0.741	3.639	2.740	3.296	2.639	0.912	2.635	1.988	1.997	1.299	1.299	1.290	13.217	0.741	0.665
Red. Algorithm	1.867	2.809	1.851	4.676	3.763	3.767	3.609	1.722	2.809	1.865	1.873	1.860	1.860	1.852	22.151	1.722	0.959
Sen. Algorithm	1.844	2.774	1.835	4.657	3.715	3.669	3.706	1.835	2.813	1.835	1.835	1.835	1.835	1.835	22.023	1.835	0.959
Pr. Algorithm	1.693	2.315	1.606	4.303	3.311	1.725	2.846	1.229	2.610	1.006	1.006	1.006	1.006	1.006	12.667	1.006	0.978

In this part, the case of IEEE 14 bus power system has been considered, whose bus topology and PMU installation position have been shown in Fig. 5.1. The

Table 5.3: Probability of delay within maximum allowed latency bound with a total of 159kHz bandwidth.

PMU bus location	2	4	5	6	7	8	9	11	13
Default Algorithm	0.004	0.737	0.999	0.999	0.908	0.004	0.991	0.997	0.299
Red. Algorithm	0.909	0.942	0.958	0.954	0.921	0.801	0.946	0.919	0.906
Sen. Algorithm	0.905	0.930	0.939	0.941	0.942	0.894	0.941	0.894	0.894
Pr. Algorithm	0.904	0.928	0.943	0.944	0.941	0.891	0.940	0.900	0.892

statistical probability of the communication delay associated to PMU at bus 2 has been given in Fig. 5.2. The Shannon capacity required for the PMU at bus 2 is 17.344kHz under the considered scenario. It can be indicated in Fig. 5.2 that the latency bound will not be met with only minimum required bandwidth. In order to counteract the fading induced communication system fluctuation, extra bandwidths are needed for a desired performance, whose quantity can be obtained via (5.22) and (5.33).
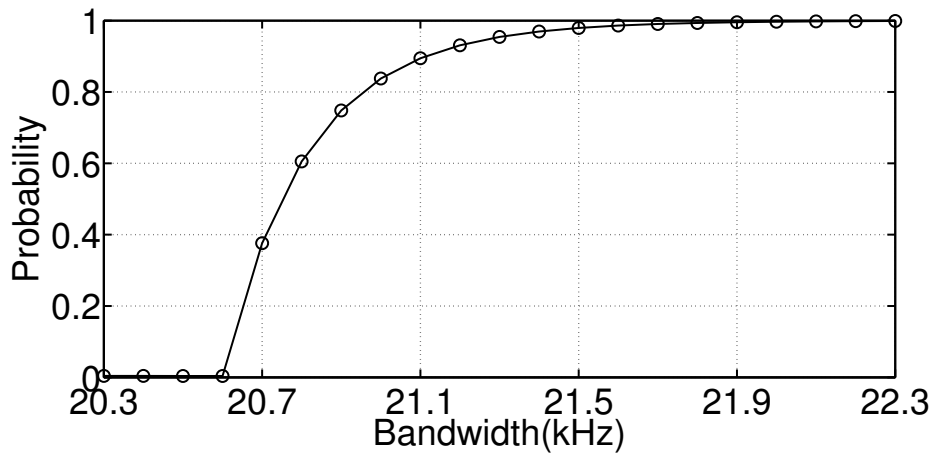
Figure 5.2: The probability of communication delay bound being met associated to PMU at bus 2 as a function of bandwidth.

The system observability redundancy under different total communication bandwidth constraints is illustrated in Fig. 5.3. Here we consider the PMU loss only results from the maximum latency bound violation. Without any PMU loss, using the PMU installation position defined in Table 5.1, the overall grid observability redundancy can be calculated to be 25. It can be seen from Fig. 5.3 that the SOR algorithm provides the best grid observability redundancy performance across different bandwidths. Specifically, with a total bandwidth of 163kHz, the proposed

SOR algorithm can provide a close performance to the situation of no PMU loss, while the default algorithm requires 169kHz to reach a similar performance.
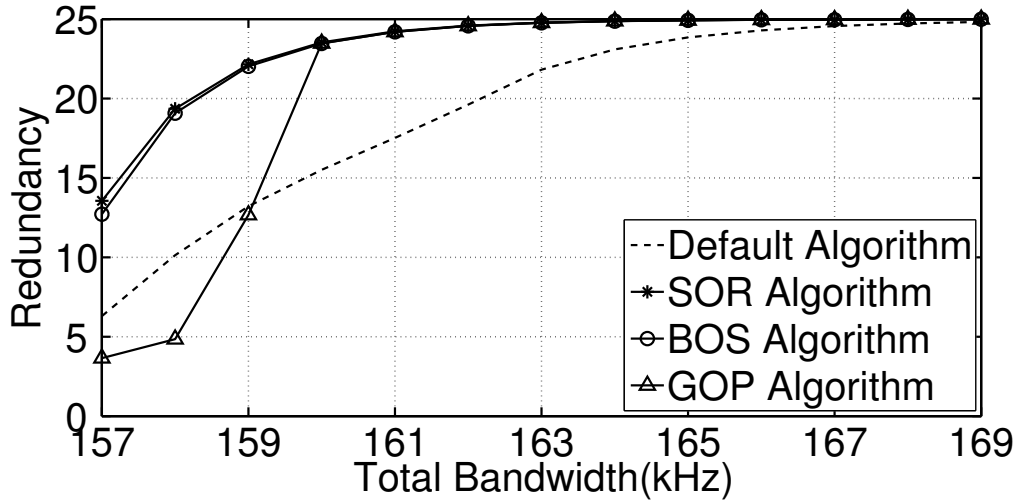

Figure 5.3: System observability redundancy performance in IEEE 14 bus case.
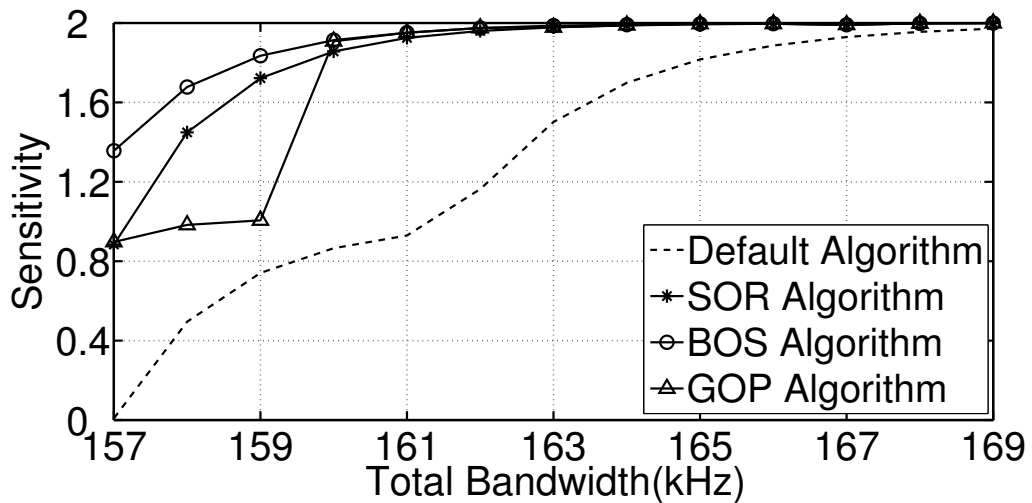
Figure 5.4: Bus observability sensitivity performance in IEEE 14 bus case.

In an ideal communication scenario, the bus observability sensitivity for the considered case is 2, which is due to the two independent sets of PMUs in the P&B method. Fig. 5.4 indicates that the BOS algorithm is capable to improve the minimum bus observability within the whole power grid. It also suggests that the SOR algorithm and BOS algorithm have better performance over the GOP algorithm, when considering redundancy and sensitivity metrics. One major reason
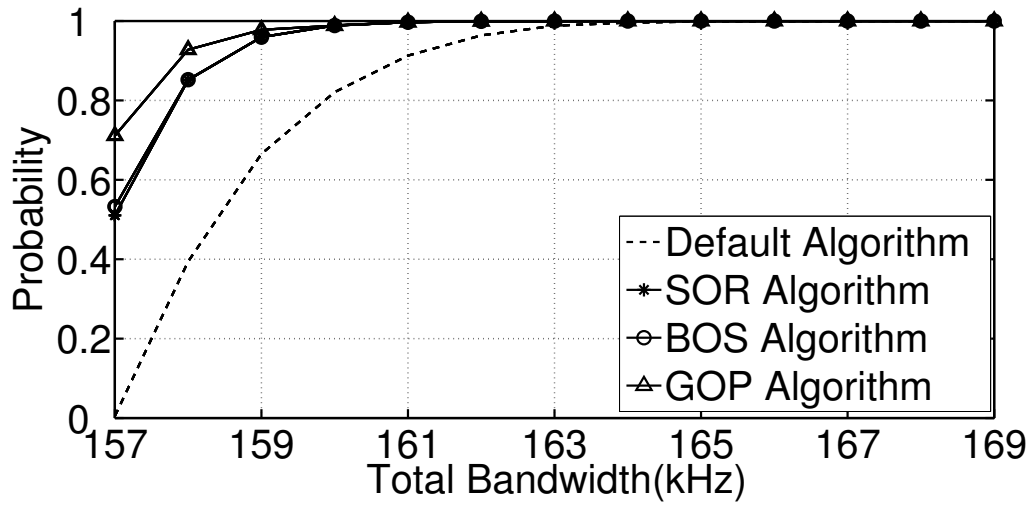
Figure 5.5: Grid observable probability performance in IEEE 14 bus case.

is that these two algorithms are both based on expected observability while the GOP algorithm focuses on the probability performance.

The GOP algorithm aims at improving the probability that individual bus observability is over the desired threshold. In this case study, the desired threshold has been set to be 1, which equals the case that the whole power system is observable. It is shown in Fig. 5.5 that the GOP algorithm provides a better statistical guarantee for the power grid to be observable than the other algorithms. It can be also noticed that, this performance gain is at the cost of a reduced overall power system observability redundancy and bus observability sensitivity, as indicated in Fig. 5.3 and Fig. 5.4.

More detailed performances related to individual buses are given in Table 5.2 and Table 5.3, where the total available bandwidth is 159kHz. It is worth mentioning that, under the considered scenario, the minimum required total channel bandwidth is calculated to be 131.87kHz using Shannon capacity theorem. But it can be inferred from Table 5.2 that, with only Shannon capacity, the system observability performance cannot meet the requirement. Using default algorithm, which provides each PMU with required Shannon bandwidth and evenly divides the extra bandwidth, the bus 8 is vulnerable to lose observability in the considered scenario. On the contrary, every bus observability can be statistically guaranteed by the SOR algorithm, BOS algorithm or GOP algorithm, where the performance has been opti-

mized for different desired performance metrics, respectively. From Table 5.2 as well as Fig.5.3 - 5.5, it can be seen that the proposed algorithms make better use of the extra bandwidth, to obtain performance improvements on system observability redundancy, bus observability sensitivity and grid observable probability, respectively.

5.5.2   IEEE 30 Bus Case Study

In order to test the performance of the proposed algorithms, the IEEE 30 bus power system test case has also been investigated. The bus topology for the IEEE 30 bus power system is given in Fig. 5.6.
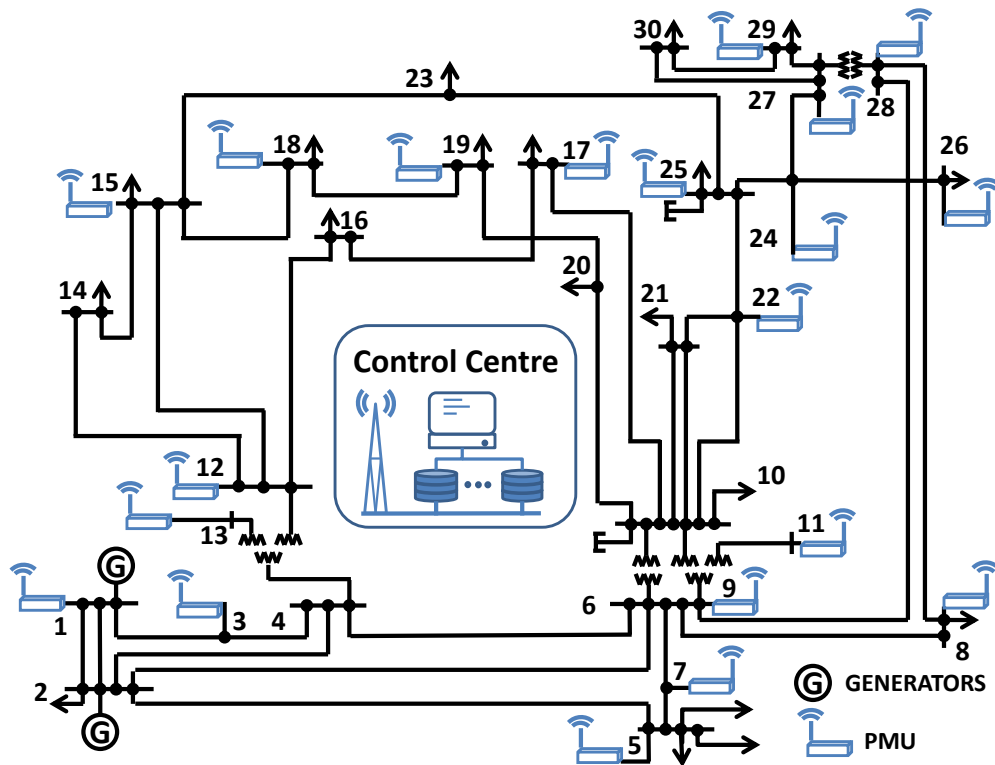
Figure 5.6: IEEE 30 bus power system with 21 PMUs.

The proposed three algorithms are oriented in the optimization of three different power system performance metrics, namely system observability redundancy, bus observability sensitivity and grid observable probability. The simulation results have been given in Fig. 5.7-5.9. It can be seen from these figures that, the three proposed algorithms have better performance over all considered performance metrics than the default algorithm in the considered scenarios.
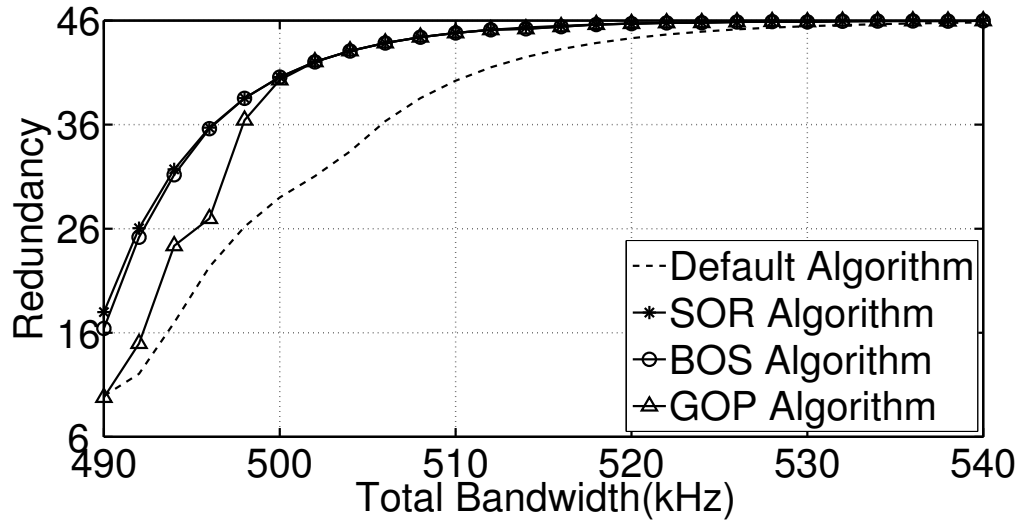
Figure 5.7: System observability redundancy performance in IEEE 30 bus case.
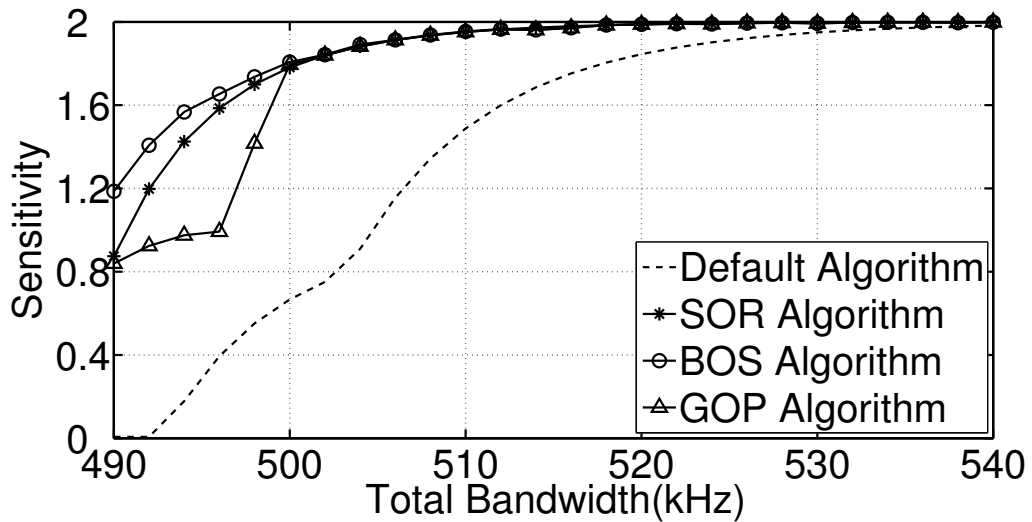
Figure 5.8: Bus observability sensitivity performance in IEEE 30 bus case.

As illustrated in Fig. 5.7, the SOR algorithm provides more redundancy than the GOP algorithm as well as the default algorithm. From the aspect of system observability redundancy, the performance gain for SOR algorithm is slightly higher than BOS algorithm. But this loss of performance gain in the BOS algorithm improves the power grid observability sensitivity, as indicated in Fig. 5.8. This is because the overall resources are constrained, which results in the situation that, the improvement of certain bus observability will be at the cost of other bus observability. Although this redundancy performance gain does not seem to be large between the
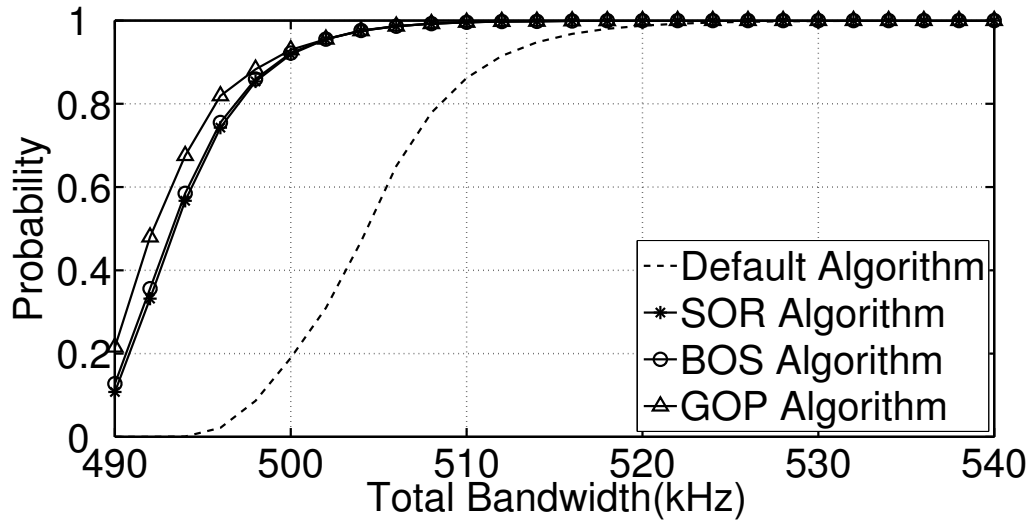
Figure 5.9: Grid observable probability performance in IEEE 30 bus case.

SOR algorithm and the GOP algorithm, it should be noticed that the redundancy performance in Fig. 5.7 targets the whole power system performance, while the sensitivity performance in Fig. 5.8 targets individual buses. With constrained total resources, the improvement of overall grid observability redundancy will be less seemingly prominent in the figures than the sensitivity performance. However, it should be noted that individual bus performances are different, as illustrated in Table 5.2 and Table 5.3.

As can be seen in Fig. 5.9, the GOP algorithm improves the probability that the power system can be observable over different total communication bandwidths. It can be also seen that the performance gain at observable probability is at the cost of a decrease in redundancy and sensitivity performances, as can be indicated from Fig. 5.7 and Fig. 5.8.

Comparing performances between IEEE 14 bus case in Fig. 5.3 - Fig. 5.5 and IEEE 30 bus case in Fig. 5.7 - Fig. 5.9, the three proposed algorithms provide better observability performance than the default algorithm, when corresponding optimized metrics are considered. But it also indicates that no single algorithm outperforms the other algorithms if all metrics are considered at the same time. The optimal algorithm depends on the considered scenario and the metric of interest.

The considered performance metrics, namely system observability redundancy, bus observability sensitivity and grid observable probability, are all formulated using

a statistical approach. In theory, the best performance, when an ideal communication system is considered, can be asymptotically approached. Yet from the discussion above, to improve the average performance, it has to increase the required overall communication resources in an exponential way. The performance gain may be marginal even with large deployment of communication resources, especially when we are close to the best performance. Hence the results also suggest that there is a trade-off between the observability performance and the bandwidth. In the considered IEEE 30 bus power system case, the power system can reach performance similar to that with ideal communication using a total bandwidth of 520 kHz.

5.6   Concluding Remarks

In this chapter, the power grid observability performance has been studied by considering both power system and communication system aspects. A corresponding analysis model has also been formulated. In order to perform the communication system cross layer analysis, as well as to consider the channel fading effect and total bandwidth constraint, the effective capacity theory has been adopted and utilized. Based on this cross scenario and cross layer analysis model, three power grid observability performance metrics have been formulated, namely system observability redundancy, bus observability sensitivity and grid observable probability. Then, corresponding improvement algorithms have been proposed via optimal communication resource allocation. The IEEE 14 bus and 30 bus power systems have been used in the case study to validate the performance of the three proposed algorithms. Results show that the proposed algorithms can help improve the power grid observability performance. Furthermore, the three proposed algorithms have the potential to be used to trade-off between the investment needed for the communication system and the required power system performance.

Chapter 6

Software Defined Radio Enabled Smart Grid Testbed

Smart grid is considered to be the next generation of the power grid, which provides a bidirectional information flow within the grid [31]. Power system and communication system are deeply coupled in the Smart Grid system, which poses a challenge on the inter discipline research, analysis and evaluation. To address this challenge, versatile Smart Grid testbeds have been proposed, which provide a safe and practical environment for the integration research in systems such as power system and communication system [116].

Smart Grid testbed is an important platform for the application development, analysis, validation, and evaluation. The field test is usually not cost effective and involves safety issue, while theoretical results lack experimental data validation. Therefore, the hardware and simulator integrated testbeds provide an alternative solution for such requirements [241]. Existing Smart Grid testbeds are mostly addressing either power system aspect or communication system aspect, where there is still a lack of platforms to emulate different power system designs and various communication technologies at the same time [117]. To make it more challenging, this inter discipline oriented platform is desired to run at real time, like the practical Smart Grid systems do.

Wireless communication is the most important technology to span the information connection throughout the Smart Grid system. But spectrum resource scarcity

is a challenge to accommodate emerging Smart Grid applications with large volumes of data. Advanced wireless communication technologies such as cognitive radio are promising in addressing this issue [242], but its integration to the Smart Grid system is still under addressed, where validation and evaluation are the key challenges [243]. Besides, Smart Grid is an integration of both power system and communication system, where these two systems are deeply coupled in most practical cases. Hence the analysis within a single system, whether power system or communication system, is not enough to fully evaluate the performance in real cases.

To address the above challenges, we propose a cognitive radio enabled Smart Grid testbed in this chapter, which is based on Software Defined Radio (SDR) and Real Time Digital Simulator (RTDS). The proposed testbed provides a framework, which supports real time evaluation of both power system and communication system. The various advanced wireless technologies can be implemented as modules, which are then integrated into the system's module pools and reloaded as required. Meanwhile, the RTDS provides closed-in-loop emulation of the power system, where devices can be connected to the RTDS or simulated by models.

The derivations and analyses of the previous chapters are focusing on the theoretical upper bounds of the system performance. Similar to Shannon capacity, the upper bounds are critical in system designing. For example, with the physical channel environment, system set-up and QoS requirements known as a priori, the effective rate theory can be used to indicate the maximum applications to be hosted within the system. To approach the upper bound performance quantified by effective rate theory is not an easy job similar to approaching Shannon capacity, but the Software Defined Smart Grid Testbed proposed in this chapter is a firm step towards this goal, which provides the platform for QoS related researches in the Smart Grid scenario, such as delay measurement, customized applications and cross-layer analysis and evaluations. These aspects will be detailed in the following sections.

6.1 Cognitive Radio Enabled Smart Grid Testbed Design

New device, algorithm or application must be first evaluated before field deployment, which is also true to the Smart Grid. Theoretical analysis is fundamental to the performance guarantee, yet it is still far from satisfied for the field deployment. But the on-site evaluation during development procedure is not practical for most cases, and it has drawbacks such as high cost and safety problem. Therefore a comprehensive testbed is a very attractive solution, which provides a safe environment for analysis, evaluation and debug. In this section, a Smart Grid testbed framework is proposed.

6.1.1 Real Time Digital Simulator (RTDS)

In power system, it is critical to evaluate new or potential control, protection or application before field deployment. Hence a lot of solutions have been used for em-

August 11, 2018

Figure 6.1: RTDS system at Durham University Smart Grid Lab.

ulating the operation of power system, both software and hardware solutions, such as Matpower on Matlab, transient network analyser (TNA) and PSCAD. These existing simulators are mostly off-line solutions, which forms the problem in mathematics and then solve them numerically. However, these off-line simulators cannot interact with the grid components in real time like a real power system does. Hence in the proposed Smart Grid testbed, the RTDS system is applied, which has the potential to operate continuously in real time with actual hardware connected in closed-loop [244].

The RTDS Simulator is the world standard for real time power system simulation. It is used by all of the worlds major protection and control equipment manufacturers, as well as by leading electric utilities, educational institutions, and research facilities around the world.

The RTDS Simulator consists of custom hardware and all-in-one software, specifically designed to perform real time ElectroMagnetic Transient (EMT) simulations. It operates continuously in real time while providing accurate results over a frequency range from DC to 3 kHz. This range provides a greater depth of analysis than traditional stability or load flow programs which study phenomenon within a very limited frequency range.

The RTDS Simulators custom hardware is capable of simulating complex networks using a typical time step of 25-50 μs. The simulator also allows for small timestep subnetworks that operate with timesteps in the range of 1-4 s for simulation of fast switching power electronic devices (e.g. VSC bridges with PWM switching). The hardware is comprised of modular chassis, each containing a powerful multicore processor and allowing scalable access through the licensing of 1 to 10 cores per chassis. Overall system expansion and full connectivity of up to 60 chassis are supported.

In the proposed Smart Grid testbed, the power system is simulated using the RTDS in real time. The RTDS provides a power system development environment, where the grid components can be connected through both high voltage interfaces or low voltage I/O interfaces. Besides, the RTDS also provides a model library with common hardware components such as generator, PV panel, wind turbine, SVC and

breakers. It also supports customized models, which provides a practical emulation of the real power system. With the RTDS system, the Smart Grid testbed is able to analyse and evaluate a wide range of power system applications, including load flow, control schemes and small signal analysis.

In the prototype RTDS system, the 4 bus power system with one wind farm [245] is modified and implemented, which is given in Fig. 6.3. The 4 bus power system is also a standard test case that is widely used in the power system researches, which involves the operation of generator, wind turbine, transmission lines, active loads, reactive loads and dynamic loads, as well as the monitor and control of power grid. The RTDS is programmed to monitor the states of these components, whose values are converted as analogue outputs on the RTDS GTFPI module. The control inputs are made via the RTDS GTAI module.

6.1.2   Software Defined Radio platform

Software defined radio (SDR) is a counterpart to the concept of hardware defined radio. In the hardware solution of a radio communication platform, each component is fulfilled by a dedicated chip or electric circuit. Yet in the SDR solutions, the hardware is replaced by a functional block or module of executable codes. In ideal SDR platform, the software defined system part should be as close to the antenna as possible. Due to this feature, the whole communication system is built up with most of its parts as software codes. A few advantages and important features about SDR is given as follows.

- *Flexibility*

  The modular design of communication system components provides the developer with much flexibility. In hardware design, the available resources and functions are predefined by the hardware's capability. Once the hardware components are implemented on board, only very limited changes are possible. While in the SDR case, the restrictions are much more relaxed. A typical example is that SDR platforms usually support various radio fronts for different protocols, while for traditional method it requires multiple radio fronts for this purpose.
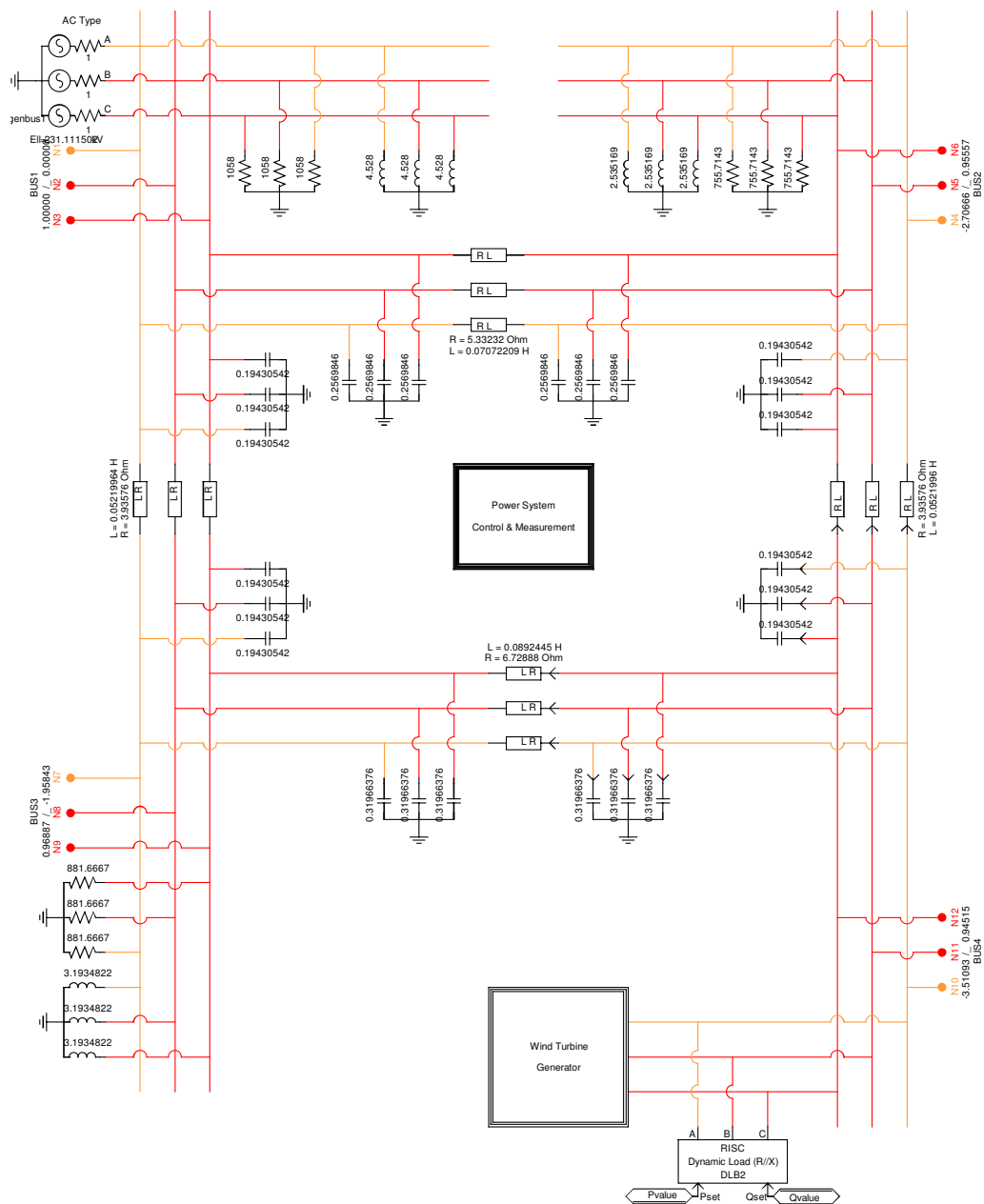
Figure 6.3: The implemented 4 bus, 2 generator power system on RTDS.

- *Reconfigurability*

  The design of SDR platform is highly reconfigurable. For some SDR platforms such as USRP, the design can be reconfigured at real time. This is a very attractive feature, which enables the communication system to adapt itself according to the environment. An important application of this feature is the Cognitive Radio system, which is able to sense the surrounding spectrum and utilize the unexploited spectrum resources.

- *Function Pool*

  As the functions are written as block or modules of codes, where the interfaces are unified for similar functions. Thus it is possible to build a function pool, which makes the implementation for different combinations of functions relatively easier and faster. A typical example is the protocol pool for SDR platform, where different communication protocols can be reloaded as required.

- *Friendly Interface*

  Most SDR supports various programming languages, such as C, C++ and Python. These languages are widely used as simulations and software based analysis. This bridges the theoretical and practical in an ideal way. For example when working with GNU Radio, the whole communication system can be loaded and called as normal functions similar to the many open source functions compatible with Python. Besides, these languages can be used as interfacing method between powerful simulation software such as Matlab and Maple.

Actually the concept of Software defined radio has been proposed long time ago, but it only comes to reality thanks to the boost of computing capability. This is because as the software defined part more close to the antenna, the more complex computations are in need. For example, a WiFi transceiver, the baseband throughput requirement can be up to hundreds or thousands megabits per second. Thus the architecture of different SDR platforms varies with its solution in addressing the computing challenges. For example, Microsoft Research Software Radio (Sora) is integrated on a PCIe extension board and runs with quad-core personal computers [246]. Another trend for the SDR development is the open source based method, where GNU Radio is a typical example. More details about GNU radio will be provided in the next part.

6.1.3 GNU Radio

One major advantage of SDR is that it shifts its dependency on dedicated hardware to the computing capability on general purpose processors. The signal processing has

been achieved via software modules. GNU Radio is a typical open source software development toolkit that provides signal processing blocks to implement software radios [247]. Due to this open source architecture, the software resources can be reused by different projects as well as compatible external RF hardware. The GNU Radio also provides a complete software simulation environment, where it runs like a traditional simulation tool without the need for any external hardware. This also leads to a wide range of choices for the compatible RF hardware, which is due to the standard and open source interface. Thus it has been widely used in amateur, research, academia and industry scenarios.

GNU Radio also provides all kinds of signal processing modules, which makes it easy to use and fast in prototyping. The core of GNU Radio provides an environment, where methods and interfaces are provided for inter blocks connections as well as the data passing between them. As another advantage of open source platform, it encourages developers to share their own codes or modules via methods like GitHub [248]. So far there have been various commonly used signal processing modules readily available, such as filters, channel codes, synchronisation elements, equalizers, demodulators, coders, decoders, and many other types of blocks which are typically found in signal processing systems [247].

In addition, GNU Radio supports C++ and Python programming language. These two languages are widely used in software development as well as academic researches. Thus these languages can not only be used for customized applications, but also for the interfaces to include advanced analysis tools and third party signal processing cores. The application has the choices to be written in Python, C++ or the combination of them during development. Python is more close to human language and provide good online debugging feature, while C++ is able to improve the computing efficiency for the performance-critical signal processing parts.

Considering the fact that Python and C++ are supported by most operating systems as well as the many choices of compatible RF hardware, the projects and their modules based on GNU Radio are with great portability. This is also a favourable feature for long evolution programmes, where updates and upgrades have been made more convenient.

6.1.4   Universal Software Radio Peripheral (USRP)

Universal Software Radio Peripheral (USRP) is the software defined radio platform provided by Ettus Research [249]. The USRP platform provides radio fronts supporting from DC to 6 GHz. The new series can also support multiple antenna systems. Ettus provides a versatile driver, i.e. USRP Hardware Driver (UHD), where APIs can be called in both C++ and Python to control the USRP hardware resources. The UHD also provides features such as FPGA image loader to customize the functions of the USRP.

With the support of UHD and the GNU Radio system, there have been various projects providing SDR based wireless communication applications, such as MIMO system, cognitive radio system and spectrum monitoring, IEEE802.11 system [250].

Unlike traditional radio communication system, SDR defines the components such as mixer and modulator/demodulator as reconfigurable software modules. This architecture enables the SDR based communication system to use different radio fronts and communication protocols with the same hardware. Therefore it makes SDR platform an ideal test and evaluate environment for new and advanced communication technologies in Smart Grid before real world deployment.

In the proposed Smart Grid testbed, we exploit the USRP platform from Ettus, which uses the GNU Radio as development environment. The GNU Radio system running at the computers is a data stream oriented signal processing platform [250]. It processes the baseband communication systems via modularized functions, where the baseband data streams are piped to or from the USRP hardware for transmission or reception. Most system components are modularized on the SDR platform, including Spectrum Sensing module, Machine Learning module, Communication Protocol Pool, Spectrum Sharing module, GUI module and Data Acquisition and Actuator module. With this modularized design, the system is able to replace any parts by reconfiguring the whole system in real time. This feature enables the testbed to be a versatile platform to evaluate, validate and compare different smart grid communication system designs.

In the prototype, the communication system is implemented on USRP N210 running with laptops. The USRP N210 is equipped with CBX daughter board,

which provides a wide range of protocol choices available between 1200-6000MHz. All modules are coded in Python or C++. The laptop communicates with the USRP N210 through a gigabit Ethernet cable. To provide better synchronising performance among different testbed sets, the GPS module BU-353 has been applied.

6.1.5   Machine Learning Enabled Spectrum Sensing

A great advantage of the Cognitive Radio technology is that it can utilize the unlicensed spectrum for data transmission. This is a very promising way to expand the systems' communication capacity without huge investment on leasing more spectrum resources. Before any transmission, the transmitter should be aware of the spectrum usage in its surroundings, which is one critical condition for the deployment of cognitive radio based transceivers. Via spectrum sensing, the transceivers can detect the existence of the primary user, who has exclusive usage of this specified spectrum. Then the unused spectrum resources can be exploited for data transmission. In this way, it mitigates the interferences to the primary users' performance. There have been a lot of options for spectrum sensing algorithms, including simple energy detection, wideband sub-Nyquist sampling [242] and machine learning.
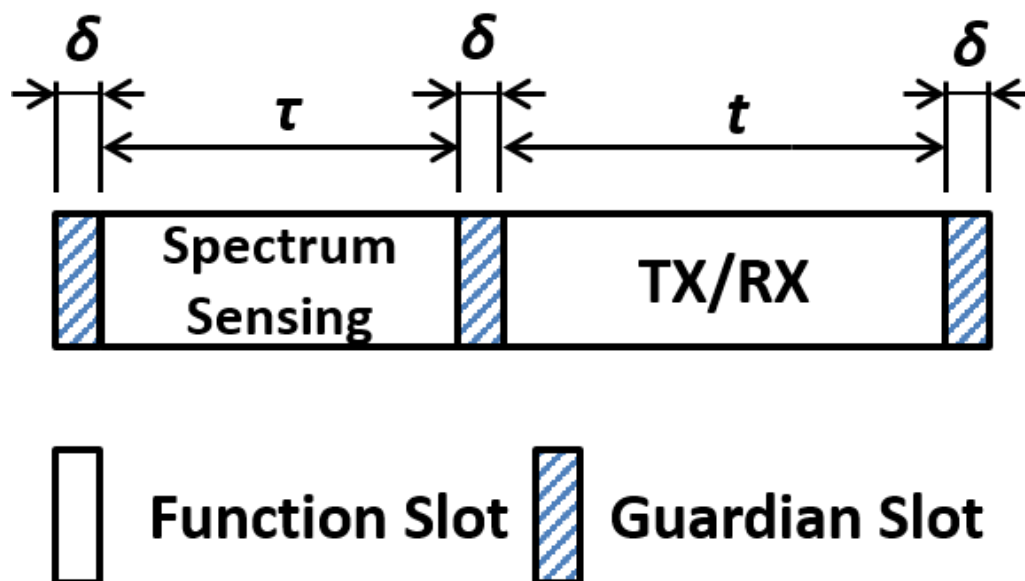
Figure 6.4: The frame of spectrum sensing enabled communication network consists of spectrum sensing slot, data transmission and reception slot and guardian slot.

In the proposed Smart Grid testbed, we exploit machine learning algorithms to perform the spectrum sensing. The key concept about spectrum sensing is to learn about the radio frequency environment. The proposed Smart Grid testbed is based on SDR platform, where multiple radio fronts can be exploited via software controls. Hence in this way, this testbed is not confined to specific wireless technologies or frequency bands as most hardware based transceivers do. Thus machine learning can be used as a more versatile spectrum sensing method, which is able to detect a wide range of frequency bands and adapt to different channel features on different frequencies. Besides, as the testbed is built upon SDR platform, it has the potential to evolve the spectrum sensing model along with environmental changes. Each cognitive radio frame can be divided into spectrum sensing slot and data transmission and/or reception slot, where guardian slots may be applied between them, as illustrated in Fig. 6.4. Within a finely synchronised network, the guardian slots are not necessary, where the efficiency of such network can be given by $\frac{t}{t+\tau}$. On one hand, increasing the sensing time τ will lead to a more accurate spectrum status result, which is essential to the spectrum access decision. On the other hand, the increase of sensing time will reduce network efficiency, which compromises the system's performance. Hence there is a trade-off between the accuracy and time performance in the spectrum sensing algorithms.

In the implemented prototype, we exploit the Extreme Learning Machine (ELM) algorithm as the spectrum sensing algorithm, which is a single hidden layer feed-forward neural network [251]. The testbed is able to perform online learning with as little as 10 scans of the frequency bands. The random neurons method is applied with sigmoid as kernel function and 500 neurons. The accuracy threshold for detection is set to be 0.95. Besides, the spectrum sensing algorithm has been modularized, where a spectrum sensing pool is enabled with various choices for different performances. Note that for similar scenarios, the trained model can be transplanted, hence the training procedure is only required when scenarios are changed or no existing model available.

The contribution of this effort is on three aspects. Firstly, although machine learning has been suggested to be beneficial especially for the applications such as

spectrum sensing, the real world verification is still under-addressed. This work is an important step towards the machine learning application in communication. Secondly, the implemented ELM based spectrum sensing is able to perform online training, which is also an effort to enable the communication nodes with the evolution ability, which is also a less addressed in practical contexts. Lastly, the machine learning part has been made as modules, which fits good with the SDR architecture. The templates and interfacing methods are of great potential to the research in similar contexts.

6.1.6   Dynamic Spectrum Sharing Mechanism

Along with the development of wireless communication technology, the spectrum scarcity problem has been more and more severe. The spectrum resource is one of the critical factors that define the upper bound of system's throughput. On one hand, it is desirable for the Smart Grid communication network to have an exclusive usage of a certain band of frequencies. But this usually requires a huge investment. On the other hand, the ISM bands are free to use, which can be exploited for data transmission. But it can be noisy and too crowded to use. Therefore, spectrum sharing method is a very attractive method to expand the systems communication capacity. As illustrated in Fig. 6.5, when the primary users' licensed spectrum resources are not exploited in any dimension such as time, frequency and space, the second user may use them for data transmission temporally. This method is usually referred to as overlay method. The other method is called underlay method, where the second users will communicate with each other under a controlled transmit power, which guarantees that the interference to the primary user is within an acceptable range when they run simultaneously. There have been also hybrid methods combining them to provide a more flexible and efficient spectrum usage [252].

In the proposed testbed design, the system has access to both licensed and unlicensed frequency band via dynamic spectrum sharing. Once the spectrum sensing results indicate spectrum opportunities, the testbed system selects the best communication channel to use. With protocol pool on the SDR platform, the testbed is able to switch to different wireless communication protocols, including but not
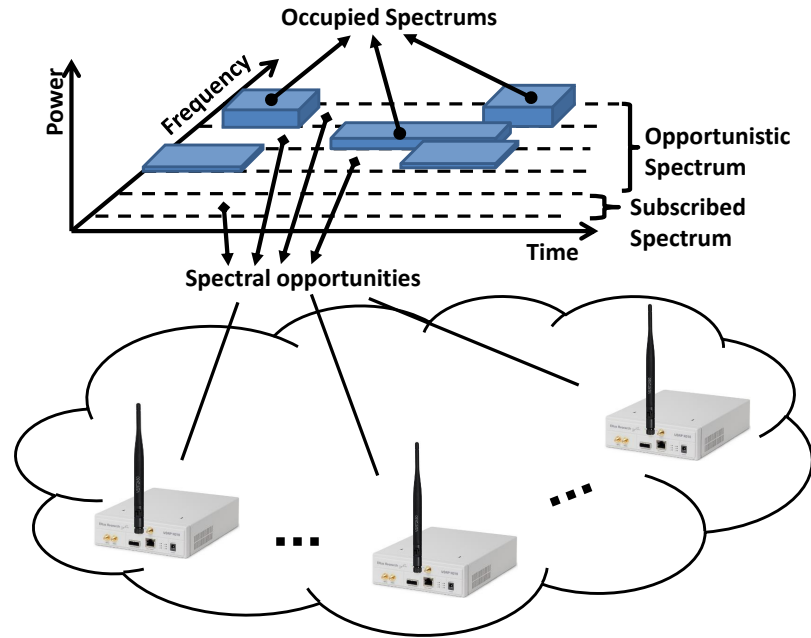
Figure 6.5: Cognitive Radio Enabled Smart Grid Communication Networks.

confined to IEEE 802.11, IEEE 802.22 and IEEE 802.15 protocols. Besides, due to the reconfigurable radio front, the proposed testbed is able to communicate at any available frequency bands, which only depends on the support of the radio frequency board module. This design enables the testbed adaptive to a wide range of scenarios, since ISM bands can be regarded as licensed to the testbed, which can be the case where no exclusive bands are available in home area smart grid application scenarios.

In the prototype, the IEEE 802.11a/p/g protocols [250] on the frequency band 2.4GHz and 5GHz have been adapted for validation purpose, where the encoding options include BPSK 1/2, BPSK 3/4, QPSK 1/2, QPSK 3/4, 16QAM 1/2, 64QAM 3/4, 64QAM 2/3 and 64QAM 3/4. A two state Finite State Machine (FSM) is used for channel access management purpose, which is illustrated in Fig. 6.6. The mechanism of the two state FSM is designed to avoid the interruption to the primary user and frequently jumping between channels, which is given as follows.

- State 0:
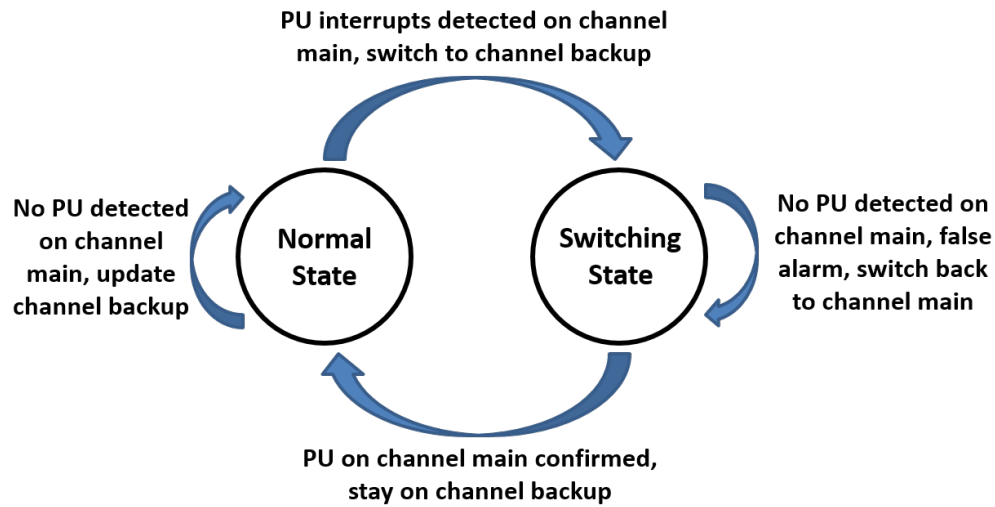
Figure 6.6: Two states Finite State Machine for channel access management.

If primary user is not using the main channel, the system stays in State 0 and updates the backup channel. Else the main channel is logged as the previous channel, then the system switches to backup channel and goes to State 1.

- State 1:
  If primary user is not using the previous channel, it is a false alarm and system switches back to the previous channel and goes to State 0. Else the system stays with this channel and goes to state 0.

6.1.7 MAC Protocol Data Unit Format

In order to be transmitted and decoded by transceivers, messages are formatted into data frames according to the applied protocols. The date passed from the upper layer will be treated as Service Data Unit (SDU), then it will be attached with some necessary information. For example, in MAC layer, the data from network layer is called MAC layer SDU (MSDU). Then it will be attached with some frame control and address information bits to form the MAC layer Protocol Unit (MPDU), which will be decoded in the MAC layer on the receiver. In the proposed Smart Grid testbed, the data to be communicated between transceivers are manipulated in the MAC layer level. The designed MSDU format is illustrated in Fig. 6.7, where the meaning of each field is given as follows.

- In Message Type field, the message type of this frame is indicated. The applied message types include control command, measurement, calibration and network command.

- In Node ID field, the data source transceiver node ID is included. Within the whole power grid, each power bus is assigned with a unique ID.

- In Data field, the information to be communicated is included. The contents vary with different message types.

- In Channel Status field, the spectrum sensing results and channel status information are included. In the prototype, the PU channel and SNR are included.

- In Spectrum Sharing Control field, the spectrum sharing related commands and data are included, which depends on the spectrum sharing mechanism. In the prototype, the backup channel is indicated in this field.

- In Time Stamp Field, the generation time for this frame is stamped in this field. This information is important for time-critical Smart Grid application.

5bytes	1byte	10bytes	6bytes	3bytes	5bytes
Message Type	Node ID	Data	Channel Status	Spectrum Sharing Control	Time Stamp
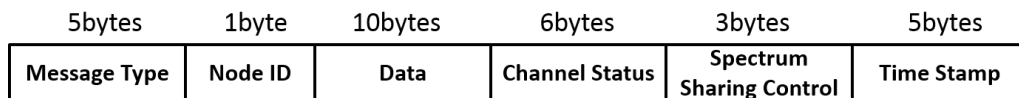
Figure 6.7: MAC layer Service Data Unit format.

6.1.8   MBED System

MBED is short for the Arm MBED IoT Device Platform, which is a fully integrated device management solution [253]. The MBED platform provides a lightweight operating system, where commonly used interfaces such as analogue, digital, I^{2}C, SPI, CAN and USB. Together with the microprocessor unit, the MBED is an ideal platform for not only control applications, but also as a data acquisition module.

The MBED provides a highly extendible platform, where extra modules can be integrated for desired features like connectivity, security and manageability. MBED is able to support various communication connection methods, such as 6LoWPAN,

Bluetooth Low Energy, Thread, LoRa, WiFi, NFC, RFID, Mobile IoT (LPWA), cellular and Ethernet between devices. For the security oriented applications, it can provide solutions such as uVisor, MBED TLS and MBED Client to secure the communication from untrusted or malicious attacks [253].

The online compiler also provides a creative environment, where mature blocks or modules are portable between different projects. It also supports C, C++ and assembly programming languages. Various interfacing functions are provided, which makes the MBED to be called as a function in other environments. For example, the MBED can be programmed to act as data acquisition and actuator modules in C, while the measurements and control commands are piped through interfaces provided in Python.

6.1.9   Data Acquisition and Actuator (DAA) Module

The data acquisition components are bridges between the SDR based communication system and the RTDS based power system. In real Smart Grid application scenarios, the data acquisition is fulfilled by different dedicated sensors, such as Voltage Meter and Watt Meter. In the meantime, the control command is executed by the actuators, such as controller and breaker.

In the proposed Smart Grid testbed, the power system operation is emulated with RTDS, where the required sensors and actuators are implemented by functions in RTDS system as well as the DAA module. The measurement outputs and control inputs are fulfilled via low voltage interfaces such as the analogue output from RTDS GTAO or RTDS GTFPI module, analogue input from RTDS GTAI module, the digital output from RTDS GTDO module and digital input from RTDS GTDI module. More sophisticated grid control modules are also supported by the designed Smart Grid testbed, where high voltage interfaces are exploited. The DAA module consists of a microcontroller and extended supportive circuits, such as bypass filter, DAC module and ADC module.

In the prototype, we apply the ARM MBED NXP LPC 1768 development board as the core of DAA module between RTDS and SDR platform. The MBED module provides versatile interfaces for various purposes, including CAN, PWM, I2C,

SPI, Serial, ADC and DAC. The MBED microcontroller is programmed to feed the USRP with RTDS GTFPI analogue outputs on demand, while the RTDS control input is achieved via RTDS GTAI interface connected with MBED Analogue Output interface.

6.2 Smart Grid Testbed Evaluation

The proposed testbed is a versatile experimental platform, which is able to perform the evaluation on both power system and communication system. In order to evaluate the proposed testbed, we implement a prototype with two USRP N210, one USRP B210, three laptops, one MBED system, one set of RTDS system and two GPS modules in the Smart Grid Laboratory at Durham University. The prototype provides an evaluation of the proposed testbed framework with all the proposed features, including power system and control system based on RTDS, data acquisition and actuator via MBED and cognitive radio enabled SDR based on USRP system. In this chapter, two evaluations including communication latency and voltage stability control application will be detailed as follows.

6.2.1 Communication Latency

Communication latency is one of the most concerned parameters in Smart Grid, which is especially true when wireless communication systems are involved. In Smart Grid, there are many delay sensitive applications, where the measurements have to be collected for a real time status monitoring, and the control commands have to be executed within a valid time period.

Therefore, in the prototype, the round trip delay performance has been evaluated. On the transmitter side, a measurement frame is tagged with UTC time as illustrated in Fig. 6.7, which is synchronised via GPS module. Once the measurement frame is decoded in the MAC layer on the receiver, a calibration frame containing the transmitted frame's time stamp is replied. Then in the MAC layer on the transmitter side, the round trip communication latency is analysed and recorded. Note that in normal operations such as the voltage stability control to be detailed in

the next part of this section, the total latency will have other contributors, such as making decisions and running power flows. Thus the evaluated time performance is the minimum achievable latency which only accounts for the communication delay.
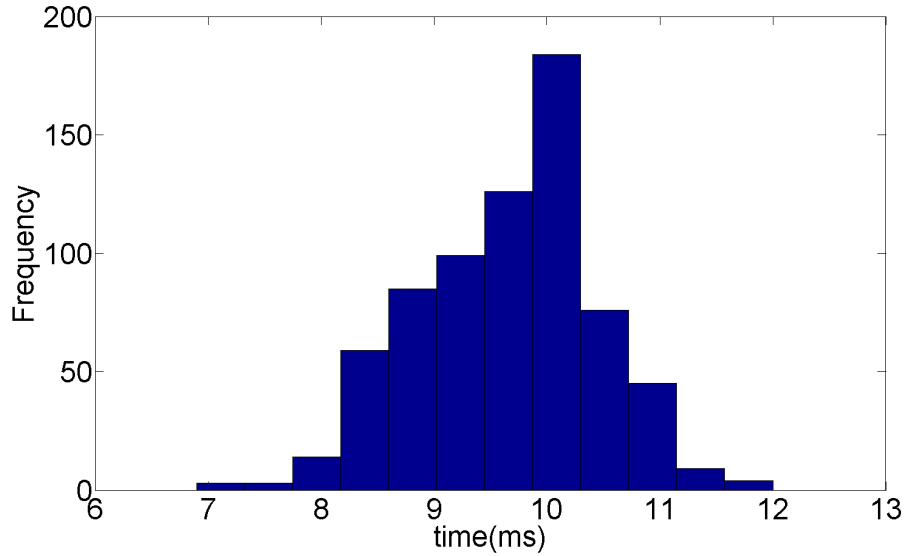

Figure 6.8: The round trip time performance.

On the transmitter side, 800 logs on the round trip time stamps are collected. The histogram of the time performance is given in Fig. 6.8. A statistical study on the data suggests that the average round trip latency is 9.68ms, where the maximum latency is 12.0ms while minimum latency is 6.9ms. Further analysis shows that the round trip delay performance can be characterized by normalized distribution, where the curve fitting algorithm suggests N(0.00968, 0.0008) is the best fit to the measured data, as shown in Fig. 6.9. The prototype can achieve a latency on the level of 10ms, which is very promising in enabling the various time critical Smart Grid applications [31].

6.2.2 Voltage Stability Control

From the power system aspect of Smart Grid, voltage stability is one of the core power quality parameters. The voltage has to be controlled within a normal range, where too high or too low voltages will damage the devices or reduce their lifetime.

In order to provide an in-depth evaluation of the prototype, a voltage stability
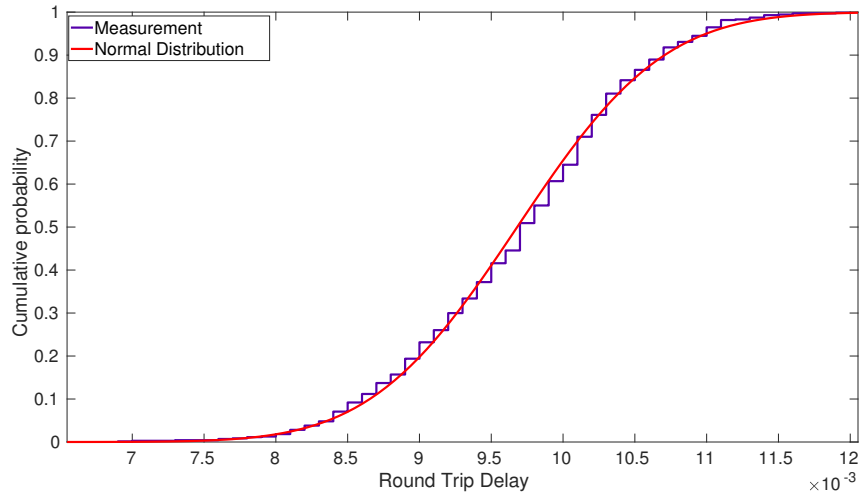
Figure 6.9: The CDF performance of measurements vs Normal distribution N(0.00968, 0.0008)

control system has been implemented and evaluated. On the RTDS, the modified 4 bus power system with one generator and one wind farm has been emulated. The wind farm attached to bus 4 is able to tune the reactive power production, which can be used to maintain the voltage stability in both local grid and whole grid. A large dynamic load is connected to bus 4, which varies with time to simulate the real cases.

Two sets of SDR platforms are exploited. One set is attached to bus 4, which is referred to as bus node set. It monitors the dynamic load and control the reactive power output from the wind farm on the RTDS via the DAA module. Another set simulates the control centre, which communicates with the bus node set to collect measurements and sends the reactive power generation values. On the control centre side, the power system state estimation is performed via the power flow algorithm, while the wind farm reactive power production is calculated via the following algorithms.

$$\Delta \mathbf{Q} = \mathbf{H} \Delta \mathbf{V}, \tag{6.1}$$

where $\Delta \mathbf{Q}$ is the required additional reactive power generation and $\mathbf{H}$ is the Jacobian matrix associated with the current power system status, which is obtained via power flow algorithm. $\Delta \mathbf{V}$ is the voltage difference between the current states and the threshold voltage magnitudes. In the implemented system, this desired threshold

voltage magnitude is set to 0.983 p.u..

The system is running with IEEE 802.11 a/g/p protocols on the 2.4GHz and 5GHz frequency band. The 5.8GHz frequency band for IEEE 802.11p is assumed to be the primary user's band, which is less crowded in spectrum and has a wider bandwidth. An ELM model is trained and exploited for the fast spectrum sensing purpose.


```
scbg46@DML-ECSPG-132: ~/Desktop/polay@gui
Communication Channel: 178 Backup channel: 182 PU channel: 000 RTDS measurement: 2.442 V
Communication Channel: 178 Backup channel: 182 PU channel: 000 RTDS measurement: 2.443 V
Communication Channel: 178 Backup channel: 182 PU channel: 000 RTDS measurement: 2.428 V

UHD Warning:
    The requested decimation is odd; the user should expect CIC rolloff.
    Select an even decimation to ensure that a halfband filter is enabled.
    decimation = dsp_rate/samp_rate -> 5 = (100.000000 MHz)/(20.000000 MHz)
No PU interruption, new back up channel  182 , we are talking at channel  178
we are talking at 178 , and the backup channel is 182
Communication Channel: 178 Backup channel: 182 PU channel: 000 RTDS measurement: 2.442 V
Communication Channel: 178 Backup channel: 182 PU channel: 000 RTDS measurement: 2.442 V
Communication Channel: 178 Backup channel: 182 PU channel: 000 RTDS measurement: 2.427 V
Communication Channel: 178 Backup channel: 182 PU channel: 000 RTDS measurement: 2.428 V
Communication Channel: 178 Backup channel: 182 PU channel: 000 RTDS measurement: 2.428 V
Communication Channel: 178 Backup channel: 182 PU channel: 000 RTDS measurement: 2.427 V
Communication Channel: 178 Backup channel: 182 PU channel: 000 RTDS measurement: 2.426 V
Communication Channel: 178 Backup channel: 182 PU channel: 000 RTDS measurement: 2.441 V
Communication Channel: 178 Backup channel: 182 PU channel: 000 RTDS measurement: 2.427 V
Communication Channel: 178 Backup channel: 182 PU channel: 000 RTDS measurement: 2.429 V

UHD Warning:
    The requested decimation is odd; the user should expect CIC rolloff.
    Select an even decimation to ensure that a halfband filter is enabled.
    decimation = dsp_rate/samp_rate -> 5 = (100.000000 MHz)/(20.000000 MHz)
PU appears! No switching! PU is using channel  174 ,but we are using channel  178
we are talking at 178 , and the backup channel is 182
Communication Channel: 178 Backup channel: 182 PU channel: 174 RTDS measurement: 2.441 V
Communication Channel: 178 Backup channel: 182 PU channel: 174 RTDS measurement: 2.443 V
Communication Channel: 178 Backup channel: 182 PU channel: 174 RTDS measurement: 2.442 V
Communication Channel: 178 Backup channel: 182 PU channel: 174 RTDS measurement: 2.428 V
Communication Channel: 178 Backup channel: 182 PU channel: 174 RTDS measurement: 2.442 V
Communication Channel: 178 Backup channel: 182 PU channel: 174 RTDS measurement: 2.427 V
Communication Channel: 178 Backup channel: 182 PU channel: 174 RTDS measurement: 2.427 V
Communication Channel: 178 Backup channel: 182 PU channel: 174 RTDS measurement: 2.442 V
Communication Channel: 178 Backup channel: 182 PU channel: 174 RTDS measurement: 2.443 V
Communication Channel: 178 Backup channel: 182 PU channel: 174 RTDS measurement: 2.427 V

UHD Warning:
    The requested decimation is odd; the user should expect CIC rolloff.
    Select an even decimation to ensure that a halfband filter is enabled.
    decimation = dsp_rate/samp_rate -> 5 = (100.000000 MHz)/(20.000000 MHz)
PU appears! No switching! PU is using channel  174 ,but we are using channel  178
we are talking at 178 , and the backup channel is 182
Communication Channel: 178 Backup channel: 182 PU channel: 174 RTDS measurement: 2.443 V
Communication Channel: 178 Backup channel: 182 PU channel: 174 RTDS measurement: 2.427 V
Communication Channel: 178 Backup channel: 182 PU channel: 174 RTDS measurement: 2.428 V
Communication Channel: 178 Backup channel: 182 PU channel: 174 RTDS measurement: 2.427 V
Communication Channel: 178 Backup channel: 182 PU channel: 174 RTDS measurement: 2.428 V
Communication Channel: 178 Backup channel: 182 PU channel: 174 RTDS measurement: 2.442 V
Communication Channel: 178 Backup channel: 182 PU channel: 174 RTDS measurement: 2.443 V
Communication Channel: 178 Backup channel: 182 PU channel: 174 RTDS measurement: 2.443 V
Communication Channel: 178 Backup channel: 182 PU channel: 174 RTDS measurement: 2.443 V
Communication Channel: 178 Backup channel: 182 PU channel: 174 RTDS measurement: 2.444 V

UHD Warning:
    The requested decimation is odd; the user should expect CIC rolloff.
    Select an even decimation to ensure that a halfband filter is enabled.
    decimation = dsp_rate/samp_rate -> 5 = (100.000000 MHz)/(20.000000 MHz)
```

Figure 6.10: PU appears in Channel 174, while the pairs are communicating on Channel 178 and the channel is maintained.

Besides, another set of SDR platform is implemented with USRP B210 to simulate the primary user, which is assumed to random appear in any channel in 5.8GHz

Figure 6.11: PU takes over the Channel 178, the communicating pairs switch to backup Channel 172 in the new communication round.

at any time. Two PU interruption scenarios have been evaluated. For the first scenario, the pair of nodes is communicating in Channel 178, while the PU appears on Channel 174. With the implemented FSM channel access management in Fig. 6.6, this pair maintains their channel but they are aware of the PU's appearance, as indicated in Fig. 6.10. In the second scenario, the pair of nodes are communicating in Channel 178, and the PU appears on Channel 178. As illustrated in Fig. 6.11, the nodes are aware of the PU's appearance. They give up the Channel 178 to the PU and successfully switch to the backup Channel 172, and their communication

link is maintained.
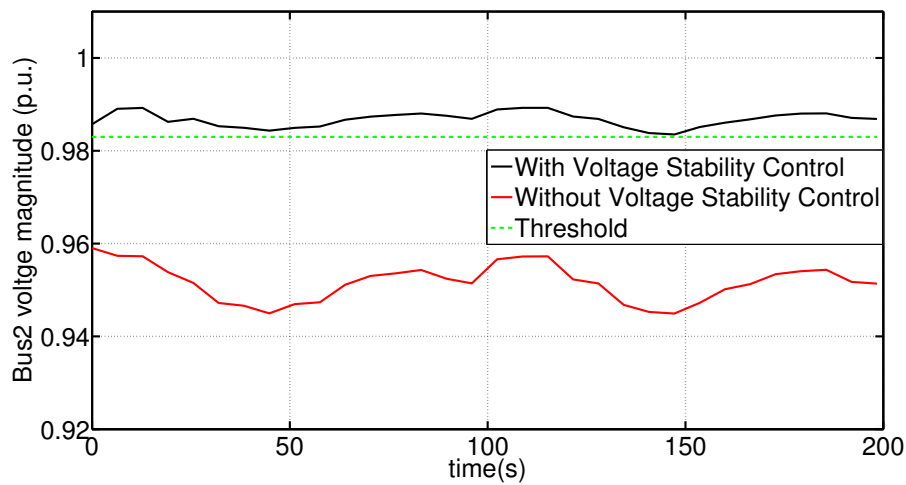
Figure 6.12: Bus 2 voltage magnitude with v.s. without voltage control.
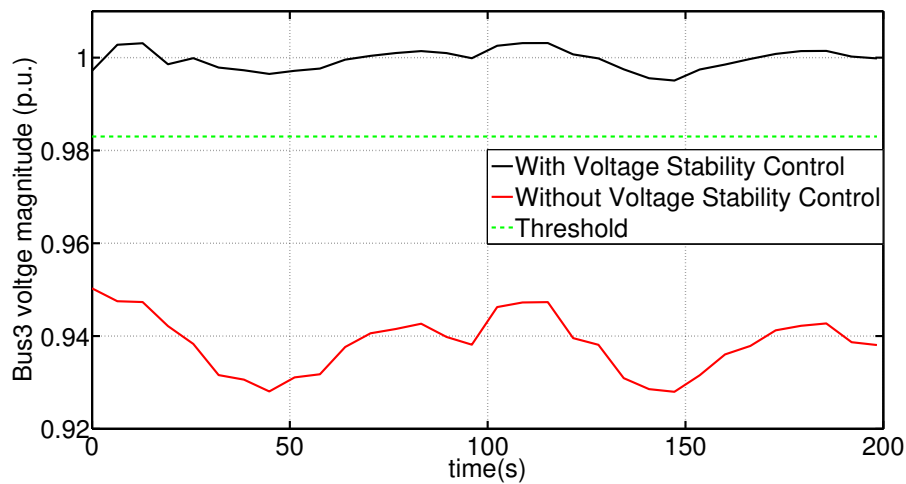
Figure 6.13: Bus 3 voltage magnitude with v.s. without voltage control.

With the real time feature of the testbed, the system is able to provide timely control to stabilize whole grid's voltage magnitudes above the threshold 0.983 p.u., as indicated in Fig. 6.12-6.14. It can be also indicated by these figures that, the voltage magnitudes are maintained within the range of 0.983-1.010 p.u., which is in a more stable state than the case without control. Also due to the timely control, the variation of the voltage magnitude profile is more desirable than the case without control.
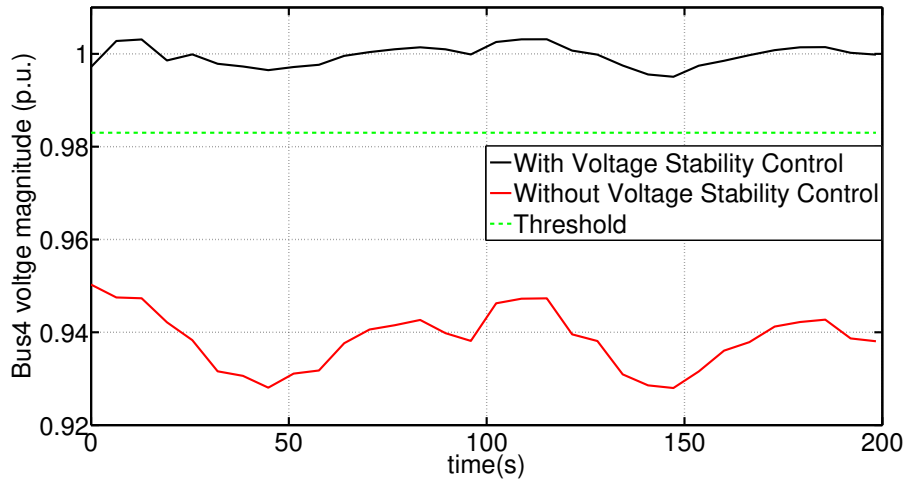
Figure 6.14: Bus 4 voltage magnitude with v.s. without voltage control.

6.3 Concluding Remarks

In this chapter, we proposed a Smart Grid testbed based on SDR platform and
RTDS system. Besides, the Cognitive Radio technology was employed in the com-
munication system, where the spectrum sensing was enabled via machine learning
algorithm. The power system was emulated via the RTDS system in real time, where
the interfaces between USRP and RTDS systems were supported by a designed DAA
module. Two evaluations were performed on the implemented prototype, including
communication latency and voltage stability control system. Results showed that
the proposed testbed can provide an average of 9.7ms round trip communication
latency, and support the real time applications such as voltage stability control.
The prototype validated that the proposed Smart Grid testbed was able to provide
a comprehensive development environment for both power system and communica-
tion system.

Chapter 7

Discussions, Conclusions and Future Works

In this chapter, the main results obtained in previous chapters will be briefly summarized and discussed, which will be focusing on the generalization of effective rate theory, effective theory application in smart grid and software defined Smart Grid testbed, respectively. Based on the discussions, future works are discussed, which will be helpful to the researches on QoS performance analysis within Smart Grid.

7.1 General Discussions on the Results

7.1.1 Generalization of Effective Rate Theory

In Chapter 3, the traditional integration based method for effective rate analysis was introduced. This framework was applied to the i.n.i.d. Weibull fading channel conditions, which complemented existing effective rate researches. In Chapter 3, a new framework was proposed for the effective rate analysis, which was based on H transform representation. Some key points about the proposed framework are discussed as follows.

Firstly, compared to the integration based framework, the proposed one further extended the effective rate analytical framework. As can be seen in Chapter 2 and the reference therein, although integration based framework was able to analyse

140

every MISO fading scenario, it was usually very hard or required extensive efforts. As illustrated in Section 4-3 Chapter 4, the analysis of SISO, i.i.d., i.n.i.d. and even correlated fading channel scenarios was more unified within the proposed framework, where the analysis complexity was transformed to obtain the MGF of the interested fading channel. The MGF was already known for most fading scenarios as listed in Table 4-4.

Secondly, the application of H transform simplified the derivation procedure involved in effective rate analysis. The key point about H transform was that it transformed the integration operation into the arithmetic of parameters. Similar to the application of Fourier transform or Laplace transform in the electronic analysis, this H transform had provided a new method for effective rate analysis, or even other researches where complex integration manipulations were involved.

Thirdly, the representation for the effective rate of many complex fading channels could be given in the analytical form, without integration operations involved. This was a very attractive feature about the proposed framework, since effective rate was also a metric, which needed to be involved in further analysis and derivations such as QoS provisioning. When the effective rate was involved in further integration operations, the H transform and H function provided versatile and more unified manipulation method.

In addition, many beneficial results were obtained based on the framework, including both analytical and asymptotic results. This included more specific representations for i.n.i.d. scenarios and asymptotic approximations covering correlated fading channels. The intermediate results were also beneficial to the study of general functions like H function, since these functions were frequently used in the analysis of engineering related researches.

Last but not the least, besides its advantages in the analytical analysis, the framework also showed potentials in numerical analysis. As illustrated in Chapter 3, in most scenarios the analytical representation of the effective rate was also in H function format with a variation of parameters. As H function was available in numerical software, such as Mathematics or Matlab, it potentially further simplified the evaluation of effective rate as a metric of the QoS performance in individual

fading channel scenarios.

7.1.2 Effective Rate Theory Application in Smart Grid QoS Analysis

As shown in Chapter 2-3, the effective rate was a versatile QoS metric, which could characterize the statistical delay performance from a cross layer view. In the latter part of Chapter 3, an initial application of effective rate on the QoS performance analysis of Smart Grid applications was presented. The analysis was performed based on specific QoS performance requirements, where minimum communication resources for a statistical delay guarantee was recommended. Further in Chapter 5, a more specific scenario was investigated, where the power system observability performance was analysed under constrained communication resources. The effective rate was applied to bridge the gaps between two systems, where three observability improvement methods were proposed. From these investigations, some discussions on the application of effective rate theory in Smart Grid QoS analysis could be given as follows, which might provide an in-depth understanding of this metric's benefits.

In the beginning, effective rate theory has the potential in bridging the research gap between power system and communication system in the study of Smart Grid. Traditionally power system and communication system are two distinct and largely separated research areas. This results in the complicated situation in the integration of such two systems, especially during the analytical researches. Although the performance metrics in either system are usually well investigated, the mutual influence is still not well addressed yet. Let alone it is essentially a complicated task to characterize some metrics within one system, such as delay in the communication system. Thus via the demonstrations in Chapter 3 and Chapter 5, effective rate as a cross layer oriented QoS metric is also a potential metric in addressing the coupling effective between power system and communication system.

Moreover, effective rate theory is also an analytical framework, which paves the way for both analytical and numerical researches on interested application performances in Smart Grid. With the further extension of existing integration based effective rate analytical framework in Chapter 3 and the new proposed MGF and

H transform based framework in Chapter 4, the analytical effective rate representation for general or specific Smart Grid scenarios can be readily available. This not only benefits the modelling of such application scenario in a theoretical way, but also provides a numerical evaluation tool for the consideration of various communication system effects, such as channel fading effects and communication resource constraints.

7.1.3   Software Defined Smart Grid Testbed

As reviewed in Chapter 2, it has attracted a lot of universities, laboratories, and institutions to build testbeds for an experimental Smart Grid environment. The proposed software defined Smart Grid testbed in Chapter 6 provides such environment with large flexibility in both power system and communication system. To be specific, the benefits of this testbed can be listed as follows.

Firstly, the RTDS system is able to support real time simulation in a wide range of power system scenarios, including system level control, transmission network, distribution network, system modelling and small scale signal simulations. Besides, the RTDS system itself is also modularized, where desired simulation scale can be achieved via extra computing cards. The available I/O cards provide versatile interfacing methods to other simulators and hardware. For example, hardware-in-the-loop can be achieved with high voltage interfaces, while various control and measurements can be realized using the analogue and digital input/output interfaces.

Secondly, the MBED system is a different trial on the interfacing method within Smart Grid testbed. The MBED system is programmed as data acquisition and actuator module, which itself acts and emulates the intelligent electrical devices (IEDs) like meters or controllers deployed in the Smart Grid. This is another dimension provided by this testbed for Smart Grid related researches. Besides, the system is also highly extendible, for example modules can be integrated to achieve a large IoT network. The application of MBED also benefits the whole testbed in the aspect of computation. As MBED itself can be programmed to perform complex control or interfacing tasks, this also reduces the signal processing burden from both communication system and power system end. The MBED is in essence a hardware platform,

but due to its programmable feature, it is integrated into the whole testbed similar to those SDR modules.

The most important aspect of this software defined Smart Grid testbed is its integration of SDR system to implement the communication system. According to the extensive reviews in Chapter 2, this is the first time that a SDR system is used to build a Smart Grid testbed. The software defined radio provides an environment similar to simulation testbeds solely based on software, where the difference is the APIs have been related to real hardware functions and resources. On the other hand, the SDR system itself is a real hardware system, where all implemented designs are readily and commercially available. Besides, since the infrastructure of a SDR based system is combinations of software defined modules, the comparisons or evaluations of new technologies and configurations are therefore facilitated.

From the above discussions, it can be concluded that the proposed software defined Smart Grid testbed is able to provide a versatile experimental environment, specifically in the aspect of implementation of different communication protocols, evaluation of Smart Grid applications in wide range of practical power system scenarios, and the emulation of IED device performances.

7.2 Future Works

As discussed in the previous section, the works introduced in this thesis brings some potential new research directions in Smart Grid QoS performance analysis. Thus some future works are identified as follows.

7.2.1 Further Extensions on Effective Rate Theory

Although effective rate theory is based on cross layer analysis within the communication system, the researches involved in Chapter 3 and Chapter 4 are all based on Physical layer and Network layer. This is also true to most existing literature, where the influence of MAC layer has been overlooked. To the best of the author's knowledge, only empirical model is available which simultaneously considers Physical layer, MAC layer and Network layer. Thus in the future work, efforts will be

put on the analytical framework to include the effects from all these three layers.

7.2.2 Effective Rate in Smart Grid Application QoS Analysis

As demonstrated in Chapter 5, the effective rate can serve as the coupling point between power system and communication system in the Smart Grid application QoS analysis. Effective rate as a QoS metric connects statistical delay performances and communication resources, thus it is possible to use similar research method to the analytical studies of other time critical Smart Grid applications. Future work will include applying effective rate to investigate real time voltage stability control and distributed renewable resources management.

7.2.3 Further extensions on Software Defined Smart Grid Testbed

The work introduced in Chapter 6 presents the framework of the proposed testbed, where a small scale prototype has been implemented. The prototype shows potential in the evaluation of real time Smart Grid applications, for example the real time voltage stability control. In the future work, several aspects will be focused on, including expanding the communication protocol pool, large scale networking, distribution network scenario, distributed renewable energy management, and wireless supported PMU.

7.3 Thesis Conclusion

In this thesis, the QoS performances in Smart Grid scenario has been studied from both theoretical and practical aspects. Effective rate theory has been studied as a potential method in addressing the coupling effects between power system and communication system. The proposed new effective rate analytical and asymptotic framework has shown its flexibility and advantages for various wireless fading channels, including SISO, MISO i.n.i.d. and correlated scenarios. Furthermore, effective

rate has been used to improve power system observability under communication constraints, which also demonstrates the potential of effective rate in addressing the general problem where power system and communication system are deeply coupled. A new software defined Smart Grid testbed framework has also been proposed, which is flexible and scalable in configuration while versatile in experimental contents. The implemented prototype and the demonstration cases have shown that the testbed is able to evaluate real time Smart Grid application performances.

Bibliography

[1] Y. Jeong, H. Shin, and M. Win, "H-transforms for wireless communication," *IEEE Transactions on Information Theory*, vol. 61, no. 7, pp. 3773–3809, July 2015.

[2] F. Yilmaz and M. S. Alouini, "A novel unified expression for the capacity and bit error probability of wireless communication systems over generalized fading channels," *IEEE Transactions on Communications*, vol. 60, no. 7, pp. 1862–1876, July 2012.

[3] United States Department of Commece National Institute of Standards and Technology Office of the National Coordinator for Smart Grid Interoperability, "NIST framework and roadmap for smart grid interoperability standards," *Release 1.0*, 2010.

[4] D. Wu and R. Negi, "Effective capacity: a wireless link model for support of quality of service," *IEEE Transactions on Wireless Communications*, vol. 2, no. 4, pp. 630–643, February 2003.

[5] C.-S. Chang and J. A. Thomas, "Effective bandwidth in high-speed digital networks," *IEEE Journal on Selected areas in Communications*, vol. 13, no. 6, pp. 1091–1100, August 1995.

[6] J. Zhang, M. Matthaiou, Z. Tan, and H. Wang, "Effective rate analysis of MISO η-μ fading channels," in *2013 IEEE International Conference on Communications*, Budapest, June 2013, pp. 5840–5844.

[7] X. Li, J. Li, L. Li, J. Jin, J. Zhang, and D. Zhang, "Effective rate of MISO systems over κ - μ shadowed fading channels," *IEEE Access*, vol. 5, pp. 10 605–10 611, June 2017.

[8] S. Akin and M. C. Gursoy, "Effective capacity analysis of cognitive radio channels for quality of service provisioning," *IEEE Transactions on Wireless Communications*, vol. 9, no. 11, pp. 3354–3364, October 2010.

[9] A. Khalek and Z. Dawy, "Energy-efficient cooperative video distribution with statistical QoS provisions over wireless networks," *IEEE Transactions on Mobile Computing*, vol. 11, no. 7, pp. 1223–1236, July 2012.

[10] M. Matthaiou, G. C. Alexandropoulos, H. Q. Ngo, and E. G. Larsson, "Analytic framework for the effective rate of MISO fading channels," *IEEE Transactions on Communications*, vol. 60, no. 6, pp. 1741–1751, June 2012.

[11] S. V. Buldyrev, R. Parshani, G. Paul, H. E. Stanley, and S. Havlin, "Catastrophic cascade of failures in interdependent networks," *Nature*, vol. 464, no. 7291, pp. 1025–1028, April 2010.

[12] Z. Feng, Q. Li, W. Li, T. A. Gulliver, and P. Zhang, "Priority-based dynamic spectrum management in a smart grid network environment," *IEEE Journal on Selected Areas in Communications*, vol. 33, no. 5, pp. 933–945, May 2015.

[13] J. Huang, H. Wang, Y. Qian, and C. Wang, "Priority-based traffic scheduling and utility optimization for cognitive radio communication infrastructure-based smart grid," *IEEE Transactions on Smart Grid*, vol. 4, no. 1, pp. 78–86, March 2013.

[14] C. E. Shannon, "A mathematical theory of communication," *ACM SIGMOBILE Mobile Computing and Communications Review*, vol. 5, no. 1, pp. 3–55, 2001.

[15] X. Fang, S. Misra, G. Xue, and D. Yang, "Smart grid–the new and improved power grid: A survey," *IEEE communications Surveys & Tutorials*, vol. 14, no. 4, pp. 944–980, December 2012.

[16] H. Farhangi, "The path of the smart grid," *IEEE Power and Energy Magazine*, vol. 8, no. 1, pp. 1–8, December 2010.

[17] I. Cisco, "Internet protocol architecture for the smart grid," 2009.

[18] I. Lamprinos, N. D. Hatziargyriou, I. Kokos, and A. D. Dimeas, "Making demand response a reality in Europe: Policy, regulations, and deployment status," *IEEE Communications Magazine*, vol. 54, no. 12, pp. 108–113, December 2016.

[19] NDRC and NEB, "Thirteenth five year plan related to major science and technology industrialization projects of smart grid," National Development and Reform Commission and National Energy Board, Tech. Rep., Dec. 2016. [Online]. Available: http://www.ndrc.gov.cn/zcfb/zcfbghwb/201612/P020161222570036010274.pdf

[20] the Government of Japan, "Strategic energy plan," the Government of Japan, Tech. Rep., Apr. 2014. [Online]. Available: http://www.enecho.meti.go.jp/en/category/others/basic_plan/pdf/4th_strategic_energy_plan.pdf

[21] I. S. G. S. Roadmap, "SMB smart grid strategic group SG3," 2010.

[22] "IEEE guide for the interoperability of energy storage systems integrated with the electric power infrastructure," *IEEE P2030.2 D9.0, December 2014*, pp. 1–136, June 2015.

[23] Microsoft, "Smart energy reference architecture SERA," Tech. Rep., 2009.

[24] S. Rohjans, M. Uslar, R. Bleiker, J. González, M. Specht, T. Suding, and T. Weidelt, "Survey of smart grid standardization studies and recommendations," in *2010 first IEEE international conference on Smart grid communications (SmartGridComm)*, 2010, pp. 583–588.

[25] *IEC 61850-5 2013: Communication networks and systems for power utility automation*, Int. Electrotechnical Commission Std., 2013.

[26] Z. Shenming and L. Guoding, "Introduction of standard IEC 61970," *Automation of Electric Power Systems*, vol. 14, pp. 1–6, 2002.

[27] W. Wang, Y. Xu, and M. Khanna, "A survey on the communication architectures in smart grid," *Computer Networks*, vol. 55, no. 15, pp. 3604–3629, October 2011.

[28] L. A. Barroso, H. Rudnick, F. Sensfuss, and P. Linares, "The green effect," *IEEE Power and Energy Magazine*, vol. 8, no. 5, pp. 22–35, September 2010.

[29] E. K. Hart, E. D. Stoutenburg, and M. Z. Jacobson, "The potential of intermittent renewables to meet electric power demand: Current methods and emerging analytical techniques," *Proceedings of the IEEE*, vol. 100, no. 2, pp. 322–334, February 2012.

[30] P. Kundur, N. J. Balu, and M. G. Lauby, *Power system stability and control*. McGraw-hill New York, 1994, vol. 7.

[31] V. C. Gungor, D. Sahin, T. Kocak, S. Ergut, C. Buccella, C. Cecati, and G. P. Hancke, "A survey on smart grid potential applications and communication requirements," *IEEE Transactions on Industrial Informatics*, vol. 9, no. 1, pp. 28–42, September 2013.

[32] D. Engel and G. Eibl, "Wavelet-based multiresolution smart meter privacy," *IEEE Transactions on Smart Grid*, vol. 8, no. 4, pp. 1710–1721, July 2017.

[33] Y. Yan, Y. Qian, H. Sharif, and D. Tipper, "A survey on smart grid communication infrastructures: Motivations, requirements and challenges," *IEEE Communications Surveys & Tutorials*, vol. 15, no. 1, pp. 5–20, February 2013.

[34] M. Chenine, K. Zhu, and L. Nordstrom, "Survey on priorities and communication requirements for PMU-based applications in the nordic region," in *2009 IEEE Bucharest PowerTech*, 2009, pp. 1–8.

[35] V. C. Güngör, D. Sahin, T. Kocak, S. Ergüt, C. Buccella, C. Cecati, and G. P. Hancke, "Smart grid technologies: communication technologies and

standards," *IEEE Transactions on Industrial Informatics*, vol. 7, no. 4, pp. 529–539, September 2011.

[36] M. You, H. Sun, J. Jiang, and J. Zhang, "Unified framework for the effective rate analysis of wireless communication systems over MISO fading channels," *IEEE Transactions on Communications*, vol. 65, no. 4, pp. 1775–1785, December 2017.

[37] D. Von Dollen *et al.*, "Report to NIST on the smart grid interoperability standards roadmap," *Electric Power Research Institute (EPRI) and National Institute of Standards and Technology*, 2009.

[38] B. Gou, "Generalized integer linear programming formulation for optimal PMU placement," *IEEE Transactions on Power Systems*, vol. 23, no. 3, pp. 1099–1104, July 2008.

[39] I. Recommendation, "E. 800: Terms and definitions related to quality of service and network performance including dependability," *ITU-T August 1994*, 1994.

[40] J. Tang and X. Zhang, "Cross-layer resource allocation over wireless relay networks for quality of service provisioning," *IEEE Journal on Selected Areas in Communications*, vol. 25, no. 4, pp. 645–656, May 2007.

[41] M.-C. Chow, *Understanding SONET/SDH: Standards and Applications*. Andan Publisher, 1996.

[42] K. Pahlavan and P. Krishnamurthy, *IEEE 802.3 Ethernet*. Wiley Telecom, 2009. [Online]. Available: http://ieeexplore.ieee.org/xpl/articleDetails.jsp?arnumber=8042052

[43] W. J. Goralski, *ADSL and DSL technologies*. McGraw-Hill Professional, 2001.

[44] J. G. Deshpande, E. Kim, and M. Thottan, "Differentiated services QoS in smart grid communication networks," *Bell Labs Technical Journal*, vol. 16, no. 3, pp. 61–81, December 2011.

[45] N. Saputro, K. Akkaya, and S. Uludag, "A survey of routing protocols for smart grid communications," *Computer Networks*, vol. 56, no. 11, pp. 2742–2771, July 2012.

[46] H. C. Ferreira, H. M. Grové, O. Hooijen, and A. Han Vinck, *Power line communication*.   Wiley Online Library.

[47] A. M. Tonello and F. Versolatto, "Bottom-up statistical PLC channel modeling part I: Random topology model and efficient transfer function computation," *IEEE Transactions on Power Delivery*, vol. 26, no. 2, pp. 891–898, April 2011.

[48] A. A. Amarsingh, H. A. Latchman, and D. Yang, "Narrowband power line communications: Enabling the smart grid," *IEEE Potentials*, vol. 33, no. 1, pp. 16–21, January 2014.

[49] B. Adebisi, A. Treytl, A. Haidine, A. Portnoy, R. U. Shan, D. Lund, H. Pille, and B. Honary, "IP-centric high rate narrowband PLC for smart grid applications," *IEEE Communications Magazine*, vol. 49, no. 12, pp. 46–54, December 2011.

[50] G. Artale, A. Cataliotti, V. Cosentino, D. D. Cara, R. Fiorelli, P. Russotto, and G. Tin, "Medium voltage smart grid: Experimental analysis of secondary substation narrow band power line communication," *IEEE Transactions on Instrumentation and Measurement*, vol. 62, no. 9, pp. 2391–2398, September 2013.

[51] S. Galli, A. Scaglione, and Z. Wang, "For the grid and through the grid: The role of power line communications in the smart grid," *Proceedings of the IEEE*, vol. 99, no. 6, pp. 998–1027, June 2011.

[52] M. Yigit, V. C. Gungor, G. Tuna, M. Rangoussi, and E. Fadel, "Power line communication technologies for smart grid applications: A review of advances and challenges," *Computer Networks*, vol. 70, pp. 366–383, September 2014.

[53] C. Cano, A. Pittolo, D. Malone, L. Lampe, A. M. Tonello, and A. G. Dabak, "State of the art in power line communications: From the applications to the

medium," *IEEE Journal on Selected Areas in Communications*, vol. 34, no. 7, pp. 1935–1952, July 2016.

[54] "IEEE standard for wireless lan medium access control (MAC) and physical layer (PHY) specifications," *IEEE Std 802.11-1997*, pp. 1–445, November 1997.

[55] "IEEE standard for information technology - telecommunications and information exchange between systems - local and metropolitan area networks specific requirements part 15.4: Wireless medium access control (MAC) and physical layer (PHY) specifications for low-rate wireless personal area networks (LR-WPANs)," *IEEE Std 802.15.4-2003*, pp. 1–670, 2003.

[56] P. Fazio, F. D. Rango, and M. Tropea, "Prediction and QoS enhancement in new generation cellular networks with mobile hosts: A survey on different protocols and conventional unconventional approaches," *IEEE Communications Surveys & Tutorials*, vol. 19, no. 3, pp. 1822–1841, March 2017.

[57] "IEEE standard for information technology– local and metropolitan area networks– specific requirements– part 22: Cognitive wireless ran medium access control (MAC) and physical layer (PHY) specifications: Policies and procedures for operation in the TV bands," *IEEE Std 802.22-2011*, pp. 1–680, July 2011.

[58] M. Chen, Y. Qian, Y. Hao, Y. Li, and J. Song, "Data-driven computing and caching in 5g networks: Architecture and delay analysis," *IEEE Wireless Communications*, vol. 25, no. 1, pp. 70–75, 2018.

[59] A. Osseiran, F. Boccardi, V. Braun, K. Kusume, P. Marsch, M. Maternia, O. Queseth, M. Schellmann, H. Schotten, H. Taoka *et al.*, "Scenarios for 5g mobile and wireless communications: the vision of the metis project," *IEEE Communications Magazine*, vol. 52, no. 5, pp. 26–35, 2014.

[60] M. Simsek, A. Aijaz, M. Dohler, J. Sachs, and G. Fettweis, "5g-enabled tactile internet," *IEEE Journal on Selected Areas in Communications*, vol. 34, no. 3, pp. 460–473, 2016.

[61] M. Marchese, *QoS over heterogeneous networks*. John Wiley & Sons, 2007.

[62] L. Rao, X. Liu, L. Xie, and W. Liu, "Coordinated energy cost management of distributed internet data centers in smart grid," *IEEE Transactions on Smart Grid*, vol. 3, no. 1, pp. 50–58, March 2012.

[63] A. Rahman, X. Liu, and F. Kong, "A survey on geographic load balancing based data center power management in the smart grid environment," *IEEE Communications Surveys & Tutorials*, vol. 16, no. 1, pp. 214–233, August 2014.

[64] M. Ghamkhari and H. Mohsenian-Rad, "Energy and performance management of green data centers: A profit maximization approach," *IEEE Transactions on Smart Grid*, vol. 4, no. 2, pp. 1017–1025, June 2013.

[65] D. Niyato, L. Xiao, and P. Wang, "Machine-to-machine communications for home energy management system in smart grid," *IEEE Communications Magazine*, vol. 49, no. 4, pp. 53–59, April 2011.

[66] H. Gharavi and B. Hu, "Multigate communication network for smart grid," *Proceedings of the IEEE*, vol. 99, no. 6, pp. 1028–1045, May 2011.

[67] S. Salous, *Radio propagation measurement and channel modelling*. John Wiley & Sons, 2013.

[68] T. S. Rappaport *et al.*, *Wireless communications: principles and practice*. prentice hall PTR New Jersey, 1996, vol. 2.

[69] D. Chen, J. Brown, and J. Y. Khan, "Performance analysis of a distributed 6LoWPAN network for the smart grid applications," in *2014 IEEE Ninth International Conference on Intelligent Sensors, Sensor Networks and Information Processing (ISSNIP)*, 2014, pp. 1–6.

[70] J. Kim, D. Kim, K.-W. Lim, Y.-B. Ko, and S.-Y. Lee, "Improving the reliability of IEEE 802.11s based wireless mesh networks for smart grid systems," *Journal of Communications and Networks*, vol. 14, no. 6, pp. 629–639, December 2012.

[71] H. Hu, D. Kaleshi, A. Doufexi, and L. Li, "Performance analysis of IEEE 802.11af standard based neighbourhood area network for smart grid applications," in *2015 IEEE 81st Vehicular Technology Conference (VTC Spring)*, 2015, pp. 1–5.

[72] R. P. Liu, G. J. Sutton, and I. B. Collings, "Power save with offset listen interval for IEEE 802.11ah smart grid communications," in *2013 IEEE International Conference on Communications (ICC)*, 2013, pp. 4488–4492.

[73] J. F. Kurose, *Computer networking: A top-down approach featuring the internet.* Pearson Education India, 2005.

[74] R. Ramaswamy, N. Weng, and T. Wolf, "Characterizing network processing delay," in *IEEE 2004 Global Telecommunications Conference (GLOBECOM'04)*, vol. 3, 2004, pp. 1629–1634.

[75] D. D. Giustina and S. Rinaldi, "Hybrid communication network for the smart grid: Validation of a field test experience," *IEEE Transactions on Power Delivery*, vol. 30, no. 6, pp. 2492–2500, December 2015.

[76] P. Kansal and A. Bose, "Bandwidth and latency requirements for smart transmission grid applications," *IEEE Transactions on Smart Grid*, vol. 3, no. 3, pp. 1344–1352, May 2012.

[77] P. Ferrari, A. Flammini, M. Loda, S. Rinaldi, D. Pagnoncelli, and E. Ragaini, "First experimental characterization of LTE for automation of smart grid," in *2015 IEEE International Workshop on Applied Measurements for Power Systems (AMPS)*, 2015, pp. 108–113.

[78] S. Rinaldi, P. Ferrari, A. Flammini, F. Gringoli, M. Loda, and N. Ali, "An application of ieee 802.11ac to smart grid automation based on IEC 61850," in *IECON 2016 - 42nd Annual Conference of the IEEE Industrial Electronics Society*, 2016, pp. 4645–4650.

[79] M. Luvisotto, Z. Pang, and D. Dzung, "Ultra high performance wireless control for critical applications: Challenges and directions," *IEEE Transactions on Industrial Informatics*, vol. 13, no. 3, pp. 1448–1459, October 2017.

[80] M. Kolenc, P. Nemček, C. Gutschi, N. Suljanović, and M. Zajc, "Performance evaluation of a virtual power plant communication system providing ancillary services," *Electric Power Systems Research*, vol. 149, pp. 46–54, August 2017.

[81] J. Stahlhut, T. Browne, G. Heydt, and V. Vittal, "Latency viewed as a stochastic process and its impact on wide area power system control signals," *IEEE Transactions on Power Systems*, vol. 23, no. 1, pp. 84–91, February 2008.

[82] A. Chamaken and L. Litz, "Joint design of control and communication in wireless networked control systems: A case study," in *2010 American Control Conference (ACC)*, 2010, pp. 1835–1840.

[83] V. C. Gungor, B. Lu, and G. P. Hancke, "Opportunities and challenges of wireless sensor networks in smart grid," *IEEE Transactions on Industrial Electronics*, vol. 57, no. 10, pp. 3557–3564, February 2010.

[84] I. Al-Anbagi, M. Erol-Kantarci, and H. T. Mouftah, "A survey on cross-layer quality-of-service approaches in wsns for delay and reliability-aware applications," *IEEE Communications Surveys & Tutorials*, vol. 18, no. 1, pp. 525–552, October 2016.

[85] G. A. Shah, V. C. Gungor, and Ö. B. Akan, "A cross-layer QoS-aware communication framework in cognitive radio sensor networks for smart grid applications." *IEEE Transactions on Industrial Informatics*, vol. 9, no. 3, pp. 1477–1485, January 2013.

[86] I. Al-Anbagi, M. Erol-Kantarci, and H. T. Mouftah, "Priority-and delay-aware medium access for wireless sensor networks in the smart grid," *IEEE Systems Journal*, vol. 8, no. 2, pp. 608–618, September 2014.

[87] H. Su and X. Zhang, "Cross-layer based opportunistic MAC protocols for QoS provisionings over cognitive radio wireless networks," *IEEE Journal on Selected Areas in Communications*, vol. 26, no. 1, pp. 118–129, January 2008.

[88] Q. Liu, X. Wang, and G. B. Giannakis, "A cross-layer scheduling algorithm with QoS support in wireless networks," *IEEE Transactions on Vehicular Technology*, vol. 55, no. 3, pp. 839–847, June 2006.

[89] Y.-J. Chang, F.-T. Chien, and C.-C. Kuo, "Cross-layer QoS analysis of opportunistic OFDM-TDMA and OFDMA networks," *IEEE Journal on Selected Areas in Communications*, vol. 25, no. 4, pp. 657–666, May 2007.

[90] Q. Zhang and Y.-Q. Zhang, "Cross-layer design for QoS support in multihop wireless networks," *Proceedings of the IEEE*, vol. 96, no. 1, pp. 64–76, December 2008.

[91] X. Zhang, J. Tang, H.-H. Chen, S. Ci, and M. Guizani, "Cross-layer-based modeling for quality of service guarantees in mobile wireless networks," *IEEE Communications Magazine*, vol. 44, no. 1, pp. 100–106, January 2006.

[92] J. Tang and X. Zhang, "Cross-layer-model based adaptive resource allocation for statistical qos guarantees in mobile wireless networks," *IEEE Transactions on Wireless Communications*, vol. 7, no. 6, pp. 2318–2328, June 2008.

[93] A. Davy, B. Meskill, and J. Domingo Pascual, "An empirical study of effective capacity throughputs in 802.11 wireless networks," in *2012 IEEE Global Communications Conference (GLOBECOM)*, 2012, pp. 1770–1775.

[94] M. Matthaiou, G. C. Alexandropoulos, H. Q. Ngo, and E. G. Larsson, "Effective rate analysis of MISO Rician fading channels," in *2012 IEEE 7th Sensor Array and Multichannel Signal Processing Workshop (SAM)*, 2012, pp. 53–56.

[95] M. You, H. Sun, J. Jiang, and J. Zhang, "Effective rate analysis in Weibull fading channels," *IEEE Wireless Communications Letters*, vol. 5, no. 4, pp. 340–343, August 2016.

[96] J. Zhang, Z. Tan, H. Wang, Q. Huang, and L. Hanzo, "The effective through-put of MISO systems over $\kappa - \mu$ fading channels," *IEEE Transactions on Vehicular Technology*, vol. 63, no. 2, pp. 943–947, February 2014.

[97] J. Zhang, L. Dai, Z. Wang, D. W. K. Ng, and W. H. Gerstacker, "Effective rate analysis of MISO systems over α-μ fading channels," in *2015 IEEE Global Communications Conference (GLOBECOM)*, 2015, pp. 1–6.

[98] M. C. Gursoy, "MIMO wireless communications under statistical queueing constraints," *IEEE Transactions on Information Theory*, vol. 57, no. 9, pp. 5897–5917, September 2011.

[99] Q. Wang, D. Wu, and P. Fan, "Effective capacity of a correlated Rayleigh fading channel," *Wireless Communications and Mobile Computing*, vol. 11, no. 11, pp. 1485–1494, November 2011.

[100] C. Zhong, T. Ratnarajah, K.-K. Wong, and M.-S. Alouini, "Effective capac-ity of correlated MISO channels," in *2011 IEEE International Conference on Communications*, Kyoto, 2011, pp. 1–5.

[101] Q. Wang, D. Wu, and P. Fan, "Effective capacity of a correlated Nakagami-m fading channel," *Wireless Communications and Mobile Computing*, vol. 12, no. 14, pp. 1225–1238, February 2012.

[102] X. Guo, L. Dong, and H. Yang, "Performance analysis for effective rate of correlated MISO fading channels," *Electronics Letters*, vol. 48, no. 24, pp. 1564–1565, November 2012.

[103] J. Zhang, M. Matthaiou, G. K. Karagiannidis, and L. Dai, "On the multivari-ate γ–γ distribution with arbitrary correlation and applications in wireless communications," *IEEE Transactions on Vehicular Technology*, vol. 65, no. 5, pp. 3834–3840, June 2016.

[104] D. Wu, "QoS provisioning in wireless networks," *Wireless Communications and Mobile Computing*, vol. 5, no. 8, pp. 957–970, November 2005.

[105] D. Wu and R. Negi, "Utilizing multiuser diversity for efficient support of quality of service over a fading channel," *IEEE Transactions on Vehicular Technology*, vol. 54, no. 3, pp. 1198–1206, May 2005.

[106] ——, "Downlink scheduling in a cellular network for quality-of-service assurance," *IEEE Transactions on Vehicular Technology*, vol. 53, no. 5, pp. 1547–1557, September 2004.

[107] X. Li and D. Wu, "Power control and channel allocation for real-time applications in cellular networks," *Wireless Communications and Mobile Computing*, vol. 8, no. 6, pp. 705–713, January 2008.

[108] A. Balasubramanian and S. Miller, "The effective capacity of a time division downlink scheduling system," *IEEE Transactions on Communications*, vol. 58, no. 1, pp. 73–78, January 2010.

[109] W. Cheng, X. Zhang, and H. Zhang, "Joint spectrum and power efficiencies optimization for statistical QoS provisionings in wireless networks," in *2012 IEEE Global Communications Conference (GLOBECOM)*, 2012, pp. 4006–4011.

[110] ——, "Joint spectrum and power efficiencies optimization for statistical QoS provisionings over SISO/MIMO wireless networks," *IEEE Journal on Selected Areas in Communications*, vol. 31, no. 5, pp. 903–915, April 2013.

[111] J. Tang and X. Zhang, "Quality-of-service driven power and rate adaptation for multichannel communications over wireless links," *IEEE Transactions on Wireless Communications*, vol. 6, no. 12, pp. 4349–4360, December 2007.

[112] ——, "Cross-layer modeling for quality of service guarantees over wireless links," *IEEE Transactions on Wireless Communications*, vol. 6, no. 12, pp. 4504–4512, December 2007.

[113] S. Agarwal, S. De, S. Kumar, and H. Gupta, "QoS-aware downlink cooperation for cell-edge and handoff users," *IEEE Transactions on Vehicular Technology*, vol. 64, no. 6, pp. 2512–2527, June 2015.

[114] M. You, X. Mou, and H. Sun, "Effective capacity analysis of smart grid communication networks," in *2015 IEEE 20th International Workshop on Computer Aided Modelling and Design of Communication Links and Networks (CAMAD)*, 2015, pp. 196–200.

[115] L. Hernandez, C. Baladron, J. M. Aguiar, B. Carro, A. J. Sanchez-Esguevillas, J. Lloret, and J. Massana, "A survey on electric power demand forecasting: future trends in smart grids, microgrids and smart buildings," *IEEE Communications Surveys & Tutorials*, vol. 16, no. 3, pp. 1460–1495, April 2014.

[116] M. H. Cintuglu, O. A. Mohammed, K. Akkaya, and A. S. Uluagac, "A survey on smart grid cyber-physical system testbeds," *IEEE Communications Surveys & Tutorials*, vol. 19, no. 1, pp. 446–464, November 2017.

[117] I. T. F. on Interfacing Techniques for Simulation Tools, S. C. Mller, H. Georg, J. J. Nutaro, E. Widl, Y. Deng, P. Palensky, M. U. Awais, M. Chenine, M. Kch, M. Stifter, H. Lin, S. K. Shukla, C. Wietfeld, C. Rehtanz, C. Dufour, X. Wang, V. Dinavahi, M. O. Faruque, W. Meng, S. Liu, A. Monti, M. Ni, A. Davoudi, and A. Mehrizi-Sani, "Interfacing power system and ICT simulators: Challenges, state-of-the-art, and case studies," *IEEE Transactions on Smart Grid*, vol. 9, no. 1, pp. 14–24, January 2018.

[118] M. D. Ilic, L. Xie, U. A. Khan, and J. M. F. Moura, "Modeling of future cyber physical energy systems for distributed sensing and control," *IEEE Transactions on Systems, Man, and Cybernetics - Part A: Systems and Humans*, no. 4, pp. 825–838, July.

[119] G. E. Moore, "Cramming more components onto integrated circuits," *Proceedings of the IEEE*, vol. 86, no. 1, pp. 82–85, January 1998.

[120] R. D. Zimmerman, C. E. Murillo-Sánchez, and R. J. Thomas, "MATPOWER: Steady-state operations, planning, and analysis tools for power systems research and education," *IEEE Transactions on Power Systems*, vol. 26, no. 1, pp. 12–19, June 2011.

[121] Matlab. [Online]. Available: https://www.mathworks.com/products/matlab.html

[122] M. J. McDonald, G. Conrad, R. Cassidy *et al.*, "Cyber effects analysis using VCSE," *Sandia National Laboratories*, 2008.

[123] D. C. Bergman, D. K. Jin, D. M. Nicol, and T. Yardley, "The virtual power system testbed and inter-testbed integration." in *CSET*, 2009, pp. 1–6.

[124] PowerWorld. [Online]. Available: https://www.powerworld.com/

[125] M. Liljenstam, J. Liu, D. Nicol, Y. Yuan, G. Yan, and C. Grier, "Rinse: The real-time immersive network simulation environment for network security exercises," in *Proceedings of the 19th Workshop on Principles of Advanced and Distributed Simulation*, 2005, pp. 119–128.

[126] M. Mallouhi, Y. Al-Nashif, D. Cox, T. Chadaga, and S. Hariri, "A testbed for analyzing security of SCADA control systems (TASSCS)," in *2011 IEEE PES Innovative Smart Grid Technologies (ISGT)*, 2011, pp. 1–7.

[127] OPNET. [Online]. Available: https://www.riverbed.com/gb/products/steelcentral/opnet.html

[128] J. Hong, S.-S. Wu, A. Stefanov, A. Fshosha, C.-C. Liu, P. Gladyshev, and M. Govindarasu, "An intrusion and defense testbed in a cyber-power system environment," in *2011 Power and Energy Society General Meeting*, 2011, pp. 1–5.

[129] C. Queiroz, A. Mahmood, and Z. Tari, "Scadasima framework for building SCADA simulations," *IEEE Transactions on Smart Grid*, vol. 2, no. 4, pp. 589–597, September 2011.

[130] OMNET++. [Online]. Available: https://www.omnetpp.org/

[131] T. Morris, A. Srivastava, B. Reaves, W. Gao, K. Pavurapu, and R. Reddi, "A control system testbed to validate critical infrastructure protection concepts,"

International Journal of Critical Infrastructure Protection, vol. 4, no. 2, pp. 88–103, August 2011.

[132] W. Su, W. Zeng, and M.-Y. Chow, "A digital testbed for a PHEV/PEV enabled parking lot in a smart grid environment," in *2012 IEEE PES Innovative Smart Grid Technologies (ISGT)*, 2012, pp. 1–7.

[133] D. M. Ingram, D. A. Campbell, P. Schaub, and G. Ledwich, "Test and evaluation system for multi-protocol sampled value protection schemes," in *2011 IEEE Trondheim PowerTech*, 2011, pp. 1–7.

[134] S. Schütte, S. Scherfke, and M. Tröschel, "Mosaik: A framework for modular simulation of active components in smart grids," in *2011 IEEE First International Workshop on Smart Grid Modeling and Simulation (SGMS)*, 2011, pp. 55–60.

[135] S. Schütte, S. Scherfke, and M. Sonnenschein, "Mosaik-smart grid simulation API," *Proceedings of SMARTGREENS*, pp. 14–24, 2012.

[136] S. Rohjans, S. Lehnhoff, S. Schtte, S. Scherfke, and S. Hussain, "Mosaik - a modular platform for the evaluation of agent-based smart grid control," in *2013 IEEE PES ISGT Europe*, 2013, pp. 1–5.

[137] T. Hess, J. Dickert, and P. Schegner, "Multivariate power flow analyses for smart grid applications utilizing mosaik," in *2016 IEEE PES Innovative Smart Grid Technologies Conference Europe (ISGT-Europe)*, 2016, pp. 1–6.

[138] A. M. Kosek, O. Lnsdorf, S. Scherfke, O. Gehrke, and S. Rohjans, "Evaluation of smart grid control strategies in co-simulation: integration of IPSYS and mosaik," in *2014 Power Systems Computation Conference*, 2014, pp. 1–7.

[139] M. Bscher, A. Claassen, M. Kube, S. Lehnhoff, K. Piech, S. Rohjans, S. Scherfke, C. Steinbrink, J. Velasquez, F. Tempez, and Y. Bouzid, "Integrated smart grid simulations for generic automation architectures with RT-LAB and mosaik," in *2014 IEEE International Conference on Smart Grid Communications (SmartGridComm)*, 2014, pp. 194–199.

[140] S. Lehnhoff, O. Nannen, S. Rohjans, F. Schlogl, S. Dalhues, L. Robitzky, U. Hager, and C. Rehtanz, "Exchangeability of power flow simulators in smart grid co-simulations with mosaik," in *2015 Workshop on Modeling and Simulation of Cyber-Physical Energy Systems (MSCPES)*, 2015, pp. 1–6.

[141] J. Haack, B. Akyol, N. Tenney, B. Carpenter, R. Pratt, and T. Carroll, "VOLTTRON: An agent platform for integrating electric vehicles and smart grid," in *2013 International Conference on Connected Vehicles and Expo (IC-CVE)*, 2013, pp. 81–86.

[142] S. Katipamula, J. Haack, G. Hernandez, B. Akyol, and J. Hagerman, "VOLT-TRON: An open-source software platform of the future," *IEEE Electrification Magazine*, vol. 4, no. 4, pp. 15–22, December 2016.

[143] D. P. Chassin, K. Schneider, and C. Gerkensmeyer, "GridLAB-D: An open-source power systems modeling and simulation environment," in *2008 IEEE/PES Transmission and distribution conference and exposition*, 2008, pp. 1–5.

[144] D. P. Chassin, J. C. Fuller, and N. Djilali, "GridLAB-D: An agent-based simulation framework for smart grids," *Journal of Applied Mathematics*, vol. 2014, pp. 1–12, June 2014.

[145] K. P. Schneider, J. C. Fuller, and D. Chassin, "Evaluating conservation voltage reduction: An application of GridLAB-D: An open source software package," in *2011 IEEE Power and Energy Society General Meeting*, 2011, pp. 1–6.

[146] A. Vaccaro, M. Popov, D. Villacci, and V. Terzija, "An integrated framework for smart microgrids modeling, monitoring, control, communication, and verification," *Proceedings of the IEEE*, vol. 99, no. 1, pp. 119–132, November 2011.

[147] J. Wan, S. Tang, Z. Shu, D. Li, S. Wang, M. Imran, and A. V. Vasilakos, "Software-defined industrial internet of things in the context of industry 4.0," *IEEE Sensors Journal*, vol. 16, no. 20, pp. 7373–7380, May 2016.

[148] X. Li, D. Li, J. Wan, A. V. Vasilakos, C.-F. Lai, and S. Wang, "A review of industrial wireless networks in the context of industry 4.0," *Wireless Networks*, vol. 23, no. 1, pp. 23–41, January 2017.

[149] National SCADA Test Bed. [Online]. Available: https://energy.gov/oe/technology-development/energy-delivery-systems-cybersecurity/national-scada-test-bed

[150] NSTB Fact Sheet. [Online]. Available: https://energy.gov/sites/prod/files/oeprod/DocumentsandMedia/NSTB_Fact_Sheet_FINAL_09-16-09.pdf

[151] J. Eto, R. Lasseter, B. Schenkman, J. Stevens, D. Klapp, H. VolkommeRr, E. Linton, H. Hurtado, and J. Roy, "Overview of the CERTS microgrid laboratory test bed," in *2009 CIGRE/IEEE PES Joint Symposium Integration of Wide-Scale Renewable Resources Into the Power Delivery System*, 2009, pp. 1–7.

[152] V. Salehi, A. Mohamed, A. Mazloomzadeh, and O. A. Mohammed, "Laboratory-based smart power system, part I: Design and system development," *IEEE Transactions on Smart Grid*, vol. 3, no. 3, pp. 1394–1404, June 2012.

[153] ——, "Laboratory-based smart power system, part II: Control, monitoring, and protection," *IEEE Transactions on Smart Grid*, vol. 3, no. 3, pp. 1405–1417, June 2012.

[154] F. Marra, D. Sacchetti, A. B. Pedersen, P. B. Andersen, C. Træholt, and E. Larsen, "Implementation of an electric vehicle test bed controlled by a virtual power plant for contributing to regulating power reserves," in *2012 IEEE Power and Energy Society General Meeting*, 2012, pp. 1–7.

[155] B. Zhao, X. Zhang, and J. Chen, "Integrated microgrid laboratory system," in *2013 IEEE Power Energy Society General Meeting*, 2013, pp. 1–1.

[156] ——, "Integrated microgrid laboratory system," *IEEE Transactions on Power Systems*, vol. 27, no. 4, pp. 2175–2185, May 2012.

[157] J. Mirkovic and T. Benzel, "Teaching cybersecurity with DeterLab," *IEEE Security & Privacy*, vol. 10, no. 1, pp. 73–76, February 2012.

[158] Grid security: Distributed controls test bed research capabilities and facilities at the distributed energy control and communication lab. [Online]. Available: https://web.ornl.gov/sci/renewables/docs/factsheets/Security-DECC.pdf

[159] South korea: Jeju island smart grid test-bed. [Online]. Available: https://www.gsma.com/iot/wp-content/uploads/2012/09/cl_jeju_09_121.pdf

[160] M. Shahidehpour and M. Khodayar, "Cutting campus energy costs with hierarchical control: The economical and reliable operation of a microgrid," *IEEE Electrification Magazine*, vol. 1, no. 1, pp. 40–56, October 2013.

[161] F. Huerta, J. Gruber, M. Prodanovic, and P. Matatagui, "A power-HIL microgrid testbed: Smart energy integration lab (SEIL)," in *2014 IEEE Energy Conversion Congress and Exposition (ECCE)*, 2014, pp. 3998–4003.

[162] M. Prodanovic, A. Rodríguez-Cabero, M. Jiménez-Carrizosa, and J. Roldán-Pérez, "A rapid prototyping environment for DC and AC microgrids: Smart energy integration lab (SEIL)," in *2017 IEEE Second International Conference on DC Microgrids (ICDCM)*, 2017, pp. 421–427.

[163] D. Hawbaker, T. Kazimer, P. Repic, E. Gleue, Q. Howard, C. Cortes, and M. Finocchio, "Cyber physical smart grid," *2015 NCUR*, 2015.

[164] NREL. [Online]. Available: https://www.nrel.gov/continuum/energy_integration/supporting_facilities.html

[165] S. Amendola, C. Occhiuzzi, and G. Marrocco, "RFID sensing networks for critical infrastructure security: A real testbed in an energy smart grid," in *2017 IEEE International Conference on RFID Technology & Application (RFID-TA)*, 2017, pp. 106–110.

[166] A. Chakrabortty and Y. Xin, "Hardware-in-the-loop simulations and verifications of smart power systems over an Exo-GENI testbed," in *2013 Second*

GENI Research and Educational Experiment Workshop (GREE), 2013, pp. 16–19.

[167] M. Weiss, A. Chakrabortty, and Y. Xin, "A multi-user network testbed for wide-area monitoring and control of power systems using distributed synchrophasors," in *Proceedings of the fourth international conference on Future energy systems*, 2013, pp. 291–292.

[168] V. P. Tran, S. Kamalasadan, and J. Enslin, "Real-time modeling and model validation of synchronous generator using synchrophasor measurements," in *2013 North American Power Symposium (NAPS)*, 2013, pp. 1–5.

[169] A. Hahn, A. Ashok, S. Sridhar, and M. Govindarasu, "Cyber-physical security testbeds: Architecture, application, and evaluation for smart grid," *IEEE Transactions on Smart Grid*, vol. 4, no. 2, pp. 847–855, March 2013.

[170] A. Ashok, S. Sridhar, A. D. McKinnon, P. Wang, and M. Govindarasu, "Testbed-based performance evaluation of attack resilient control for agc," in *2016 Resilience Week (RWS)*, 2016, pp. 125–129.

[171] V. Venkataramanan, P. Wang, A. Srivastava, A. Hahn, and M. Govindarasu, "Interfacing techniques in testbed for cyber-physical security analysis of the electric power grid," in *2017 Workshop on Modeling and Simulation of Cyber-Physical Energy Systems (MSCPES)*, 2017, pp. 1–6.

[172] M. J. Stanovich, I. Leonard, K. Sanjeev, M. Steurer, T. P. Roth, S. Jackson, and M. Bruce, "Development of a smart-grid cyber-physical systems testbed," in *2013 IEEE PES Innovative Smart Grid Technologies (ISGT)*, 2013, pp. 1–6.

[173] B. Chen, K. L. Butler-Purry, A. Goulart, and D. Kundur, "Implementing a real-time cyber-physical system test bed in RTDS and OPNET," in *2014 North American Power Symposium (NAPS)*, 2014, pp. 1–6.

[174] O. Bassey, B. Chen, K. L. Butler-Purry, and A. Goulart, "Implementation of wide area control in a real-time cyber-physical power system test bed," in *2017 North American Power Symposium (NAPS)*, 2017, pp. 1–6.

[175] C. B. Vellaithurai, S. S. Biswas, and A. K. Srivastava, "Development and application of a real-time test bed for cyber–physical system," *IEEE Systems Journal*, vol. 11, no. 14, pp. 2192–2203, November 2017.

[176] Y. Yang, H. Jiang, K. McLaughlin, L. Gao, Y. Yuan, W. Huang, and S. Sezer, "Cybersecurity test-bed for IEC 61850 based smart substations," in *2015 IEEE Power & Energy Society General Meeting*, 2015, pp. 1–5.

[177] Y. Yang, K. McLaughlin, L. Gao, S. Sezer, Y. Yuan, and Y. Gong, "Intrusion detection system for IEC 61850 based smart substations," in *2016 Power and Energy Society General Meeting (PESGM)*, 2016, pp. 1–5.

[178] Y. Yang, H.-Q. Xu, L. Gao, Y.-B. Yuan, K. McLaughlin, and S. Sezer, "Multidimensional intrusion detection system for IEC 61850-based SCADA networks," *IEEE Transactions on Power Delivery*, vol. 32, no. 2, pp. 1068–1078, August 2017.

[179] U. Adhikari, T. Morris, and S. Pan, "WAMS cyber-physical test bed for power system, cybersecurity study, and data mining," *IEEE Transactions on Smart Grid*, vol. 8, no. 6, pp. 2744–2753, March 2017.

[180] V. Krishnan, R. Liu, A. Askerman, A. Srivastava, D. Bakken, and P. Panciatici, "Resilient cyber infrastructure for the minimum wind curtailment remedial control scheme," in *2017 IEEE Industry Applications Society Annual Meeting*, 2017, pp. 1–7.

[181] R. Liu, A. K. Srivastava, D. E. Bakken, A. Askerman, and P. Panciatici, "Decentralized state estimation and remedial control action for minimum wind curtailment using distributed computing platform," *IEEE Transactions on Industry Applications*, vol. 53, no. 6, pp. 5915–5926, August 2017.

[182] S. Tan, W. Z. Song, S. Yothment, J. Yang, and L. Tong, "Scoreplus: An integrated scalable cyber-physical experiment environment for smart grid," in *2015 12th Annual IEEE International Conference on Sensing, Communication and Networking (SECON)*, 2015, pp. 381–389.

[183] S. Tan, W.-Z. Song, Q. Dong, and L. Tong, "Score: Smart-grid common open research emulator," in *2012 IEEE Third International Conference on Smart Grid Communications (SmartGridComm)*, 2012, pp. 282–287.

[184] J. Ahrenholz, C. Danilov, T. R. Henderson, and J. H. Kim, "CORE: A real-time network emulator," in *2008 IEEE Military Communications Conference*, 2008, pp. 1–7.

[185] G. Koutsandria, R. Gentz, M. Jamei, A. Scaglione, S. Peisert, and C. Mc-Parland, "A real-time testbed environment for cyber-physical security on the power grid," in *Proceedings of the First ACM Workshop on Cyber-Physical Systems-Security and/or Privacy*, 2015, pp. 67–78.

[186] H. G. Aghamolki, Z. Miao, and L. Fan, "A hardware-in-the-loop SCADA testbed," in *2015 North American Power Symposium (NAPS)*, 2015, pp. 1–6.

[187] Opal-RT. [Online]. Available: https://www.opal-rt.com/

[188] A. R. R. Matavalam and V. Ajjarapu, "Implementation of user defined models in a real-time cyber physical test-bed," in *2016 National Power Systems Conference (NPSC)*, 2016, pp. 1–6.

[189] M. Matin, G. Ilya, and S. Mohammed. Test bed for a cyber-physical system based on integration of advanced power laboratory and extensible messaging and presence protocol. [Online]. Available: https://www.ece.cmu.edu/~electriconf/posterpdf_2015/Matin_Meskin_Poster.pdf

[190] R. Belkacemi, A. Feliachi, M. Choudhry, and J. E. Saymansky, "Multi-agent systems hardware development and deployment for smart grid control applications," in *2011 IEEE Power and Energy Society General Meeting*, 2011, pp. 1–8.

[191] M. Kabir-Querrec, S. Mocanu, J.-M. Thiriet, and E. Savary, "A test bed dedicated to the study of vulnerabilities in IEC 61850 power utility automation networks," in *2016 IEEE 21st International Conference on Emerging Technologies and Factory Automation (ETFA)*, 2016, pp. 1–4.

[192] D. Wu and R. Negi, "Effective capacity-based quality of service measures for wireless networks," *Mobile Networks and Applications*, vol. 11, no. 1, pp. 91–99, February 2006.

[193] IEEE VTC Committee on Radio Propagation, "Coverage prediction for mobile radio systems operating in the 800/900 MHz frequency range," *IEEE Transactions on Vehicular Technology*, vol. 37, no. 1, pp. 3–72, February 1988.

[194] Y. Ibdah and Y. Ding, "Mobile-to-mobile channel measurements at 1.85 GHz in suburban environments," *IEEE Transactions on Communications*, vol. 63, no. 2, pp. 466–475, February 2015.

[195] H. Hashemi, "The indoor radio propagation channel," *Proceedings of the IEEE*, vol. 81, no. 7, pp. 943–968, July 1993.

[196] M. Matthaiou and C. Zhong, "Low-SNR analysis of MIMO Weibull fading channels," *IEEE Communications Letters*, vol. 16, no. 5, pp. 694–697, May 2012.

[197] F. Yilmaz and M.-S. Alouini, "Sum of Weibull variates and performance of diversity systems," in *Proc. ICWCMC: Connecting the World Wirelessly*, Leipzig, 2009, pp. 247–252.

[198] F. W. Olver, D. W. Lozier, R. F. Boisvert, and C. W. Clark, *NIST handbook of mathematical functions*. Washington, DC: Cambridge University Press, 2010.

[199] Z. Ji, C. Dong, Y. Wang, and J. Lu, "On the analysis of effective capacity over generalized fading channels," in *2014 IEEE International Conference on Communications (ICC)*, Sydney, 2014, pp. 1977–1983.

[200] G. Cui, A. Maio, V. Carotenuto, and L. Pallotta, "Performance prediction of the incoherent detector for a weibull fluctuating target," *IEEE Transactions on Aerospace and Electronic Systems*, vol. 50, no. 3, pp. 2176–2184, March 2014.

[201] M. Di Renzo, F. Graziosi, and F. Santucci, "Channel capacity over generalized fading channels: A novel MGF-based approach for performance analysis and design of wireless communication systems," *IEEE Transactions on Vehicular Technology*, vol. 59, no. 1, pp. 127–149, January 2010.

[202] A. Mathai, R. K. Saxena, and H. J. Haubold, *The H-function: theory and applications.* Springer Science & Business Media, Oct. 2009.

[203] A. Lozano, A. M. Tulino, and S. Verdú, "Multiple-antenna capacity in the low-power regime," *IEEE Transactions on Information Theory*, vol. 49, no. 10, pp. 2527–2544, October 2003.

[204] S. Verdú, "Spectral efficiency in the wideband regime," *IEEE Transactions on Information Theory*, vol. 48, no. 6, pp. 1319–1343, August 2002.

[205] E. Tanghe, W. Joseph, L. Verloock, L. Martens, H. Capoen, K. Van Herwegen, and W. Vantomme, "The industrial indoor channel: large-scale and temporal fading at 900, 2400, and 5200 MHz," *IEEE Transactions on Information Theory*, vol. 7, no. 7, pp. 2740–2751, July 2008.

[206] R. Bultitude, "Measurement, characterization and modeling of indoor 800/900 MHz radio channels for digital communications," *Communications Magazine, IEEE*, vol. 25, no. 6, pp. 5–12, June 1987.

[207] C. Fox, "The G and H functions as symmetrical Fourier kernels," *Transactions of the American Mathematical Society*, vol. 98, no. 3, pp. 395–429, March 1961.

[208] C. D. Bodenschatz, "Finding an *H*-function distribution for the sum of independent H-function variates," Ph.D. dissertation, University of Texas Austin, 1992.

[209] R. Saxena, "On the H-function of n variables," *Kyungpook Math J*, vol. 17, pp. 221–226, 1977.

[210] K. Gupta and S. Agrawal, "Fractional integral formulae involving a general class of polynomials and the multivariable H function," *Proceedings Mathematical Sciences*, vol. 99, no. 2, pp. 169–173, August 1989.

[211] P. Agarwal, S. V. Rogosin, E. T. Karimov, and M. Chand, "Generalized fractional integral operators and the multivariable H function," *Journal of Inequalities and Applications*, vol. 2015, no. 1, p. 350, November 2015.

[212] L. C. Andrews and L. C. Andrews, *Special functions of mathematics for engineers*. Oxford University Press Oxford, 1998, vol. 2.

[213] H. M. Srivastava and B. Kashyap, *Special functions in queuing theory and related stochastic processes.*, 1982.

[214] B. C. Carlson, *Special functions of applied mathematics*. Academic Press, 1977.

[215] H. Exton, *Multiple hypergeometric functions and applications*. Horwood, 1976.

[216] M. D. Springer, *The Algebra of Random variables*. New York, NY, USA: Wiley, 1979.

[217] B. D. Carter, "On the probability distribution of rational functions of independent H-function variates," Ph.D. dissertation, University of Arkansas, Fayetteville, AR, USA, 1972.

[218] S. D. Kellogg, "Algebraic functions of H-functions with specific dependency structure," Ph.D. dissertation, University of Texas Austin, Austin, TX, USA, 1984.

[219] J. I. D. Cook, "The H-function and probability density functions of certain algebraic combinations of independent random variables with H-function proba-

bility distribution," Ph.D. dissertation, University of Texas, Austin, TX, USA, 1981.

[220] Y. Jeong, J. W. Chong, H. Shin, and M. Win, "Intervehicle communication: Cox-Fox modeling," *IEEE Journal on Selected Areas in Communications*, vol. 31, no. 9, pp. 418–433, September 2013.

[221] J. Zhang, L. Dai, Z. Wang, D. W. K. Ng, and W. H. Gerstacker, "Effective rate analysis of MISO systems over $\alpha - \mu$ fading channels," in *2014 IEEE Global Communications Conference (GLOBECOM)*, 2014, pp. 1–6.

[222] H. Srivastava and M. Garg, "Some integrals involving a general class of polynomials and the multivariable H-function," 1986.

[223] S. Gaboury and R. Tremblay, "An expansion theorem involving H-function of several complex variables," *International Journal of Analysis*, vol. 2013, pp. 1–7, November 2013.

[224] H. Srivastava and R. Panda, "Expansion theorems for the H function of several complex variables," *J. Reine Angew. Math*, vol. 288, pp. 129–145, December 1976.

[225] H. Srivastava and N. Singh, "The integration of certain products of the multivariable H-function with a general class of polynomials," *Rendiconti del Circolo Matematico di Palermo*, vol. 32, no. 2, pp. 157–187, 1983.

[226] B. D. Carter and M. D. Springer, "The distribution of products, quotients and powers of independent H-function variates," *SIAM J. Appl. Math.*, vol. 33, no. 4, pp. 542–558, August 1977.

[227] H. Srivastava, "A class of generalised multiple hypergeometric series arising in physical and quantum chemical applications," *Journal of Physics A: Mathematical and General*, vol. 18, no. 5, pp. 227–234, 1985.

[228] R. Barakat, "Weak-scatterer generalization of the K-density function with application to laser scattering in atmospheric turbulence," *J. OSA. A.*, vol. 3, no. 4, pp. 401–409, April 1986.

[229] I. S. Gradshteyn and I. M. Ryzhik, *Table of integrals, series, and products*, 6th ed. Academic Press, 2000.

[230] P. Bithas, "Weibull-gamma composite distribution: alternative multipath/shadowing fading model," *Electronics Letters*, vol. 45, no. 14, pp. 749–751, July 2009.

[231] F. Yilmaz and M. S. Alouini, "Product of the powers of generalized Nakagami-m variates and performance of cascaded fading channels," in *2009 IEEE Global telecommunications conference (GLOBECOM 2009)*, Honolulu, 2009, pp. 1–8.

[232] H. R. Alhennawi, M. M. H. E. Ayadi, M. H. Ismail, and H. A. M. Mourad, "Closed-form exact and asymptotic expressions for the symbol error rate and capacity of the H -function fading channel," *IEEE Transactions on Vehicular Technology*, vol. 65, no. 4, pp. 1957–1974, April 2016.

[233] T. Routtenberg, R. Concepcion, and L. Tong, "PMU-based detection of voltage imbalances with tolerance constraints," *IEEE Transactions on Power Delivery*, vol. 32, no. 1, pp. 484–494, February 2017.

[234] N. H. Abbasy and H. M. Ismail, "A unified approach for the optimal PMU location for power system state estimation," *IEEE Transactions on Power Systems*, vol. 24, no. 2, pp. 806–813, May 2009.

[235] T. T. Kim and H. V. Poor, "Strategic protection against data injection attacks on power grids," *IEEE Transactions on Smart Grid*, vol. 2, no. 2, pp. 326–333, June 2011.

[236] A. A. Khalek, C. Caramanis, and R. W. Heath, "Delay-constrained video transmission: Quality-driven resource allocation and scheduling," *IEEE Journal of Selected Topics in Signal Processing*, vol. 9, no. 1, pp. 60–75, February 2015.

[237] X. Bei, Y. J. Yoon, and A. Abur, "Optimal placement and utilization of phasor measurements for state estimation," *PSERC Publication*, pp. 05–20, 2005.

[238] D. Bertsekas, A. Nedić, and A. Ozdaglar, *Convex Analysis and Optimization*, ser. Athena Scientific optimization and computation series. Athena Scientific, 2003.

[239] V. Kekatos, G. B. Giannakis, and B. Wollenberg, "Optimal placement of phasor measurement units via convex relaxation," *IEEE Transactions on Power Systems*, vol. 27, no. 3, pp. 1521–1530, February 2012.

[240] "IEEE standard for synchrophasor data transfer for power systems," *IEEE Std C37.118.2-2011 (Revision of IEEE Std C37.118-2005)*, pp. 1–53, December 2011.

[241] W. Tushar, C. Yuen, B. Chai, S. Huang, K. L. Wood, S. G. Kerk, and Z. Yang, "Smart grid testbed for demand focused energy management in end user environments," *IEEE Wireless Communications*, vol. 23, no. 6, pp. 70–80, December 2016.

[242] H. Sun, W.-Y. Chiu, J. Jiang, A. Nallanathan, and H. V. Poor, "Wideband spectrum sensing with sub-nyquist sampling in cognitive radios," *IEEE Transactions on Signal Processing*, vol. 60, no. 11, pp. 6068–6073, November 2012.

[243] A. A. Khan, M. H. Rehmani, and M. Reisslein, "Cognitive radio for smart grids: Survey of architectures, spectrum sensing mechanisms, and networking protocols," *IEEE Communications Surveys & Tutorials*, vol. 18, no. 1, pp. 860–898, September 2016.

[244] L.-F. Pak, V. Dinavahi, G. Chang, M. Steurer, and P. F. Ribeiro, "Real-time digital time-varying harmonic modeling and simulation techniques IEEE task force on harmonics modeling and simulation," *IEEE Transactions on Power Delivery*, vol. 22, no. 2, pp. 1218–1227, April 2007.

[245] W. S. J. John Grainger, *Power System Analysis*. MCGRAW HILL BOOK CO, 1994.

[246] Microsoft Research. [Online]. Available: https://www.microsoft.com/en-us/research/project/microsoft-research-software-radio-sora/

[247] GNURadio. [Online]. Available: https://www.gnuradio.org/

[248] GitHub. [Online]. Available: https://github.com/

[249] Ettus. [Online]. Available: https://www.ettus.com/

[250] B. Bloessl, M. Segata, C. Sommer, and F. Dressler, "Performance assessment of IEEE 802.11p with an open source SDR-based prototype," *IEEE Transactions on Mobile Computing*, no. 99, pp. 1–1, September 2017.

[251] G.-B. Huang, H. Zhou, X. Ding, and R. Zhang, "Extreme learning machine for regression and multiclass classification," *IEEE Transactions on Systems, Man, and Cybernetics, Part B (Cybernetics)*, vol. 42, no. 2, pp. 513–529, April 2012.

[252] S. K. Sharma, T. E. Bogale, L. B. Le, S. Chatzinotas, X. Wang, and B. Ottersten, "Dynamic spectrum sharing in 5g wireless networks with full-duplex technology: Recent advances and research challenges," *IEEE Communications Surveys & Tutorials*, vol. 20, no. 1, pp. 674–707, November 2017.

[253] MBED. [Online]. Available: https://www.mbed.com/